－ 三重大学　工学研究科　電気電子工学専攻　修士論文　－

"Improving System Performance of Solar-Wind Hybrid Power System by Numerical Simulation and Frequency Analysis of PV Cell Cooperating System"

令和 2 年度

三重大学大学院　工学研究科　電気電子工学専攻

Mukkaew Sittisombat

Abstract

Since there was an awareness of the negative environmental impact from carbon dioxide emission from conventional power generating system which fossil fuel, coal, and natural gas were involved, the trend of renewable energy usage was arisen as the global annual additions of renewable power capacity in 2019 is 74% higher than in 2013. The trend will continue in the same direction as it is stated in the road map to 2050 for the global energy transformation that renewable energy share in power generation should be increased to 86% with annual solar PV and wind additions up to 360 and 240 GW per year respectively.

To achieve those aims, the efficiency of the renewable power generating system must be considered, especially to overcome obstacles due to unpredictable characteristics of natural power sources. To combine the sources is one of the promising solutions. Therefore, hybrid power generation was introduced. In our research, the wind power is added to the existing photo-voltaic (PV) power generation system to increase the efficiency of the system from the lack of solar irradiation during night time and unpleasant weather conditions, hence PV Cell Cooperating System (PVCCS) is given as its name.

The PVCCS is comprised of the PV power generation system (PVPGS), the emulating circuit, an electric double-layer capacitor (EDLC), a bi-directional boost chopper, a filter, a power conditioner system (PCS) and a simplified grid. As there are many nonlinear elements included in the system, the purpose of this study is to investigate the frequency response of them by numerical and frequency analyses and verified simulations. To analyze the frequency characteristic, the transfer functions are derived by the state-space averaging method and analyzed by Bode, Nyquist, and Lyapunov Stability Criterion. The trial and error method is used to define the PI parameters to make the system more stable. Therefore, an evaluation to improve the system performance can be conducted. The stability and efficiency of the system are improved after the evaluating processes are done.

Acknowledgements

Table of Contents

List of Figures

List of Tables

Chapter 1

Introduction

1.1. Background and purpose

At the present, the trend of renewable energy usage has arisen, [1] the main reason was that there was an awareness of the negative environmental impact from the emission of CO_2 [2] from conventional power generating system in which fossil fuel, coal, and natural gas were involved [3]. As shown in Fig. 1.1, the CO_2 emission from coal has increased from around 9,000 MT in 1990 to around 15,000 MT in 2017. The trend is also the same for oil and natural gas but with slower increasing rate.

CO2 emissions by energy source, World 1990-2017

MT CO2

IEA. All rights reserved.

● Coal   ● Oil   ● Natural gas   ● Other
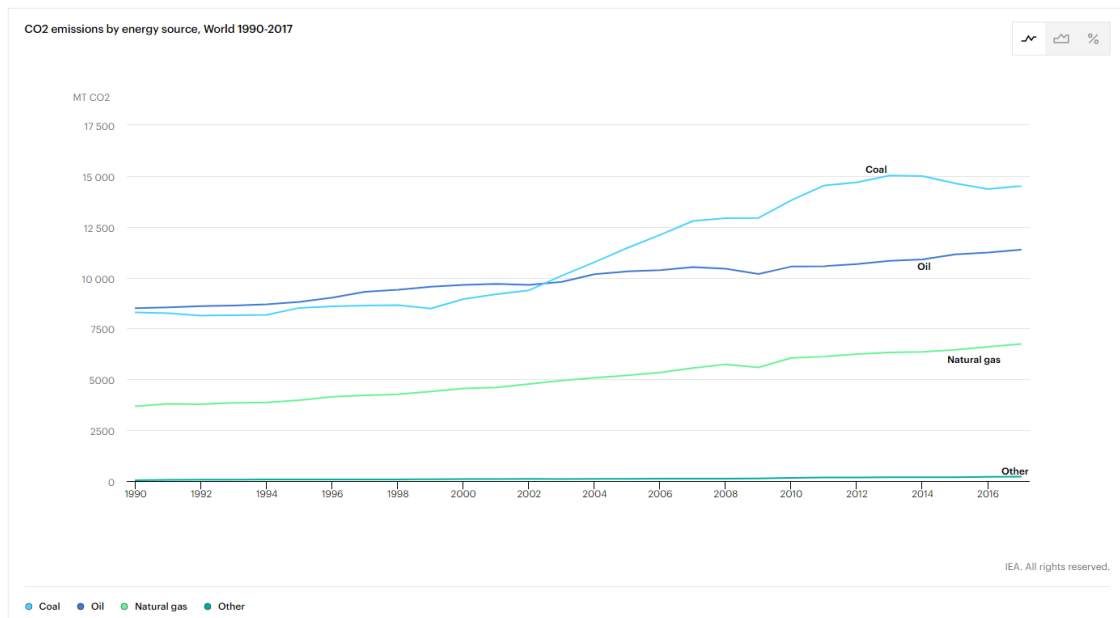
Figure 1.1 World carbon dioxide emission by energy source from $1990 - 2017$

Annual Additions of Renewable Power Capacity, by Technology and Total, 2013-2019

Additions by technology (Gigawatts)

More than **200** gigawatts added in 2019

Solar PV
Wind power
Hydropower
Bio-power, geothermal, ocean power, CSP

Note: Solar PV capacity data are provided in direct current (DC). Data are not comparable against technology contributions to electricity generation.

Figure 1.2 Annual addition of renewable power capacity by technology and total 2013-2019

Total primary energy supply (EJ/yr)

TPES increases **40%** by 2050 under **current and planned policies**

Accelerated deployment of **renewables** and **energy efficiency** result in **30%** decline in TPES

Renewable
Non-renewable
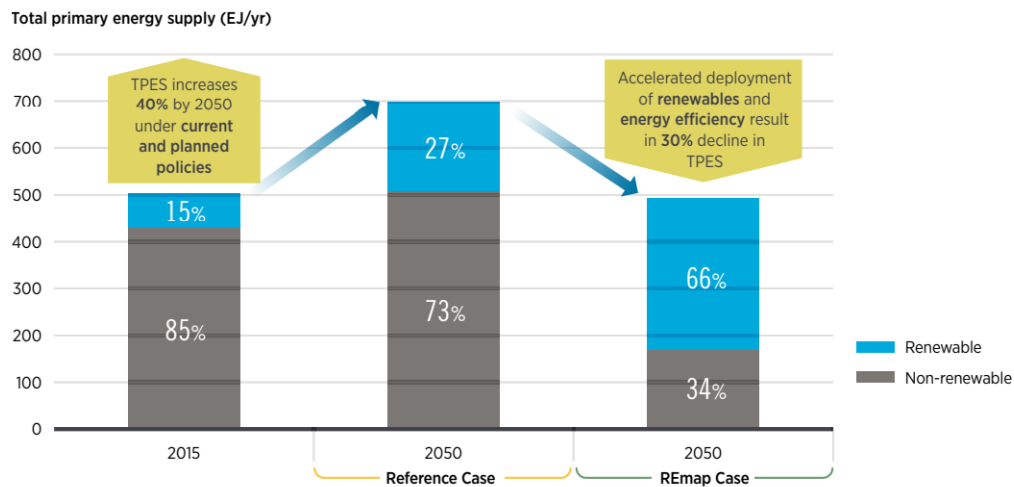
Figure 1.3 The aim for the global share of renewable energy to reach two-thirds by 2050

The annual addition of renewable power capacity is promising especially the solar PV which increased nearly 120 GW and following by around 60 GW of the wind power as shown in Fig. 1.2. The trend will be continued in this manner into the future and there is an aim for the global share of the renewable energy to reach two-thirds by 2050. [4]

To reach such a marvelous goal, there are a lot of obstacles to overcome to efficient the renewable power generating system due to unpredictable characteristics of natural power sources. To combine the sources is one of the promising solutions. Therefore, the hybrid

2

power generation was introduced.
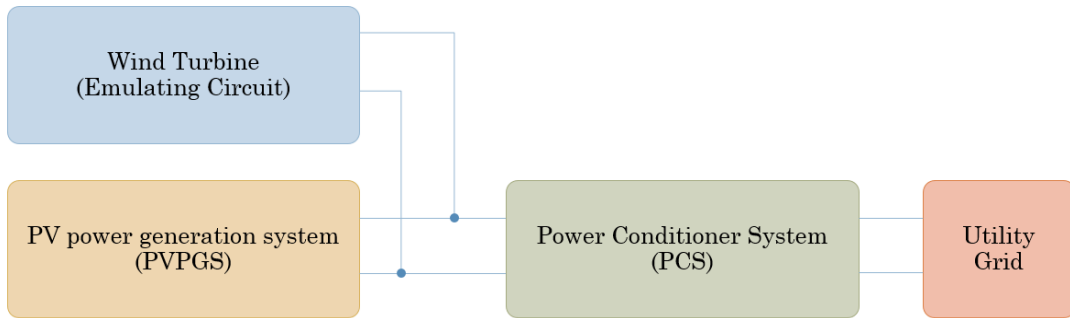
Figure 1.4 PV cell cooperating system diagram

In our research, the wind power generation system is retrofitted to the existed photovoltaic (PV) power generation system to increase the efficiency of the system from the lack of solar irradiation during night time and unpleasant weather conditions, hence PV Cell Cooperating System is given as its name as shown in Fig. 1.4.

It is necessary to study the characteristics of the PV power generation system (PVPGS) and emulate them in order to retrofit a wind turbine to the previously installed system. As a result, the emulating circuit was made which consists of a current source imitating the power from the wind turbine, an electric double-layer capacitors (EDLC) smoothing the fluctuating wind power, inductors and a capacitor as parts of the DC/DC converter. A bi‐directional chopper is introduced as the converter topology in this study. After the emulating conditions are satisfied, the emulating circuit and the PVPGS are connected to the power conditioner system (PCS). Subsequently the adjusted output power from the PCS is fed to the grid. Although, in this research the grid is simplified to ideal condition by using a battery with grid voltage instead of an inverter converting DC to AC.
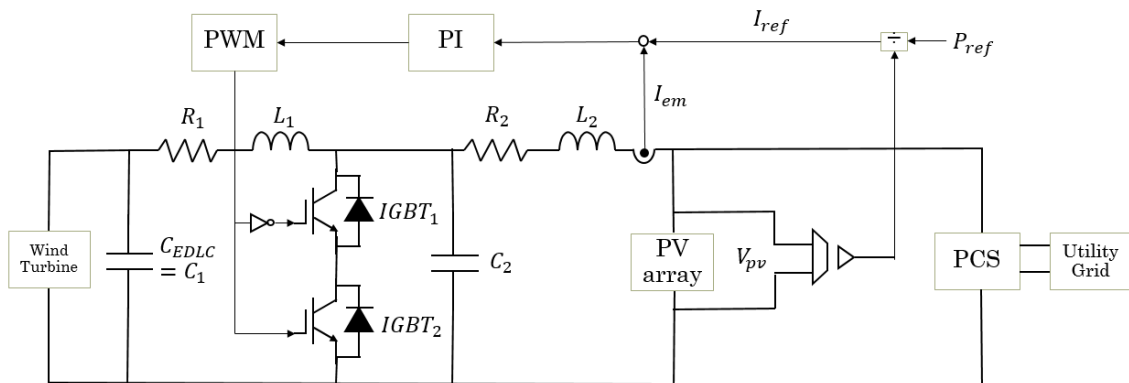
Figure 1.5 The schematic of PV cell cooperating system

3

The purpose of this study is to investigate the frequency response of the PV Cell Cooperating System by numerical and frequency analyses and verified simulations to judge the stability and propose new controller parameters to enhance the stability and efficiency of the whole system.

To analyze the frequency characteristic, the transfer function is derived from the state-space averaging method. The trial and error method is used to select the PI controller parameters. Then 16 cases of arbitrary gains and time constants are analyzed by Bode and Nyquist stability criteria. The step response is also used to depict the time behavior of the outputs of the system. From the test, there are 8 stable cases, among them, two promising cases are chosen as they possess the quality of highly responsive.

Therefore, the PV cell cooperating system performance is improved. The stability and efficiency of the system are enhanced after the evaluating processes are done.

1.2. Composition of the thesis

There are 5 chapters in this thesis:

Chapter 1 introduces general background, purpose, and the contribution of the thesis.

Chapter 2 is the Theory Section which includes the explanation of Wind Power Generation System, Photovoltaic Power Generation System, Hybrid Energy System, and PV Cell Cooperating System.

In chapter 3, the Method Section describes State – Space Analysis Method and Frequency Analysis Methods including Bode Stability Criterion, Nyquist Stability Criterion and step response.

In chapter 4, parameters, control methods of the system, analysis methods, simulation results and the analyze of the results are presented.

In chapter 5, conclusions and future works are mentioned.

1.3. Contributions

In this thesis, the transfer function of the PV cell cooperating system is derived and novel proper PI controller parameters are proposed. The stability judgement is conducted by using Bode and Nyquist stability criterions.

Chapter 2

Theory Section

2.1. Wind Power Generation System

The wind is a clean, free, and readily available renewable energy source. Each day, around the world, wind turbines are capturing the wind's power and converting it to electricity. Wind power generation plays an increasingly important role in the way we power our world – in a clean, sustainable manner. [5]

Over the last three decades, wind turbines have significantly evolved as the global wind market grows continuously and rapidly. By the end of 2009, the world capacity reached a total of 160 GW. In the global electricity market, wind energy penetration is projected to rise from 1% in 2008 to 8% in 2035. This is achieved simply by developing larger wind turbines and employing more in the wind farm. In terms of the size, large wind turbines of the MW order began to appear in the EU, the US and now in China and India. Typically, the large installed wind turbines in utility grids are between 1.5-5MW whilst 7.5 and 10 MW are under extensive development. Nowadays, modern wind turbines are reliable, quiet, cost-effective and commercially competitive while the wind turbine technologies are proven and mature. At present, technical challenges are generally associated with ever-growing wind turbine size, power transmission, energy storage, energy efficiency, system stability and fault tolerance.

| Under 750 | 750 – 2250 | 2250 – 3750 | 3750 – 5000 | Over 5000 |
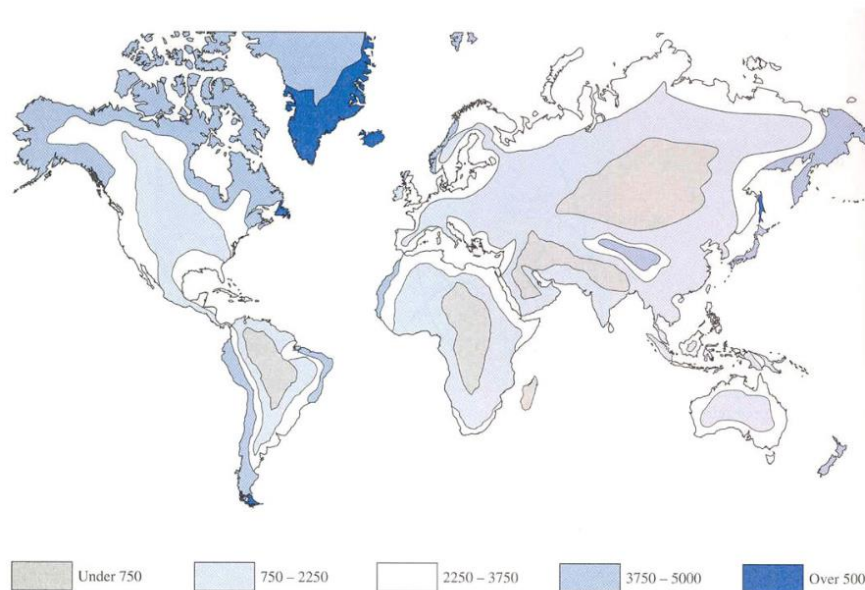
Figure 2.1 The world's energy potential for land-based wind turbines (estimated energy output in kWh/kW from a wind turbine that is dimensioned for 11 m/s)

Currently, wind power is widely recognized as a main feasible source of renewables which can be utilized economically in large quantity. A world map for wind energy potential is illustrated in Fig. 2.1. Taking the United Kingdom for example, the usable offshore wind energy alone is enough to provide three times more than the required electricity consumption in the country, given sufficient support. However, wind power fluctuates by its nature and such applications demand high reliability and high availability while the market is still looking to reduce weight, complexity and operational costs. [6]

2.1.1. Wind Turbine Generators

One of limiting factors in wind turbines lies in their generator technology. There is no consensus among academics and industry on the best wind turbine generator technology. Traditionally, there are three main types of wind turbine generators (WTGs) which can be considered for the various wind turbine systems, these being direct current (DC), alternating current (AC) synchronous and AC asynchronous generators. In principle, each can be run at fixed or variable speed. Due to the fluctuating nature of wind power, it is advantageous to operate the WTG at variable speed which reduces the physical stress on the turbine blades and drive train, and which improves system aerodynamic efficiency and torque transient behaviors.

6

2.2. Photovoltaic Power Generation System

The solar photovoltaic power generation system is mainly composed of photovoltaic cells, a solar controller, a storage battery, and so on. When the output power is required to be 220 V or 110 V, an inverter is necessary. The development of solar photovoltaic cells has been very rapid. It has been used in various industry and agriculture fields.

The use of solar energy is growing strongly around the world, in part due to the rapidly declining costs of solar panel manufacturing. [7]

2.1.1 Basics of PV cell

2.1.1.1. Electrical circuit model

Semiconductor materials which are operated by the photoelectric effect [8] form PV cells. When sunlight comes to the PV cell, the solar photons break the bonds of valence electrons and move the electron up to higher energy in the conduction band of semiconductor [8] as displayed in Figure 2.2. The movement of these electrons in the external circuit can transmit the electricity.
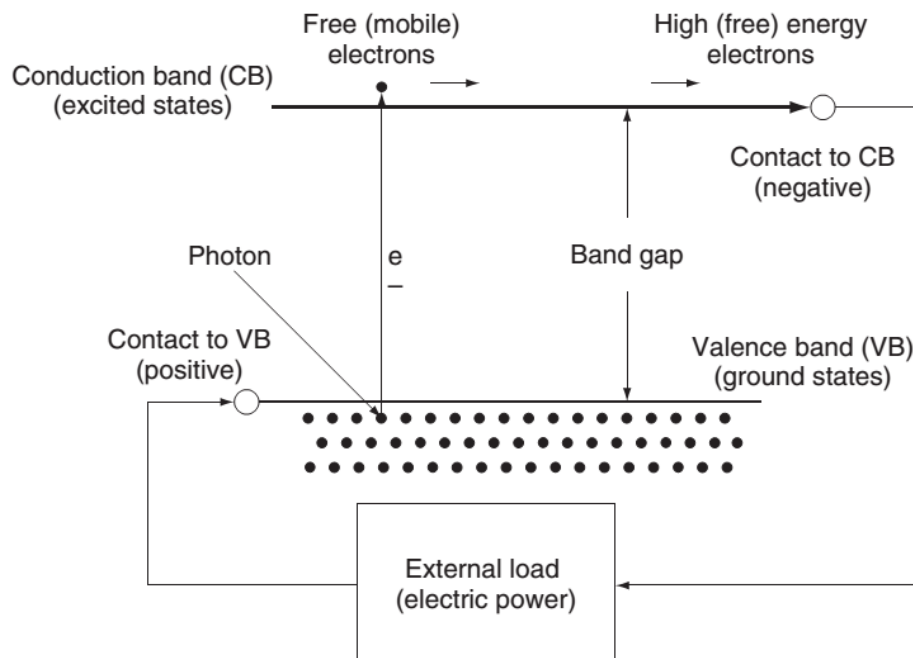
Figure 2.2 Operation principle of PV cell [8]

As a result, the solar module which is composed of many connected PV cells can generate the direct current (DC) after absorbing the sunlight. The PV cell is modeled by the equivalent electrical circuit as shown in Figure 2.2:
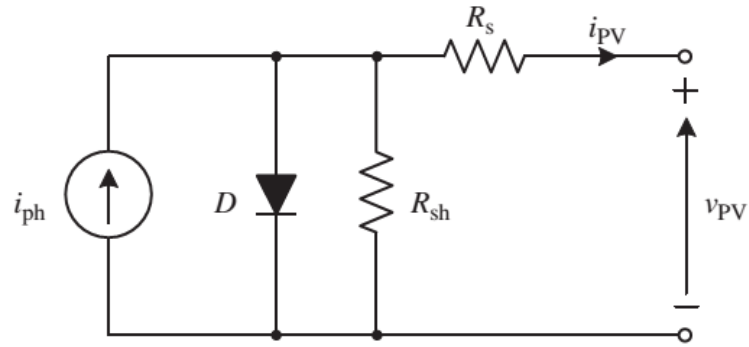
Figure 2.3 The electrical model of PV cell

The equation [9] that describes a PV cell is:

$$i_{pv} = i_L - i_0 \left(e^{\frac{q(v_{pv} + i_{pv}R_s)}{nKT}} - 1 \right) - \frac{v_{pv} + i_{pv}R_s}{R_{sh}}$$

(2.1)

where the parameters are listed in table 2.1 as below

Table 2.1 PV cell parameters

Variable	Parameter
v_{pv}	output voltage of PV cell (V)
i_{pv}	output current of PV cell (A)
R_s	Cell series parasitic resistance (Ω)
R_{sh}	Cell shunt parasitic resistance (Ω)
q	Electronic charge: 1.6×10^{-19} (Coulombs)
K	Boltzmann constant: 1.38×10^{-23} (J/K)
T	Absolute temperature in unit Kelvin
i_0	Cell reverse saturation current: 10^{-12} (A/cm^2)
i_{ph}	Cell photocurrent
n	Ideality factor of diode

2.1.1.2. I-V characteristic

Operation of the current and voltage a solar panel under different conditions of solar irradiation and temperature is presented by I–V characteristic curve in Figure 2.4.

8
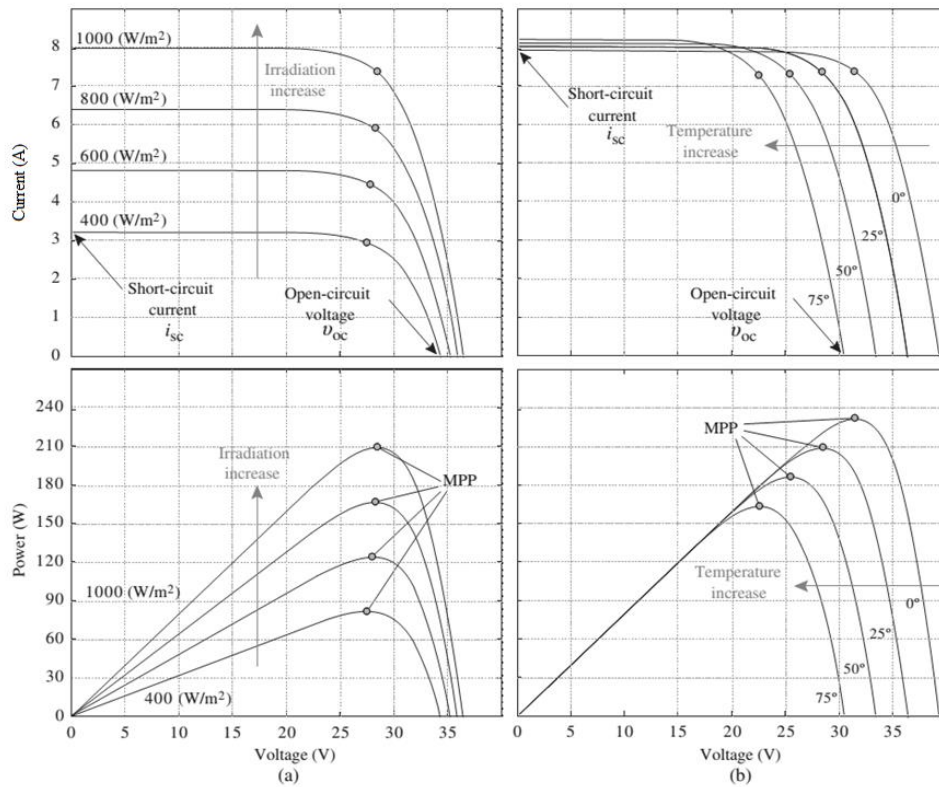
Figure 2.4 I-V characteristic of solar panel [10]

The output voltage of the solar panel changes slightly while the output current is strongly influenced [10] by the various values of solar irradiation. In contrast, the output current of the solar panel alters slightly while the output voltage is significantly affected by the changing of the temperature.

In the I–V characteristic curve, there is a special combination point of current and voltage of the solar panel, by which the power achieves the maximum value. The point at which the solar panel can supply maximum electrical power is the maximum power point (MPP). This maximum power point value changes in the I–V characteristic curve of the solar panel in accordance with the impact of the solar irradiation and temperature at different times.

When the solar panel connects with a passive load, the I–V curve of the load will intersect the I–V characteristic curve of the solar panel and determine the power transmitted by the solar module, but it is not the MPP value in the I–V characteristic curve of the solar panel. To resolve this technical problem, a DC–DC or DC–AC power converter can be used to adjust the load curve characteristic and intersect the solar panel I–V characteristic curve at the MPP, this content will be discussed in next parts.

9

2.3. Hybrid Energy System

A hybrid power system is an emerging power generation technique which involves a combination of different energy systems, mostly renewables for optimal output configuration. [11] In this research, it is in the form of the solar-wind hybrid power generation system combining between the existed PV power generation system and the retrofitted wind turbine. Therefore, PV Cell Cooperating System is called as its name. It will be explained in detailed in the next topic.

2.4. PV Cell Cooperating System

The PV cell cooperating system is a hybrid energy system combining between the existed PV power generation system and the retrofitted wind turbine. Both wind and PV power generation system are connected to the power conditioner system which will convert the power and feed it to the utility grid. The diagram of the whole system is displayed in Fig. 2.5.
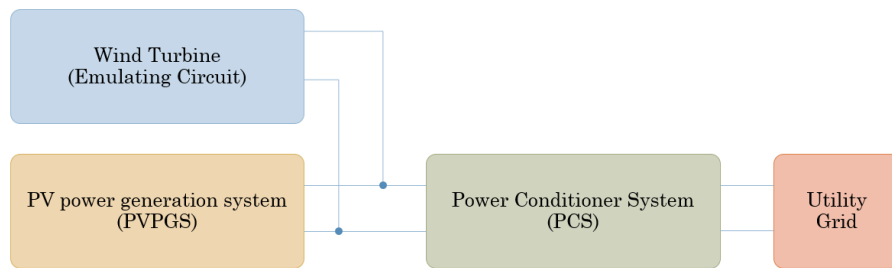
Figure 2.5 PV cell cooperating system diagram

The control schematic of the PV cell cooperating system is shown in Fig. 2.6. The theories of those elements and the control methods of the system will be explained in the following part.
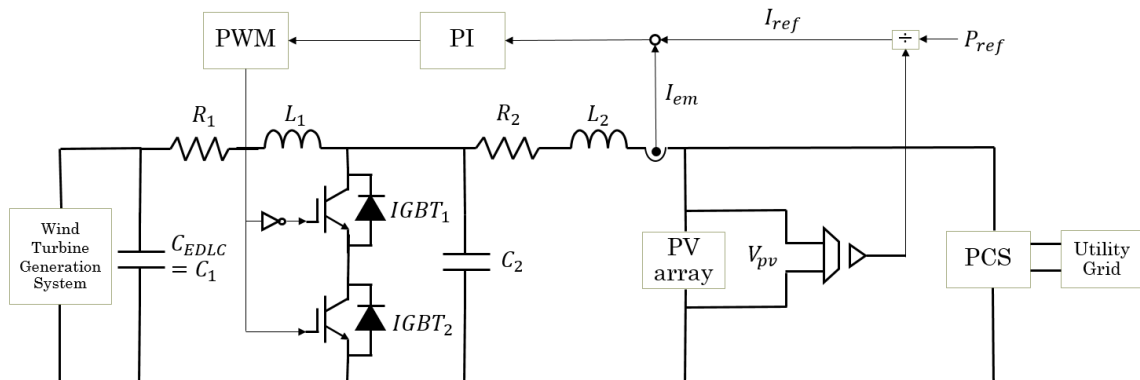
Figure 2.6 Control schematic of PV cell cooperating system

10

2.4.1. Electric Double Layer Capacitor

Electric double layer capacitor (EDLC) is the electric energy storage system based on charge–discharge process in an electric double layer on porous electrodes, which are used as memory back-up devices because of their high cycle efficiencies and their long life-cycles. A schematic illustration of EDLC is shown in Fig. 2.7.
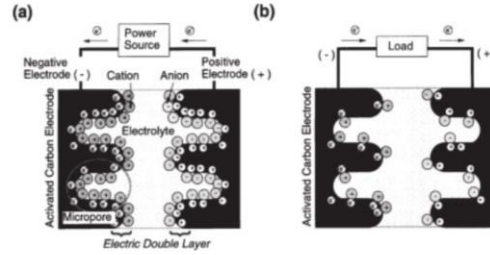
Figure 2.7 Schematic illustration of EDLC (a) charge state (b) discharge state

Recently, EDLCs have been proposed as the sub-power source for the hybrid electric vehicle because of its higher power density (larger than 1000 $W \cdot kg^{-1}$) and fast charge–discharge ability. Because the energy density of EDLC is only several $Wh \cdot kg^{-1}$, much lower than that of rechargeable batteries, an improvement in the capacitance of EDLC is required. The energy density of EDLC can be expressed as follows:

$$E = \frac{CV^2}{2} \tag{2.2}$$

where E is electric energy stored in the capacitor, C is capacitance, and V is applied voltage. The above correlation suggests that stability to electrochemical decomposition of the electrolyte, that is the electrochemical window of the electrolyte, is a key factor in energy storage, because the energy of EDLC varies as the square of applied voltage. Therefore, EDLC with a non-aqueous electrolyte has essentially a higher energy density than the aqueous type EDLC because non-aqueous electrolytes have wider electrochemical windows ($\approx$ 3 V) compared with aqueous electrolytes ($\approx$ 1 V). [12]

2.4.2. Insulated Gate Bipolar Transistor

IGBT stands for insulated-gate bipolar transistor. It is a bipolar transistor with an insulated gate terminal. The IGBT combines, in a single device, a control input with a MOS structure and a bipolar power transistor that acts as an output switch. IGBTs are suitable for high-voltage, high-current applications. They are designed to drive high-power applications with a low-power input. [13]
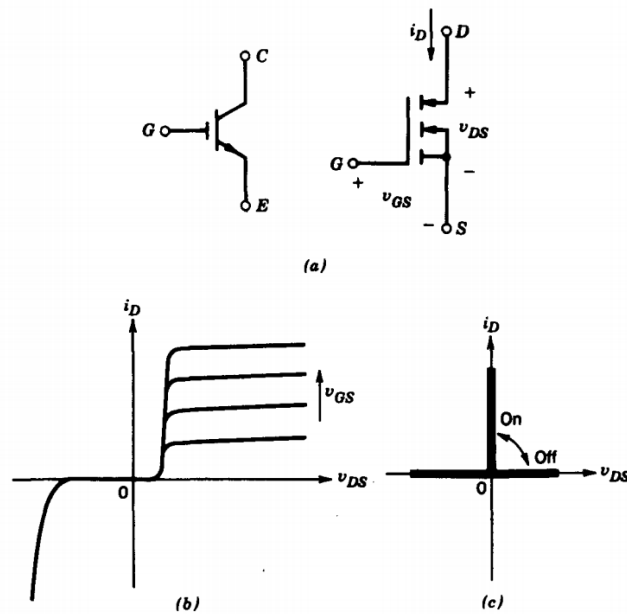
Figure 2.8 An IGBT (a) symbol, (b) i-v characteristics, (c) idealized characteristics

The circuit symbol for an IGBT is shown in Fig. 2.8a and its i-v characteristics are shown in Fig. 2.8b. The IGBTs have some of the advantages of the MOSFET, the BJT, and the GTO combined. Similar to the MOSFET, the IGBT has a high impedance gate, which requires only small amount of energy to switch the device. Like the BJT, the IGBT has a small on-state voltage even in devices with large blocking voltage ratings (for example, Von is 2-3 V in a 1000-V device). Similar to the GTO, IGBTs can be designed to block negative voltages, as their idealized switch characteristics shown in Fig. 2.8c indicate.

IGBTs have turn-on and turn-off times on the order of 1 µs and are available in module ratings as large as 1700 V and 1200 A. Voltage ratings of up to $2-3$ kV are projected. [14]

2.4.3. Pulse Width Modulation

Pulse width modulation (PWM) is an alternative method of harmonic control. The power electronic switches are repetitively turned on and blocked several times during each half cycle. The sequential switching instants are selected in a coordinated manner, to satisfy simultaneous requirements, i.e. to develop the desired fundamental voltage and to eliminate selected low order harmonics. IGBTs and IGCTs require much lower switching energy than GTOs and are better suited to applications that use PWM techniques. Multi-module arrangements are necessary to obtain high ratings. [15]

The principle of the sinusoidal PWM scheme for the two-level converter is illustrated in Fig. 2.9, where v_{ma}, v_{mb} and v_{mc} are the three-phase sinusoidal modulating waves and

v_{cr} is the triangular carrier wave. The fundamental-frequency component in the inverter output voltage can be controlled by amplitude modulation index

$$m_a = \frac{\hat{V}_m}{\hat{V}_{cr}}$$

(2.3)

where $\hat{V}_m$ and $\hat{V}_{cr}$ are the peak values of the modulating and carrier waves, respectively. The amplitude modulation index ma is usually adjusted by varying $\hat{V}_m$ while keeping $\hat{V}_{cr}$ fixed. The frequency modulation index is defined by

$$m_f = \frac{f_{cr}}{f_m}$$

(2.4)

where f_m and f_{cr} are the frequencies of the modulating and carrier waves, respectively.
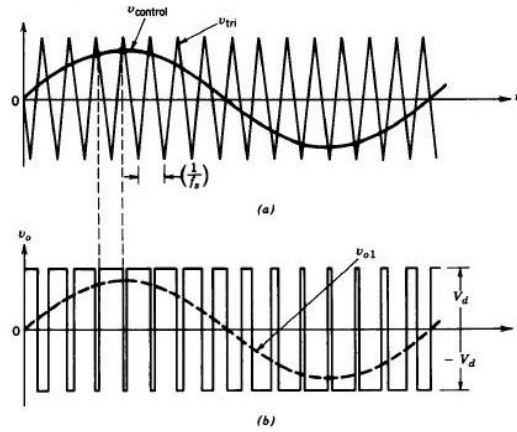
Figure 2.9 sinusoidal PWM scheme for the two-level converter [16]

2.4.4. DC-DC Converter

The main function of the DC/DC converter in the PCS is to convert the power from solar modules to the highest power by using maximum power point tracking (MPPT) method. There are some typical types of DC/DC converter such as boost converter, buck converter, buck-boost converter, and bi-direction converter can be used in the solar power systems. [17]

2.4.4.1. Boost converter

Boost converter [18], [19], [20] is used to increase the input voltage and the output voltage is always larger than the input voltage. When the switch is on, the diode is reversed biased, and it is isolating the output stage. The input generates energy to the inductor. When the switch is off, the output stage receives energy from the inductor and from the input.

13
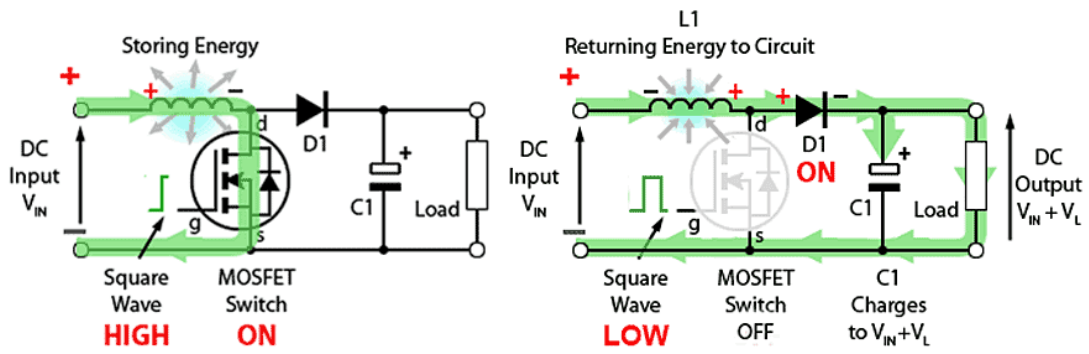
Figure 2.10 Boost converter [21]

The relationship among input voltage V_{in}, output voltage V_{out} and duty cycle D of switch in boost converter in the steady-state is shown in the equation as below:

$$\frac{V_{out}}{V_{in}} = \frac{1}{1-D}$$

(2.5)

2.4.4.2. Buck converter

The function of Buck converter [18], [22], [23] is to lower the input voltage and the output voltage is smaller than the input voltage. When the switch is on, the diode is reversed biased, it is supplying the load with current and this initially current is also stored in the inductor. When the switch is off, the energy stored in the inductor is released back to the output stage as shown in Figure 2.11.
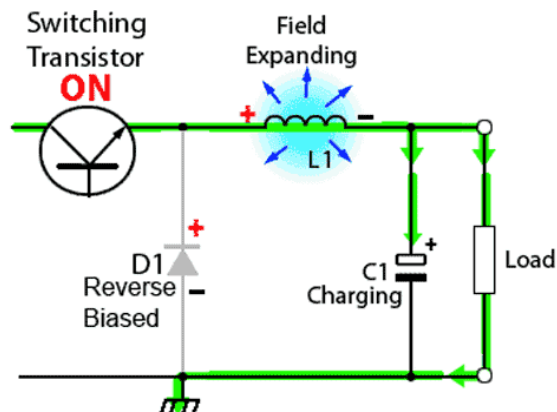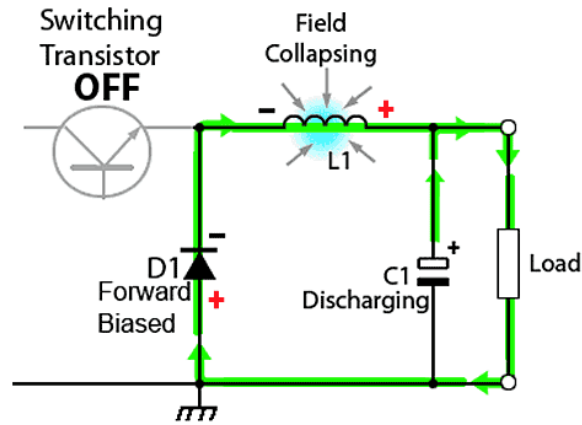
Figure 2.11 Buck converter [24]

The relationship of input voltage V_{in}, output voltage V_{out} and duty cycle D of switch in buck converter in a steady-state is displayed in the following equation.

$$\frac{V_{out}}{V_{in}} = D \qquad (2.6)$$

2.4.4.3. Buck-boost converter

Buck-boost converter [18], [25], [26] is used to control DC power supplies and the output voltage can be regulated to be higher or lower than the input voltage. In other words, the buck-boost converter combines the operation modes of either the buck converter and the boost converter. In Figure 2.12, when the switch 1 are on and off while switch 2 is off, this converter works in buck mode. In contrast, when the switch 1 is on while switch 2 are on and off, this converter operates in boost mode.
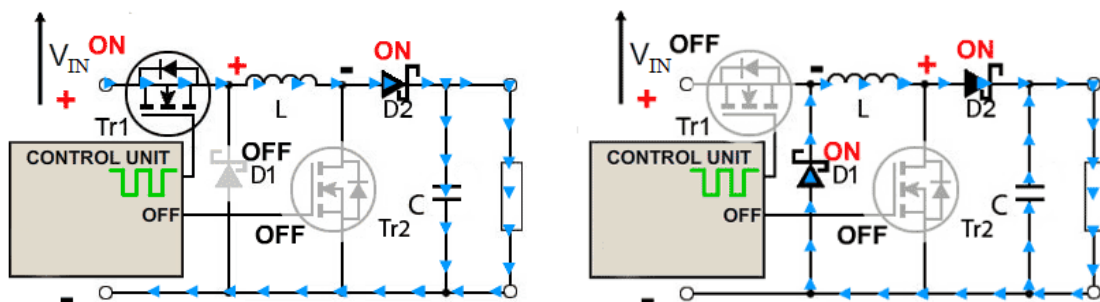
2. Operation in Buck mode

15
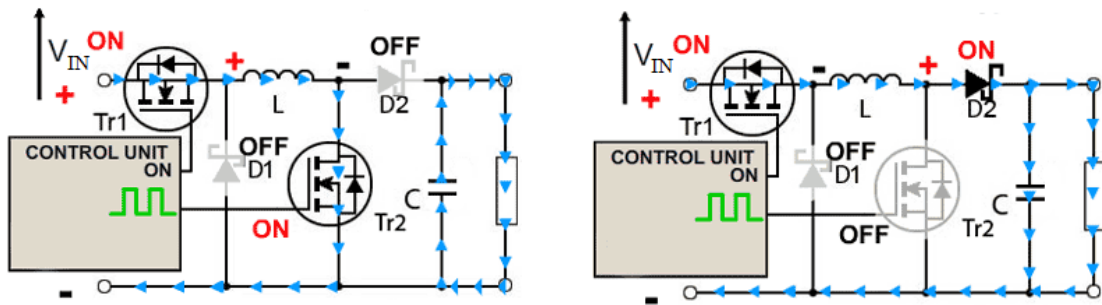
ii. Operation in Boost mode

Figure 2.12 Buck-boost converter [27]

In a steady-state condition, the relationship of input voltage V_{in}, output voltage V_{out} and duty cycle D of switch in buck – boost converter is:

$$\frac{V_{out}}{V_{in}} = \frac{D}{1-D}$$

(2.7)

2.4.4.4. Bidirectional converter

A bidirectional converter [28], [29], [30] can transmit current in both directions, but can support the voltage in only one direction. There are two-quadrant switches in the bidirectional converter, by which energy can move in both directions.

In boost mode, bidirectional converter operates in accordance with the principle of a typical boost converter. In this mode, the switch S2 behaves as a diode by sending zero to its gate.
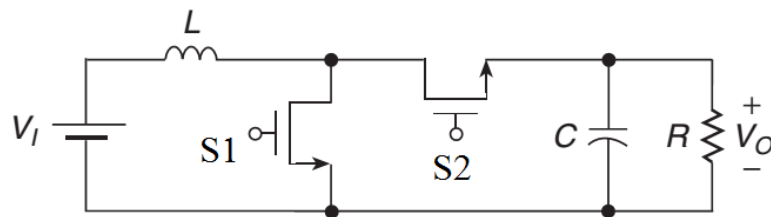
Figure 2.13 Bidirectional converter in boost mode

16

2.4.5. Maximum Power Point Tracking (MPPT)
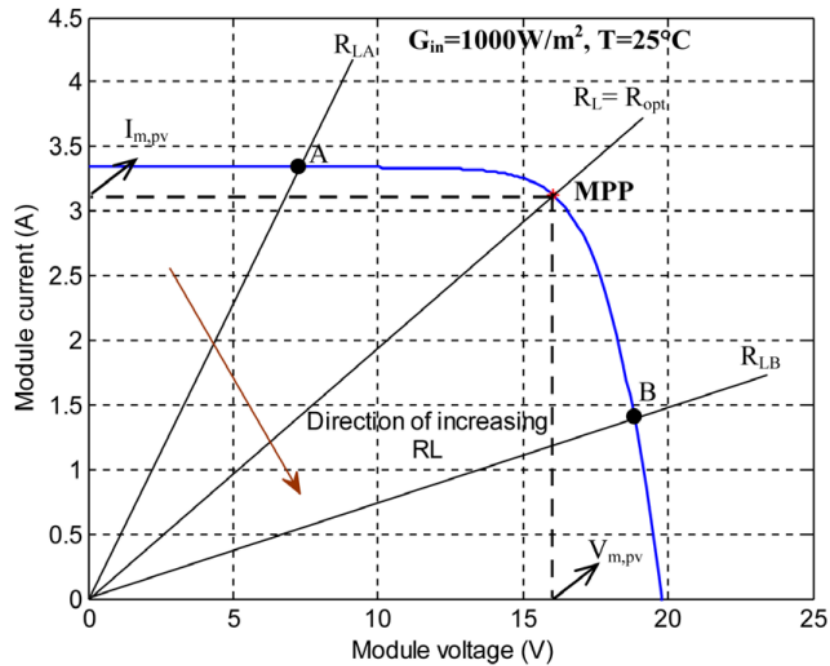
Figure 2.14 Operating point of a PV module with different resistive load [31]

When a solar array is directly connected to a load, the system's operating point will be at the intersection (A or B) of the I–V curve of the PV array and load line is shown in Figure 2.14. In general, this operating point is not at the MPP so the solar array must usually be oversized to ensure that the load's power requirements can be supplied. However, this will increase the system cost and energy losses. [31]

In order to solve this problem, a DC–DC or DC–AC power converter can control the load curve characteristic and intersect the PV curve at the MPP. The control techniques for the power converter are maximum power point tracking (MPPT) methods.

2.4.5.1. Impedance matching

A DC/DC converter which interface between load and module, serve the purpose of transferring maximum power from PV module to the load. According to the impedance matching principle [32], [33], the power output of a circuit is maximum when the source impedance matches with the load impedance.

When PV is connected directly to a load, the working point of PV will be determined by load characteristic. Load resistance is defined as follows:

$$R_{load} = \frac{V_{out}}{I_{out}} \tag{2.8}$$

where V_{out} is output voltage, I_{out} is output current

The maximum load of solar panel is:

$$R_{MPP} = \frac{V_{MPP}}{I_{MPP}} \tag{2.9}$$

where V_{MPP} is maximum voltage, I_{MPP} is maximum current

When the value of the largest load matches the value of R_{max}, the transmission power from PV to load will be the largest capacity. So, MPPT will match the impedance of the load with the largest load impedance of solar panel with the help of the DC-DC converter.
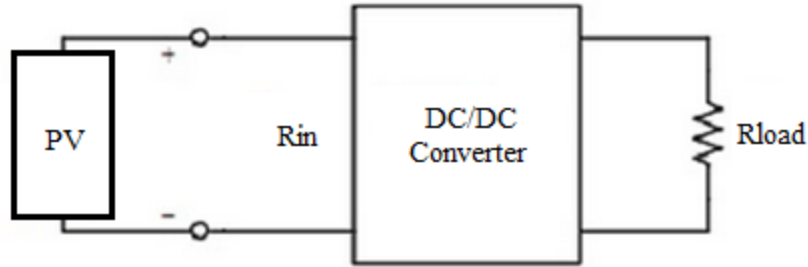
Figure 2.15 PV system with DC/DC converter

With Boost converter according to Equation (2.5) as mentioned above:

$$\frac{V_{out}}{V_{in}} = \frac{1}{1-D}$$

where V_{out} is output voltage, V_{in} is input voltage, D is duty cycle

To assume

$$P_{in} = P_{out} \tag{2.10}$$

where P_{out} is output power, P_{in} is input power

Then:

$$\frac{I_{in}}{I_{out}} = \frac{V_{out}}{V_{in}} \tag{2.11}$$

where I_0 is output current, I_i is input current

$$I_{in} = \frac{I_{out}}{1-D} \tag{2.12}$$

18

So:

$$R_{in} = \frac{V_{in}}{I_{in}} = (1-D)^2 \frac{V_{out}}{I_{out}} = (1-D)^2 R_{load} \qquad (2.13)$$

Thus, the value of R_{in} is adjusted in accordance with R_{MPP} by modifying the value of D. R_{in} varies from R_{load} to 0 as D varies from 0 to 1 correspondingly.

2.4.5.2. Perturb and Observe (P&O) algorithm
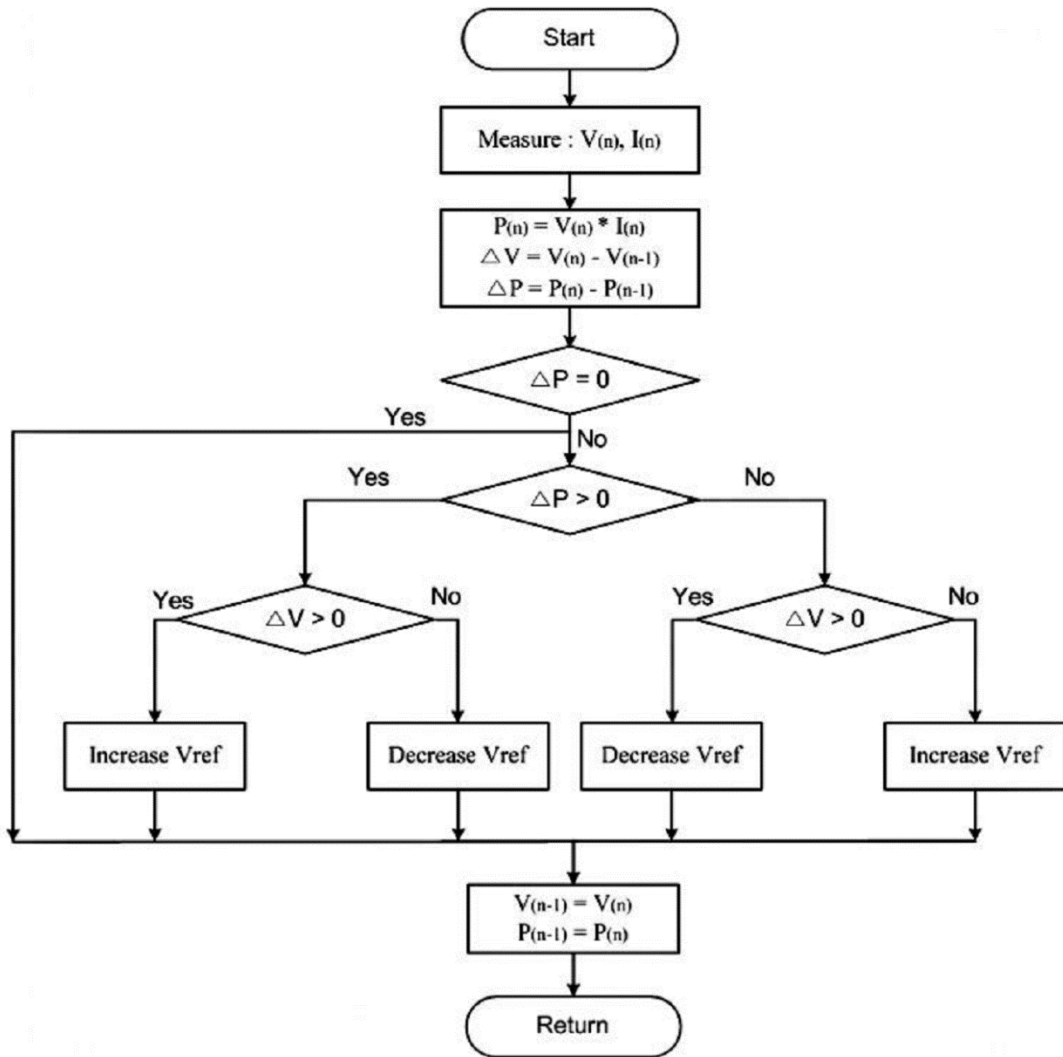
$$V_{ref} = V_{ref} (n\text{-}1) \pm \triangle V$$

Figure 2.16 Flowchart of P&O algorithm

There are many MPPT methods [34], [35], [36], [22], [37] but the Perturb and Observe (P&O) algorithm [38] is selected for the PV system in this study because it is the most commonly used in practice and the implementation is easy. Perturb and Observe (P&O)

consisting of a continuous reference voltage search process to reach the MPP. The search is performed by perturbing the reference voltage and then measuring the system response (observing) to determine the direction of the next perturbation. The reference voltage perturbations are performed in the direction in which the power should increase.

The perturbation in the reference voltage is always of the same magnitude while the sign is determined by the power variation. If the power has increased from the last sample, the sign of the perturbation is maintained. If the power has decreased, the sign is reversed.

2.4.5.3. MPPT control structure with DC/DC converter in boost mode
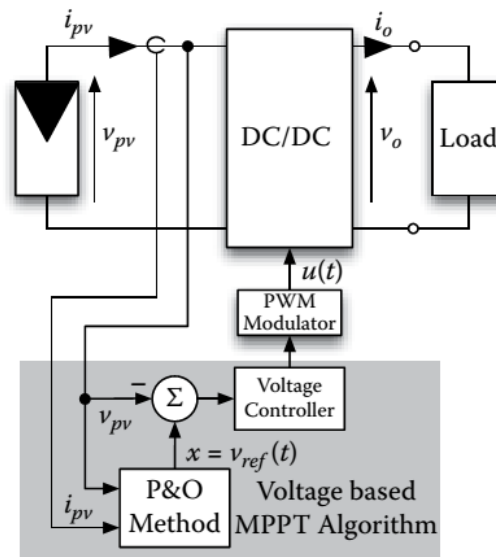
Figure 2.17 Diagram of the MPPT control system [38]

Fig. 2.17 shows a block diagram of a classic control system used to perform MPPT in the solar system with a DC/DC converter in boost mode. The PV system current i_{pv} and voltage v_{pv} measurements are required for the P&O MPPT algorithm which generates the reference voltage v_{ref}. MPPT technique will compare the PV array voltage v_{pv} with a constant reference voltage v_{ref}, which corresponds to the maximum power point voltage. A linear proportional-integral (PI) controller is used to reduce the error between reference voltage v_{ref} and the PV system voltage v_{pv} by varying the duty cycle of the DC/DC converter, which is modulated using carrier-based PWM. The gate signal controls the switch of the DC/DC converter.

2.4.6. PID Control

A PID controller is very useful and can solve a wide range of control problems. [39] More than 95% of all industrial control problems are solved by PID control, although many of

these controllers are proportional-integral (PI) controllers because derivative action is often not included.

The reason why on-off control often gives rise to oscillations is that the system overreacts since a small change in the error makes the actuated variable change over the full range. This effect is avoided in proportional control, where the characteristic of the controller is proportional to the control error for small errors. This can be achieved with the control law

$$u = \begin{cases} u_{max} & if \ e \geq e_{max}, \\ k_p e & if \ e_{min} < e < e_{max}, \\ u_{min} & if \ e \leq e_{min}, \end{cases} \tag{2.14}$$

where k_p is the controller gain, $e_{min} = u_{min}/k_p$, and $e_{max} = u_{max}/k_p$. The interval (e_{min}, e_{max}) is called the linear range because the behavior of the controller is linear when the error is in this interval:

$$u = k_p(r - y) = k_p e \quad if \ e_{min} \leq e \leq e_{max}, \tag{2.15}$$

While a vast improvement over on-off control, proportional control has the drawback that the process variable often deviates from its reference value. If some level of control signal is required for the system to maintain a desired value, then we must have e $= 0 in order to generate the requisite input. This can be avoided by making the control action proportional to the integral of the error:

$$u(t) = k_i \int_0^t e(\tau) d\tau \tag{2.16}$$

This control form is called integral control, and k_i is the integral gain. It can be shown through simple arguments that a controller with integral action has zero steady-state error. The catch is that there may not always be a steady state because the system may be oscillating. In addition, if the control action has magnitude limits, as in equation (2.14), an effect known as "integrator windup" can occur and may result in poor performance unless appropriate "anti-windup" compensation is used. Despite the potential drawbacks, which can be overcome with careful analysis and design, the benefits of integral feedback in providing zero error in the presence of constant disturbances have made it one of the most used forms of feedback.

An additional refinement is to provide the controller with an anticipative ability by using a prediction of the error. A simple prediction is given by the linear extrapolation

$$e(t + T_d) \approx e(t) + T_d \frac{de(t)}{dt} \tag{2.17}$$

which predicts the error T_d time units ahead. Combining proportional, integral, and derivative control, we obtain a controller that can be expressed mathematically as

$$u(t) = k_p e(t) + k_i \int_0^t e(\tau) d\tau + k_d \frac{de(t)}{dt} \tag{2.18}$$

The control action is thus a sum of three terms: the present as represented by the

proportional term, the past as represented by the integral of the error, and the future as represented by a linear extrapolation of the error (the derivative term). This form of feedback is called a proportional-integral-derivative (PID) controller and its action is illustrated in Fig. 2.18.
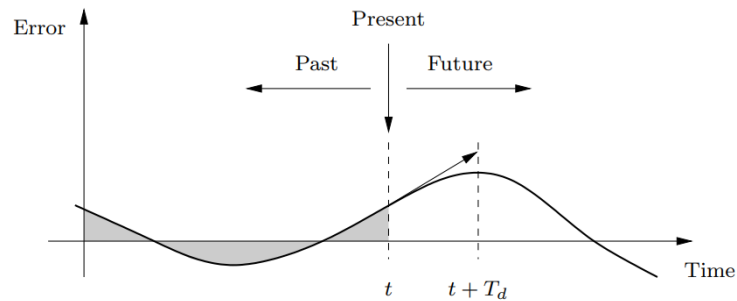
Figure 2.18 Action of a PID controller

2.5. Conclusion

In this chapter, the theories related to wind power generation system, photovoltaic power generation system, hybrid energy system, and PV cell cooperating system including EDLC, IGBT, PWM, DC-DC Converter, MPPT and PID control are described. In the next section, the methods that will be used to analyse the PV cell cooperating system will be explained.

Chapter 3

Method Section

3.1. State – Space Analysis Method

State – space analysis method is a formal method for deriving the small-signal ac equations of a switching converter which uses the state-space matrix description of linear circuits.

3.1.1. The basic state-space averaged model

Given: a PWM converter, operating in continuous conduction mode, with two subintervals during each switching period. During subinterval 1, when the switches are in position 1, the converter reduces to a linear circuit that can be described by the following state equations:

$$K \frac{dx(t)}{dt} = A_1 x(t) + B_1 u(t) \tag{3.1}$$

$$y(t) = C_1 x(t) + E_1 u(t) \tag{3.2}$$

During subinterval 2, when the switches are in position 2, the converter reduces to another linear circuit, that can be described by the following state equations:

$$K \frac{dx(t)}{dt} = A_2 x(t) + B_2 u(t) \tag{3.3}$$

$$y(t) = C_2 x(t) + E_2 u(t) \tag{3.4}$$

3.1.2. Equilibrium (dc) state-space averaged model

Provided that the natural frequencies of the converter, as well as the frequencies of variations of the converter inputs, are much slower than the switching frequency, then the state-space averaged model that describes the converter in equilibrium is

$$0 = AX + BU \tag{3.5}$$

$$Y = CX + EU \tag{3.6}$$

where the averaged matrices are

$$A = DA_1 + D'A_2 \tag{3.7}$$

$$B = DB_1 + D'B_2 \tag{3.8}$$

$$C = DC_1 + D'C_2 \tag{3.9}$$

$$E = DE_1 + D'E_2 \tag{3.10}$$

and the equilibrium dc components are

$$X = \text{equilibrium (dc) state vector}$$

$$U = \text{equilibrium (dc) input vector}$$

$$Y = \text{equilibrium (dc) output vector}$$

$$D = \text{equilibrium (dc) duty cycle}$$

3.1.3. Solution of equilibrium averaged model

Equilibrium state-space averaged model:

$$0 = AX + BU \tag{3.5}$$

$$Y = CX + EU \tag{3.6}$$

Solution for **X** and **Y**:

$$X = -A^{-1}BU \tag{3.11}$$

$$Y = -CA^{-1}B + EU \tag{3.12}$$

3.1.4. Small-signal ac state-space averaged model

$$K\frac{d\hat{x}(t)}{dt} = A\hat{x}(t) + B\hat{u}(t) + \{(A_1 - A_2)X + (B_1 - B_2)U\}\hat{d}(t) \tag{3.13}$$

$$\hat{y}(t) = C\hat{x}(t) + E\hat{u}(t) + \{(C_1 - C_2)X + (E_1 - E_2)U\}\hat{d}(t) \tag{3.14}$$

Where

$$\hat{x}(t) = \text{small} - \text{signal (ac) perturbation in state vector}$$

$$\hat{u}(t) = \text{small} - \text{signal (ac) perturbation in input vector}$$

$$\hat{y}(t) = \text{small} - \text{signal (ac) perturbation in output vector}$$

$$\hat{d}(t) = \text{small} - \text{signal (ac) perturbation in duty cycle}$$

So, if we can write the converter state equations during subintervals 1 and 2, then we can always find the averaged dc and small-signal ac models

3.1.5. Averaged state equations: quiescent operating point

The averaged (nonlinear) state equations:

$$K \frac{d\langle x(t)\rangle_{T_s}}{dt} = (d(t)A_1 + d'(t)A_2)\langle x(t)\rangle_{T_s} + (d(t)B_1 + d'(t)B_2)\langle u(t)\rangle_{T_s} \qquad (3.15)$$

$$\langle y(t)\rangle_{T_s} = (d(t)C_1 + d'(t)C_2)\langle x(t)\rangle_{T_s} + (d(t)E_1 + d'(t)E_2)\langle u(t)\rangle_{T_s} \qquad (3.16)$$

The converter operates in equilibrium when the derivatives of all elements of $\langle x(t)\rangle_{T_s}$ are zero. Hence, the converter quiescent operating point is the solution of

$$0 = AX + BU \qquad (3.5)$$
$$Y = CX + EU \qquad (3.6)$$

Where

$$A = DA_1 + D'A_2 \qquad (3.7)$$
$$B = DB_1 + D'B_2 \qquad (3.8)$$
$$C = DC_1 + D'C_2 \qquad (3.9)$$
$$E = DE_1 + D'E_2 \qquad (3.10)$$

And

$$X = equilibruim\ (dc)\ state\ vector$$
$$U = equilibruim\ (dc)\ input\ vector$$
$$Y = equilibrium\ (dc)\ output\ vector$$
$$D = equilibrium\ (dc)\ duty\ cycle$$

3.1.6. Averaged state equations: perturbation and linearization

Let
$$\langle x(t)\rangle_{T_s} = X + \hat{x}(t) \qquad (3.11)$$
$$\langle u(t)\rangle_{T_s} = U + \hat{u}(t) \qquad (3.12)$$
$$\langle y(t)\rangle_{T_s} = Y + \hat{y}(t) \qquad (3.13)$$
$$d(t) = D + \hat{d}(t) \ \rightarrow \ d'(t) = D' - \hat{d}(t) \qquad (3.14, 3.15)$$

With
$$\|U\| \gg \|\hat{u}(t)\| \qquad (3.16)$$
$$D \gg \|\hat{d}(t)\| \qquad (3.17)$$
$$\|X\| \gg \|\hat{x}(t)\| \qquad (3.18)$$
$$\|Y\| \gg \|\hat{y}(t)\| \qquad (3.19)$$

Substitute into averaged state equations

$$K \frac{d\left(X + \hat{x}(t)\right)}{dt} = \left(\left(D + \hat{d}(t)\right)A_1 + \left(D' - \hat{d}(t)\right)A_2\right)\left(X + \hat{x}(t)\right)$$

$$+ \left(\left(D + \hat{d}(t)\right)B_1 + \left(D' - \hat{d}(t)\right)B_2\right)\left(U + \hat{u}(t)\right) \qquad (3.20)$$

$$\left(Y + \hat{y}(t)\right) = \left(\left(D + \hat{d}(t)\right)C_1 + \left(D' - \hat{d}(t)\right)C_2\right)\left(X + \hat{x}(t)\right)$$

$$+ \left(\left(D + \hat{d}(t)\right)E_1 + \left(D' - \hat{d}(t)\right)E_2\right)\left(U + \hat{u}(t)\right) \qquad (3.21)$$

$$K\frac{d\hat{x}(t)}{dt} \underbrace{\phantom{K\frac{d\hat{x}(t)}{dt}}}_{first-order\ ac} = \underbrace{(AX + BU)}_{dc\ terms} + \underbrace{A\hat{x}(t) + B\hat{u}(t) + \{(A_1 - A_2)X + (B_1 - B_2)U\}\hat{d}(t)}_{first-order\ ac\ terms}$$

$$+ \underbrace{(A_1 - A_2)\hat{x}(t)\hat{d}(t) + (B_1 - B_2)\hat{u}(t)\hat{d}(t)}_{second-order\ nonlinear\ terms} \qquad (3.22)$$

$$\underbrace{(Y + \hat{y}(t))}_{dc\ +\ 1st\ order\ ac} = \underbrace{(CX + EU)}_{dc\ terms} + \underbrace{C\hat{x}(t) + E\hat{u}(t) + \{(C_1 - C_2)X + (E_1 - E_2)U\}\hat{d}(t)}_{first-order\ ac\ terms}$$

$$+ \underbrace{(C_1 - C_2)\hat{x}(t)\hat{d}(t) + (E_1 - E_2)\hat{u}(t)\hat{d}(t)}_{second-order\ nonlinear\ terms} \qquad (3.23)$$

3.1.7. Linearized small-signal state equations

Dc terms drop out of equations. Second-order (nonlinear) terms are small when the small-signal assumption is satisfied. We are left with:

$$K\frac{d\hat{x}(t)}{dt} = A\hat{x}(t) + B\hat{u}(t) + \{(A_1 - A_2)X + (B_1 - B_2)U\}\hat{d}(t) \qquad (3.24)$$

$$\hat{y}(t) = C\hat{x}(t) + E\hat{u}(t) + \{(C_1 - C_2)X + (E_1 - E_2)U\}\hat{d}(t) \qquad (3.25)$$

This is the desired result.

3.1.8 Obtain transfer function from state-space averaging equation

From the linear system analysis, equations can be written in matrix form as [40]

$$\dot{x} = Ax + Bu \qquad (3.26)$$

Where x is the state vector, A is the state coefficient matrix, u is the source vector, and B is the source coefficient matrix. If either A or B contains a function of x or u, then it is a nonlinear system. For the case of a linear system, the DC solution is obtained by setting Equation … to zero to yield

$$x = -A^{-1}Bu \qquad (3.27)$$

Where A^{-1} is the inverse of the state coefficient matrix. The inverse of a matrix is the adjoint matrix divided by its determinant. It should be noted that the determinant of A must be nonzero for a valid DC solution. Taking the Laplace transform of Equation … gives

$$sX(s) = AX(s) + BU(s) \qquad (3.28)$$

Or

$$X(s) = (sI - A)^{-1}BU(s) \tag{3.29}$$

Where I is the identity matrix having the same dimension as A. The transfer function is

$$\frac{X(s)}{U(s)} = (sI - A)^{-1}B \tag{3.30}$$

3.2. Frequency Analysis Methods

3.2.1. Bode Stability Criterion

The steady-state sinusoidal frequency-response of a circuit is described by the phasor transfer function $H(j\omega)$. A Bode plot is a graph of the magnitude (in dB) or phase of the transfer function versus frequency. It may be helpful to review some properties of transfer functions, the decibel scale, and properties of the log function.

3.2.1.1. Poles, Zeroes, and Stability

The s-domain transfer function is always a rational polynomial function of the form

$$H(s) = K\frac{N(s)}{D(s)} = K\frac{s^m + a_{m-1}s^{m-1} + a_{m-2}s^{m-2} + \cdots a_1 s + a_0}{s^n + b_{n-1}s^{n-1} + b_{n-2}s^{n-2} + \cdots b_1 s + b_0} \tag{3.31}$$

As we have seen already, the polynomials in the numerator and denominator are factored to find the poles and zeroes; these are the values of s that make the numerator or denominator zero. If we write the zeroes as $z_1, z_2, z_3 \cdots$ etc., and similarly write the poles as $p_1, p_2, p_3 \cdots$, then $H(s)$ can be written in factored form as

$$H(s) = K\frac{(s-z_1)(s-z_2)\cdots(s-z_m)}{(s-p_1)(s-p_2)\cdots(s-p_n)} \tag{3.32}$$

The pole and zero locations can be real or complex. When the roots are real, they are called simple poles or simple zeros. When the roots are complex, they always occur in pairs that are complex conjugates of each other.

Another important observation is that stable networks must always have poles and zeroes in the left-half of the complex s-plane, such that the real parts of the poles/zeroes will be negative. As an example, let us assume a stable network with simple poles at $p_1 = -1$ and $p_2 = -10$. The transfer function would then be

$$H(s) = \frac{1}{(s-p_1)(s-p_2)} = \frac{1}{(s+1)(s+10)} \tag{3.33}$$

Thus, for stable networks we always will find terms of the form $(s + a)$ in the denominator, where a is a positive number. Students sometimes get confused by the use of $(s - p)$ or $(s + a)$ to represent the same pole location; just remember that the poles are the values of s that make the denominator zero, i.e. $s = p$ or $s = -a$ in this example; clearly these will

represent the same pole if $p = -a$, and will represent a stable pole if $Re\{a\} > 0$ or $Re\{p\} < 0$.

When there are multiple roots at the same location the denominator will contain factors of the form $(s + a)^r$, where r is an integer that tells us how many times the root is repeated. For example, a critically damped second-order response would have $r = 2$.

When the stable network includes a complex-conjugate pole pair, we can represent the pole locations as $s = -\alpha \pm j\beta$ where α and β are both positive real numbers. The transfer function will then have a factor of the form

$$H(s) = \frac{1}{[s-(-\alpha+j\beta)][s-(-\alpha-j\beta)]} = \frac{1}{s^2+2\alpha s+\alpha^2+\beta^2} = \frac{1}{(s+\alpha)^2+\beta^2} \tag{3.34}$$

and thus, all the coefficients in the denominator are positive, even though the roots in fact have negative real parts. For reasons which will become clear later it is more convenient to write the second-order polynomial in the "standard form"

$s^2 + 2\xi\omega_n s + \omega_n^2$ 1.5

where ω_n is called the corner frequency or break point, and ξ is called the damping factor. Comparing (1.4) and (1.5) we can relate the corner frequency and damping factor to the poles using

$$\omega_n = \sqrt{\alpha^2 + \beta^2} \tag{3.35}$$

$$\xi = \frac{\alpha}{\omega_n} = \frac{\alpha}{\sqrt{\alpha^2+\beta^2}} \tag{3.36}$$

3.2.1.2. Decibel Scale and Log Functions

Logarithmic scales are useful when plotting functions that vary over many orders of magnitude. We are interested in the frequency response of circuits over a wide range of frequencies, so it makes sense to use a logarithmic scale for frequencies as well as signal intensity. Electrical engineers use the base-ten logarithm function and denote that as "log", reserving "ln" for the natural log function (base e), such that

$$log x \equiv log_{10} x \qquad ln x \equiv log_e x \tag{3.37}$$

$$log AB = log A + log B \tag{3.38}$$

$$log A/B = log A - log B \tag{3.39}$$

$$log y^x = x \log y \tag{3.40}$$

The "bel" scale which is named after inventor Alexander Graham Bell is defined as the log-base-ten of the ratio of two signal "intensities" (quantities relating to the power or energy associated with the signal). In circuits work we are often interested in the output-to-input power ratio, P_{out}/P_{in}, but the bel scale can be used to compare any two like quantities. Since there are 10 "decibels" per bel the power ratio in dB is defined as

$$10log_{10}\frac{P_{out}}{P_{in}} \qquad \text{(power ratio in dB)} \qquad (3.41)$$

Each time the power increases by a factor of ten, the power ratio in dB increases linearly by 10dB. Since power is related to the square of voltage or current, the dB scale for those quantities becomes (assuming identical source and load impedances)

$$10log_{10}\frac{V_{out}^2}{V_{in}^2} = 20log_{10}\frac{V_{out}}{V_{in}} \qquad \text{(voltage ratio in dB)} \qquad (3.42)$$

In most cases our transfer function is a voltage or current ratio, so we will use $20log|H(j\omega)|$ to compute the magnitude in dB.

A logarithmic scale like the dB scale prove to be a great advantage when dealing with circuit transfer functions, which are always of the form of a rational polynomial function as in (1.2). Two related terms we will use in our discussion of frequency response plots are "decade" and "octave". A decade change in frequency is a factor of ten. So, for example, 1 kHz is a decade above 100 Hz and a decade below 10 kHz. An "octave" is a factor of two, so similarly 1 kHz is an octave above 500 Hz and an octave below 2 kHz.

3.2.1.3. Stability Criteria

3.2.1.3.1. Gain Margin

Gain margin (G.M.) is the gap of magnitude that tells how far the system is from being unstable. The greater the gain margin, the greater the stability of the system. The gain margin refers to the amount of gain, which can be increased or decreased without making the system unstable. It is usually expressed as a magnitude in dB.

The gain margin can be defined from the following steps. [41]
- Find the frequency where the PHASE becomes -180 degrees.
- Find the GAIN, **G (in dB)**, at the SAME FREQUENCY.
- Then, the GAIN MARGIN (G.M.) can be defined as

$$\text{G.M.} = \textbf{0 - G dB} \qquad (3.43)$$

3.2.1.3.2. Phase Margin

The phase margin is the gap of phase that tells how far the system is from being unstable. The greater the **Phase Margin** (PM), the greater will be the stability of the system. The phase margin refers to the amount of phase, which can be increased or decreased without making the system unstable. It is usually expressed as a phase in degrees.

The phase margin can be defined from the following steps.
- Find the frequency where the GAIN is 0 dB.

- Find the PHASE, P (in degrees), at this SAME FREQUENCY
- Then, the PHASE MARGIN can be defined as:

$$\text{Phase Margin} = + P + 180 \text{ degrees} \tag{3.44}$$
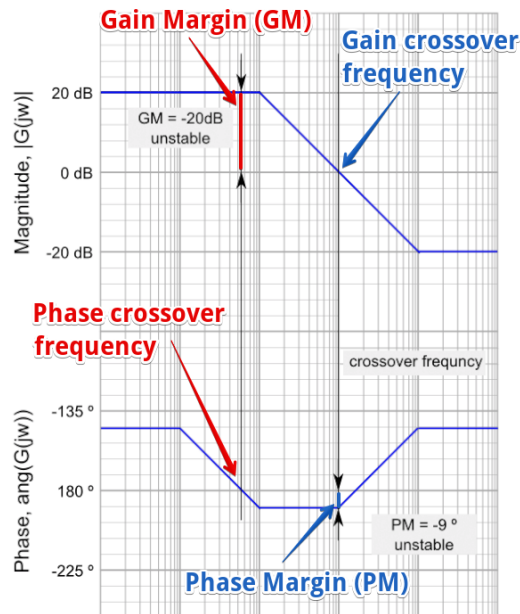
Figure 3.1 How to find gain and phase margin [42]

3.2.2. Nyquist Stability Criterion

It is a graphical technique for determining the stability of LTI system. Considering the closed loop system shown in Fig. 3.2
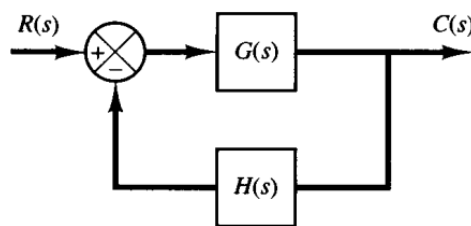

Figure 3.2 Closed loop system diagram

the transfer function is expressed as

$$\frac{C(s)}{R(s)} = \frac{G(s)}{1 + G(s)H(s)} \tag{3.45}$$

For stability, all the roots of the characteristic equation 1+GH(s) = 0 must lie in the left-

half plane. Note that open loop transfer function of a stable system may have poles in the left half plane. Nyquist stability criteria relates the open-loop transfer functions and the poles of the characteristic function.

3.2.2.1. Cauchy's argument principle

- Let $F(s)$ denotes a complex function that is a ration of two polynomials, i.e.

$$F(s) = \frac{polynomial}{polynomial} \tag{3.46}$$

- Let (x, y) represent a point in the s-plane.
- By direct substitution of (x, y) in $F(s)$, $F(s)$ will take a complex value
- Consider now a contour Γs drawn in the complex s-plane, the by substituting of all points on the contour in $F(s)$, we get another contour in $F(s)$ plane.
- The process described above is called contour mapping
- Cauchy argument principal states that
    o a contour encompassing BUT NOT PASSING through any number of zeros and poles of a function $F(s)$, can be mapped to another plane (the $F(s)$ plane) by the function $F(s)$.
    o The resulting contour $\Gamma F(s)$ will encircle the origin of the $F(s)$ plane N times, where N = Z = P, where Z and P are respectively the number of zeros and poles of $F(s)$ inside the contour Γs.
- Note that we count encirclements in the $F(s)$ plane in the same sense as the contour Γs and that encirclements in the opposite direction are negative encirclements.

3.2.2.2. Nyquist Stability Criteria

- Nyquist stability criteria is based on Cauchy's argument principle of complex variables.
- For stability analysis of closed loops systems, the chosen complex contour should cover the entire right half plane.
- Such path is called Nyquist path and consists of a semicircle starting at $-\infty$ to ∞.
- By Cauchy Argument Principle, the mapped Nyquist contour in GH(s)−plane makes a number of clock-wise encirclements around the origin equals the number of zeros of GH(s) in the right-half complex plane minus the poles of GH(s) in the right-half complex plane.
- For stability analysis, we need to check if 1+GH(s) has any zeros in the RHP or not. Noting that only difference between mapping 1 +GH(s) and mapping GH(s) is the addition of one, which is equivalent to a linear shift in the origin.

- Hence, we can use the mapped Nyquist contour of the open loop to investigate the stability of the closed loop system.
- Before delving into the details of the stability analysis procedure, it is important to point out the following facts
    - the zeros of $1 + GH(s)$ are the poles of the closed-loop system, and
    - the poles of $1 + GH(s)$ are same as the poles of $G(s)$

3.2.2.3. Application of Nyquist Stability Criteria

- let P be the number of poles of $GH(s)$ [same as $1+GH(s)$] encircled by Γs (in other words poles in the RHP for Nyquist path), and
- Z be the number of zeros of $1 + GH(s)$ encircled by Γs. Z is the number of poles of the closed loop system in the right half plane.
- The resultant contour in the GH(s)-plane, $\Gamma GH(s)$ shall encircle (clockwise) the point $(-1 + j0)$ N times such that $N = Z = P$.
- Stability Test
    - Unstable open-loop systems (P>0), we must have Z=0 to ensure stability. Hence, we should have N=-P, i.e. counter-clockwise encirclements. If N $\neq$ 6= $-P$, then some of the unstable poles have not moved to the LHP.
    - Stable open-loop systems (P=0), therefore N=Z. For stability, there must be no encirclement to -1. In this case, it is sufficient to consider only the positive frequency values of ω.
- If Nyquist plot passes through -1+j0 point, this indicates that the system has close loop poles on $j\omega$ axis

3.3. Conclusion

This chapter presented state-space averaging method, frequency analysis methods including Bode and Nyquist stability criterion. In the next section, these methods will be used to analyse the PV cell cooperating system.

Chapter 4

Analysis

4.1. Control method of the system

4.1.1. Control system of the PV cell cooperating system
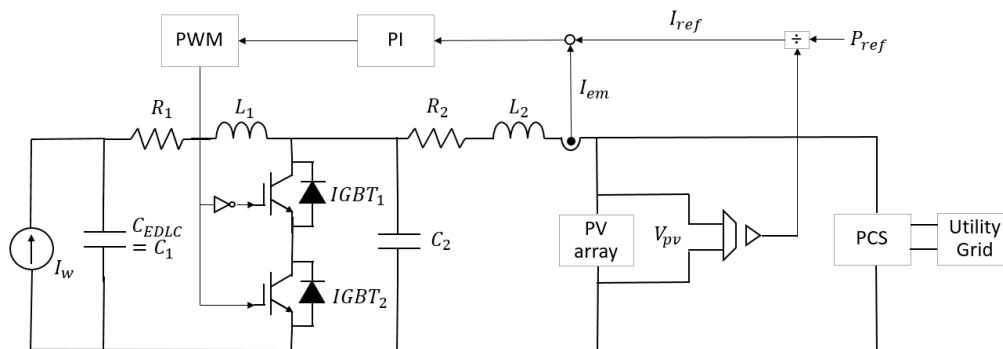
Figure 4.1 Control schematic of PV Cell Cooperating System

Fig. 4.1 presents the control method of the PVCCS. The emulating current of the PVCCS is regulated to follow the reference current value I_{ref} calculated by dividing the reference power P_{ref} by the MPP voltage V_{pv} of the PV array with the support of a current control loop. The PI controller reduces the difference between the emulating current I_{em} of the PVCCS and the reference current I_{ref}. The emulating voltage value V_{em}, which is the output voltage of the PV cell cooperating system, matches the MPP voltage value V_{pv} of the PV array. The output gate signals from the Pulse Width Modulation (PWM) adjust the switches of the boost DC/DC power converter. The inverter portion of the PCS and the utility grid have been replaced with DC power supplies.

4.2. Analysis Methods

The circuit diagram of the PVCCS is shown below.

Figure 4.2 Circuit diagram of the PV Cell Cooperating System

Figure 4.3 Circuit diagram of the PV Cell Cooperating System for defining circuit equations of averaged state equation mode A
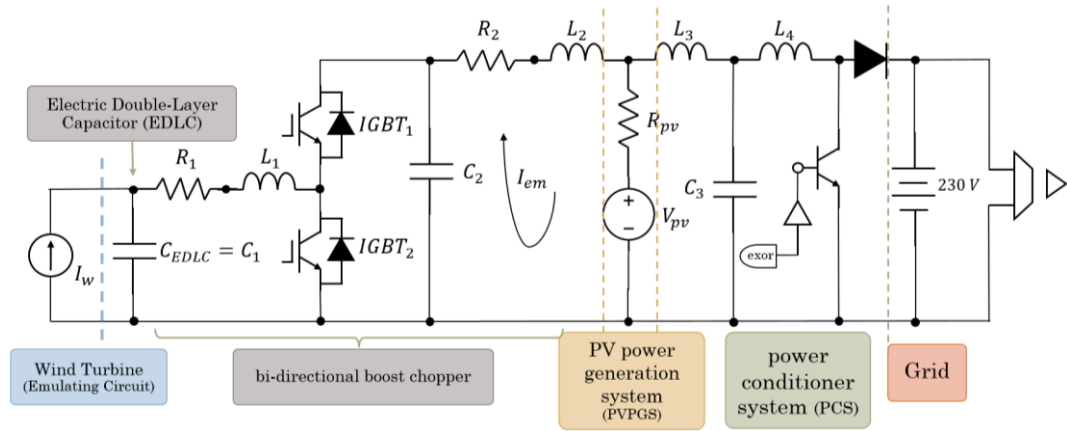
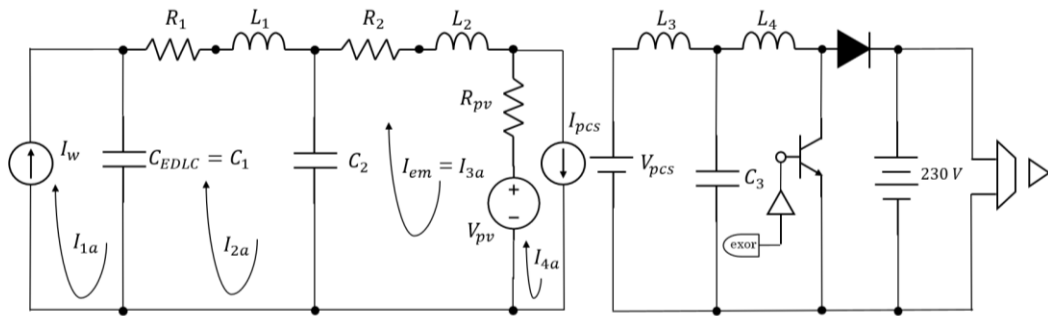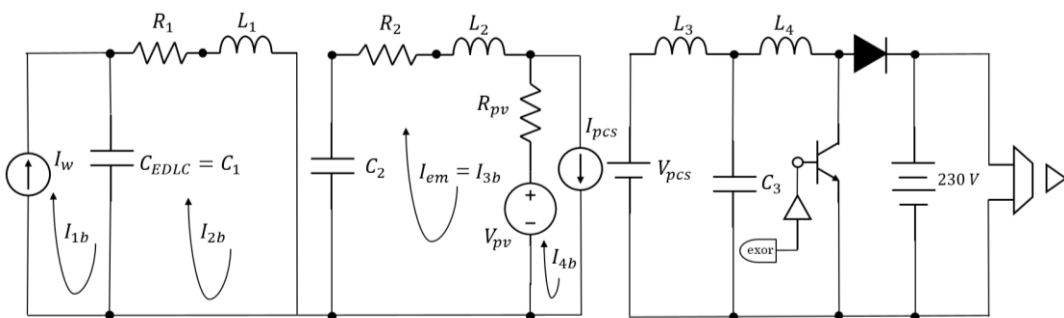

Figure 4.4 Circuit diagram of the PV Cell Cooperating System for defining circuit equations of averaged state equation mode B

4.2.1. Deriving Transfer Function by State-Space Averaging Method

From mode A as shown in Fig. 4.3. The state equations are derived as follows.

$$\frac{dx_a(t)}{dt} = A_a x_a(t) + B_a u_a(t)$$

$$
\begin{bmatrix} \dfrac{di_{2a}(t)}{dt} \\ \dfrac{di_{3a}(t)}{dt} \\ \dfrac{dv_{c1a}(t)}{dt} \\ \dfrac{dv_{c2a}(t)}{dt} \end{bmatrix}
=
\begin{bmatrix}
-\dfrac{R_1}{L_1} & 0 & -\dfrac{1}{L_1} & \dfrac{1}{L_1} \\
0 & -\dfrac{(R_2+R_{pv})}{L_2} & 0 & -\dfrac{1}{L_2} \\
\dfrac{1}{C_1} & 0 & 0 & 0 \\
-\dfrac{1}{C_2} & \dfrac{1}{C_2} & 0 & 0
\end{bmatrix}
\begin{bmatrix} i_{2a}(t) \\ i_{3a}(t) \\ v_{c1a}(t) \\ v_{c2a}(t) \end{bmatrix}
+
\begin{bmatrix}
0 & 0 \\
0 & \dfrac{1}{L_2} \\
-\dfrac{1}{C_1} & 0 \\
0 & 0
\end{bmatrix}
\begin{bmatrix} i_{wa}(t) \\ v_{pva}(t) \end{bmatrix}
$$

From mode B as shown in Fig. 4.4. The state equations are derived as follows.

$$\frac{dx_b(t)}{dt} = A_b x_b(t) + B_b u_b(t)$$

$$
\begin{bmatrix} \dfrac{di_{2b}(t)}{dt} \\ \dfrac{di_{3b}(t)}{dt} \\ \dfrac{dv_{c1b}(t)}{dt} \\ \dfrac{dv_{c2b}(t)}{dt} \end{bmatrix}
=
\begin{bmatrix}
-\dfrac{R_1}{L_1} & 0 & -\dfrac{1}{L_1} & 0 \\
0 & -\dfrac{(R_2+R_{pv})}{L_2} & 0 & -\dfrac{1}{L_2} \\
\dfrac{1}{C_1} & 0 & 0 & 0 \\
0 & \dfrac{1}{C_2} & 0 & 0
\end{bmatrix}
\begin{bmatrix} i_{2b}(t) \\ i_{3b}(t) \\ v_{c1b}(t) \\ v_{c2b}(t) \end{bmatrix}
+
\begin{bmatrix}
0 & 0 \\
0 & \dfrac{1}{L_2} \\
-\dfrac{1}{C_1} & 0 \\
0 & 0
\end{bmatrix}
\begin{bmatrix} i_{wb}(t) \\ v_{pvb}(t) \end{bmatrix}
$$

Combine the first and the second interval, the following equation is obtained.

$$
\begin{bmatrix} \dfrac{di_2(t)}{dt} \\ \dfrac{di_3(t)}{dt} \\ \dfrac{dv_{c1}(t)}{dt} \\ \dfrac{dv_{c2}(t)}{dt} \end{bmatrix}
=
\begin{bmatrix}
-\dfrac{R_1}{L_1} & 0 & -\dfrac{1}{L_1} & \dfrac{d}{L_1} \\
0 & -\dfrac{(R_2+R_{pv})}{L_2} & 0 & -\dfrac{1}{L_2} \\
\dfrac{1}{C_1} & 0 & 0 & 0 \\
-\dfrac{d}{C_2} & \dfrac{1}{C_2} & 0 & 0
\end{bmatrix}
\begin{bmatrix} i_2(t) \\ i_3(t) \\ v_{c1}(t) \\ v_{c2}(t) \end{bmatrix}
+
\begin{bmatrix}
0 & 0 \\
0 & \dfrac{1}{L_2} \\
-\dfrac{1}{C_1} & 0 \\
0 & 0
\end{bmatrix}
\begin{bmatrix} i_w(t) \\ v_{pv}(t) \end{bmatrix}
$$

Substitute the following equations as perturbation and linearization method.

$$d(t) = D + \hat{d}(t) \qquad for\ A_a$$
$$d'(t) = D' - \hat{d}(t) \qquad for\ A_b$$

$$A_a = \begin{bmatrix} -\dfrac{R_1}{L_1}(D+\hat{d}(t)) & 0 & -\dfrac{(D+\hat{d}(t))}{L_1} & \dfrac{D+\hat{d}(t)}{L_1} \\[2mm] 0 & -\dfrac{(R_2+R_{pv})(D+\hat{d}(t))}{L_2} & 0 & -\dfrac{(D+\hat{d}(t))}{L_2} \\[2mm] \dfrac{D+\hat{d}(t)}{C_1} & 0 & 0 & 0 \\[2mm] \dfrac{-D-\hat{d}(t)}{C_2} & \dfrac{D+\hat{d}(t)}{C_2} & 0 & 0 \end{bmatrix}$$

$$A_b = \begin{bmatrix} -\dfrac{R_1}{L_1}(D'-\hat{d}(t)) & 0 & \dfrac{-D'+\hat{d}(t)}{L_1} & 0 \\[2mm] 0 & -\dfrac{(R_2+R_{pv})(D'-\hat{d}(t))}{L_2} & 0 & \dfrac{-D'+\hat{d}(t)}{L_2} \\[2mm] \dfrac{D'-\hat{d}(t)}{C_1} & 0 & 0 & 0 \\[2mm] 0 & \dfrac{D'-\hat{d}(t)}{C_2} & 0 & 0 \end{bmatrix}$$

Multiply the A_a and A_b with the state vectors

$$x(t) = X + \hat{x}(t)$$

$$\begin{bmatrix} i_2(t) \\ i_3(t) \\ v_{c1}(t) \\ v_{c2}(t) \end{bmatrix} = \begin{bmatrix} I_2 + \hat{i}_2(t) \\ I_3 + \hat{i}_3(t) \\ V_{C1} + \hat{v}_{c1}(t) \\ V_{C2} + \hat{v}_{c2}(t) \end{bmatrix}$$

$$A_a = \begin{bmatrix} -\dfrac{R_1}{L_1}\left(D+\hat{d}(t)\right)\left(I_2+\hat{i}_2(t)\right) - \dfrac{\left(D+\hat{d}(t)\right)\left(V_{C1}+\hat{v}_{c1}(t)\right)}{L_1} + \dfrac{(D+\hat{d}(t))(V_{C2}+\hat{v}_{c2}(t))}{L_1} \\[3mm] -\dfrac{(R_2+R_{pv})\left(D+\hat{d}(t)\right)\left(I_3+\hat{i}_3(t)\right)}{L_2} - \dfrac{(D+\hat{d}(t))(V_{C2}+\hat{v}_{c2}(t))}{L_2} \\[3mm] \dfrac{D+\hat{d}(t)(I_2+\hat{i}_2(t))}{C_1} \\[3mm] \dfrac{(-D-\hat{d}(t))(I_2+\hat{i}_2(t))}{C_2} + \dfrac{(D+\hat{d}(t))(I_3+\hat{i}_3(t))}{C_2} \end{bmatrix}$$

$$A_b = \begin{bmatrix} -\dfrac{R_1}{L_1}\left(D'-\hat{d}(t)\right)\left(I_2+\hat{i}_2(t)\right) + \dfrac{(-D'+\hat{d}(t))(V_{C1}+\hat{v}_{c1}(t))}{L_1} \\[3mm] -\dfrac{(R_2+R_{pv})\left(D'-\hat{d}(t)\right)\left(I_3+\hat{i}_3(t)\right)}{L_2} + \dfrac{(-D'+\hat{d}(t))(V_{C2}+\hat{v}_{c2}(t))}{L_2} \\[3mm] \dfrac{(D'-\hat{d}(t))(I_2+\hat{i}_2(t))}{C_1} \\[3mm] \dfrac{(D'-\hat{d}(t))(I_3+\hat{i}_3(t))}{C_2} \end{bmatrix}$$

$$A = A_a + A_b =$$

$$
\begin{bmatrix}
\frac{1}{L_1}\{-R_1 D I_2 - R_1 D \hat{i}_2(t) - R_1 \hat{d}(t) I_2 - R_1 \hat{d}(t) \hat{i}_2(t) - D V_{C1} - D \hat{v}_{c1}(t) - V_{C1} \hat{d}(t) - \hat{v}_{c1}(t) \hat{d}(t) + D V_{C2} + D \hat{v}_{c2}(t) \\
+ V_{C2} \hat{d}(t) + \hat{v}_{c2}(t) \hat{d}(t) - R_1 I_2 D' - R_1 D' \hat{i}_2(t) + R_1 I_2 \hat{d}(t) + R_1 \hat{i}_2(t) \hat{d}(t) - V_{C1} D' - \hat{v}_{c1}(t) D' + V_{C1} \hat{d}(t) + \hat{v}_{c1}(t) \hat{d}(t)\} \\[6pt]
\frac{1}{L_2}\{-R_2 D I_3 - R_2 \hat{d}(t) I_3 - R_{pv} D I_3 - R_{pv} \hat{d}(t) I_3 - R_2 D \hat{i}_3(t) - R_2 \hat{d}(t) \hat{i}_3(t) - R_{pv} D \hat{i}_3(t) - R_{pv} \hat{d}(t) \hat{i}_3(t) - V_{C2} D \\
- \hat{v}_{c2}(t) D - V_{C2} \hat{d}(t) - \hat{v}_{c2}(t) \hat{d}(t) - R_2 D' I_3 + R_2 \hat{d}(t) I_3 - R_{pv} D' I_3 + R_{pv} \hat{d}(t) I_3 - R_2 D' \hat{i}_3(t) + R_2 \hat{d}(t) \hat{i}_3(t) \\
- R_{pv} D' \hat{i}_3(t) + R_{pv} \hat{d}(t) \hat{i}_3(t) - D' V_{C2} - D' \hat{v}_{c2}(t) + \hat{d}(t) V_{C2} + \hat{d}(t) \hat{v}_{c2}(t)\} \\[6pt]
\frac{1}{C_1}\{D I_2 + D \hat{i}_2(t) + \hat{d}(t) I_2 + \hat{d}(t) \hat{i}_2(t) + D' I_2 + D' \hat{i}_2(t) - \hat{d}(t) I_2 - \hat{d}(t) \hat{i}_2(t)\} \\[6pt]
\frac{1}{C_2}\{-D I_2 - D \hat{i}_2(t) - \hat{d}(t) I_2 - \hat{d}(t) \hat{i}_2(t) + D I_3 + D \hat{i}_3(t) + \hat{d}(t) I_3 + \hat{d}(t) \hat{i}_3(t) \\
+ D' I_3 + D' \hat{i}_3(t) - \hat{d}(t) I_3 - \hat{d}(t) \hat{i}_3(t)\}
\end{bmatrix}
$$

Only first-order AC terms,

$$
\begin{bmatrix}
\frac{1}{L_1}\{-R_1 D \hat{i}_2(t) - R_1 \hat{d}(t) I_2 - D \hat{v}_{c1}(t) - V_{C1} \hat{d}(t) + D \hat{v}_{c2}(t) + V_{C2} \hat{d}(t) \\
- R_1 D' \hat{i}_2(t) + R_1 I_2 \hat{d}(t) + R_1 I_2 \hat{d}(t) - \hat{v}_{c1}(t) D' + V_{C1} \hat{d}(t)\} \\[6pt]
\frac{1}{L_2}\{-R_2 \hat{d}(t) I_3 - R_{pv} \hat{d}(t) I_3 - R_2 D \hat{i}_3(t) - R_{pv} D \hat{i}_3(t) - \hat{v}_{c2}(t) D - V_{C2} \hat{d}(t) + R_2 \hat{d}(t) I_3 \\
+ R_{pv} \hat{d}(t) I_3 - R_2 D' \hat{i}_3(t) - R_2 D' \hat{i}_3(t) - D' V_{C2} + \hat{d}(t) V_{C2}\} \\[6pt]
\frac{1}{C_1}\{D \hat{i}_2(t) + \hat{d}(t) I_2 + D' \hat{i}_2(t) - \hat{d}(t) I_2\} \\[6pt]
\frac{1}{C_2}\{-D \hat{i}_2(t) - \hat{d}(t) I_2 + D \hat{i}_3(t) + \hat{d}(t) I_3 + D' \hat{i}_3(t) - \hat{d}(t) I_3\}
\end{bmatrix}
$$

Rewrite first-order AC terms

$$
\begin{bmatrix}
\frac{1}{L_1}\{-R_1 D \hat{i}_2(t) - D \hat{v}_{c1}(t) + D \hat{v}_{c2}(t) + V_{C2} \hat{d}(t) - R_1 D' \hat{i}_2(t) - \hat{v}_{c1}(t) D'\} \\[6pt]
\frac{1}{L_2}\{-R_2 D \hat{i}_3(t) - R_{pv} D \hat{i}_3(t) - \hat{v}_{c2}(t) D - R_2 D' \hat{i}_3(t) - R_{pv} D' \hat{i}_3(t) - D' V_{C2}\} \\[6pt]
\frac{1}{C_1}\{D \hat{i}_2(t) + D' \hat{i}_2(t)\} \\[6pt]
\frac{1}{C_2}\{-D \hat{i}_2(t) - \hat{d}(t) I_2 + D \hat{i}_3(t) + D' \hat{i}_3(t)\}
\end{bmatrix}
$$

Extract constant terms from the state vectors from A

$$
\underbrace{\begin{bmatrix}
-\dfrac{R_1(D+D')}{L_1} & 0 & \dfrac{-D-D'}{L_1} & \dfrac{D}{L_1} \\[10pt]
0 & \dfrac{-R_2(D+D') - R_{pv}(D+D')}{L_2} & 0 & \dfrac{-D-D'}{L_2} \\[10pt]
\dfrac{D+D'}{C_1} & 0 & 0 & 0 \\[10pt]
-\dfrac{D}{C_2} & \dfrac{D+D'}{C_2} & 0 & 0
\end{bmatrix}}_{\mathbb{A}}
\begin{bmatrix} \hat{i}_2(t) \\ \hat{i}_3(t) \\ \hat{v}_{c1}(t) \\ \hat{v}_{c2}(t) \end{bmatrix}
+ \underbrace{\begin{bmatrix} \dfrac{V_{c2}}{L_1} \\[6pt] 0 \\[6pt] 0 \\[6pt] -\dfrac{I_2}{C_2} \end{bmatrix}}_{\mathbb{B}} [\hat{d}(t)]
$$

Laplace Transform $(s - \mathbb{A}(D))^{-1}\mathbb{B}$

$$(s - \mathbb{A}(D)) = \begin{bmatrix} s + \dfrac{R_1(D + D')}{L_1} & 0 & \dfrac{-D - D'}{L_1} & \dfrac{D}{L_1} \\[3mm] 0 & s + \dfrac{R_2(D + D') + R_{pv}(D + D')}{L_2} & 0 & \dfrac{-D - D'}{L_2} \\[3mm] \dfrac{D + D'}{C_1} & 0 & s & 0 \\[3mm] -\dfrac{D}{C_2} & \dfrac{D + D'}{C_2} & 0 & s \end{bmatrix}$$

$(s - \mathbb{A}(D))^{-1} =$

$$\begin{bmatrix} s\left(s\left(s + \frac{(D+D')R_2 + (D+D')R_{pv}}{L_2}\right) - \frac{(-D'-D)(D+D')}{C_2L_2}\right) & \frac{D(D+D')s}{C_2L_1} & (s-\mathbb{A}(D))^{-1}{}_{13} & \frac{-Ds\left(s + \frac{(D+D')R_2 + (D+D')R_{pv}}{L_2}\right)}{L_1} \\[3mm] \frac{DD's + D^2 s}{C_2L_2} & (s-\mathbb{A}(D))^{-1}{}_{22} & \frac{D'^2 D + 2D'D^2 + D^3}{C_2L_1L_2} & (s-\mathbb{A}(D))^{-1}{}_{24} \\[3mm] (s-\mathbb{A}(D))^{-1}{}_{31} & -\frac{D(D+D')^2}{C_1C_2L_1} & (s-\mathbb{A}(D))^{-1}{}_{33} & \frac{D(D+D')\left(s + \frac{(D+D')R_2 + (D+D')R_{pv}}{L_2}\right)}{C_1L_1} \\[3mm] \frac{Ds\left(s + \frac{(D+D')R_2 + (D+D')R_{pv}}{L_2}\right)}{C_2} & (s-\mathbb{A}(D))^{-1}{}_{42} & (s-\mathbb{A}(D))^{-1}{}_{43} & (s-\mathbb{A}(D))^{-1}{}_{44} \end{bmatrix}$$

$(D'^4 + D^4 + D^3\left(C_2(R_2 + R_{pv}) + C_1(R_1 + R_2 + R_{pv})\right)s + D'^3\left(4D + C_1R_1s + C_2(R_2 + R_{pv})s\right) + C_1C_2s^4L_1L_2 + DC_1C_2s^3(R_2L_1 + R_{pv}L_1 + R_1L_2)$

$+ D^2s^2\left(C_2L_2 + C_1(C_2R_1(R_2 + R_{pv}) + L_1 + L_2)\right) + D'^2\left(6D^2 + 3D\left(C_1R_1 + C_2(R_2 + R_{pv})\right)s + s^2\left(C_1(C_2R_1(R_2 + R_{pv}) + L_1) + C_2L_2\right)\right) +$

$D'(4D^3 + D^2\left(3C_2(R_2 + R_{pv}) + C_1(3R_1 + R_2 + R_{pv})\right)s + 2Ds^2\left(C_1(C_2R_1(R_2 + R_{pv}) + L_1) + C_2L_2\right) + C_1C_2s^3(R_2L_1 + R_{pv}L_1 + R_1L_2)))$

$$(s - \mathbb{A}(D))^{-1}{}_{13} = -\frac{(-D'-D)\left(s\left(s + \frac{(D+D')R_2 + (D+D')R_{pv}}{L_2}\right) - \frac{(-D'-D)(D+D')}{C_2L_2}\right)}{L_1}$$

$$(s - \mathbb{A}(D))^{-1}{}_{22} = s^3 + \frac{D'^2 s + 2DD's + D^2 s}{C_1L_1} + \frac{D^2 s}{C_2L_1} + \frac{D'R_1s^2 + DR_1s^2}{L_1}$$

$$(s - \mathbb{A}(D))^{-1}{}_{24} = -\frac{(-D'-D)\left(s\left(s + \frac{(D+D')R_1}{L_1}\right) - \frac{(-D'-D)(D+D')}{C_1L_1}\right)}{L_2}$$

$$(s - \mathbb{A}(D))^{-1}{}_{31} = -\frac{(D+D')\left(s\left(s + \frac{(D+D')R_2 + (D+D')R_{pv}}{L_2}\right) - \frac{(-D'-D)(D+D')}{C_2L_2}\right)}{C_1}$$

$$(s - \mathbb{A}(D))^{-1}{}_{33} = \left(s^2 + \frac{D^2}{C_2L_1} + \frac{D'R_1s}{L_1} + \frac{DR_1s}{L_1}\right)\left(s + \frac{(D+D')R_2 + (D+D')R_{pv}}{L_2}\right) - \frac{(-D'-D)(D+D')\left(s + \frac{(D+D')R_1}{L_1}\right)}{C_2L_2}$$

$$(s - \mathbb{A}(D))^{-1}{}_{42} = \frac{(D+D')\left(s\left(s + \frac{(D+D')R_1}{L_1}\right) - \frac{(-D'-D)(D+D')}{C_1L_1}\right)}{C_2}$$

$$(s - \mathbb{A}(D))^{-1}{}_{43} = -\frac{(-D'-D)D\left(s + \frac{(D+D')R_2 + (D+D')R_{pv}}{L_2}\right)}{C_2L_1}$$

$$(s - \mathbb{A}(D))^{-1}{}_{44} = \left(s\left(s + \frac{(D+D')R_1}{L_1}\right) - \frac{(-D'-D)(D+D')}{C_1L_1}\right)\left(s + \frac{(D+D')R_2 + (D+D')R_{pv}}{L_2}\right)$$

$$(s - \mathbb{A}(D))^{-1}\mathbb{B} =$$

$$\begin{bmatrix} C_1 s(D'^2 V_{C2} + D^2(V_{C2} - (R_2 + R_{pv})I_2) + D'(2DV_{C2} + C_2(R_2 + R_{pv})sV_{C2} - D(R_2 + R_{pv})I_2) + C_2 s^2 V_{C2} L_2 + Ds(C_2(R_2 + R_{pv})V_{C2} - I_2 L_2)) \\ ((D + D')(2DD'I_2 + D^2 I_2 + DC_1 s(V_{C2} + R_1 I_2) + I_2(D'^2 + D'C_1 R_1 s + C_1 s^2 L_1))) \\ -(((D + D')(D'^2 V_{C2} + D^2(V_{C2} - (R_2 + R_{pv})I_2) + D'(2DV_{C2} + C_2(R_2 + R_{pv})sV_{C2} - D(R_2 + R_{pv})I_2) \\ + C_2 s^2 V_{C2} L_2 + Ds(C_2(R_2 + R_{pv})V_{C2} - I_2 L_2))) \\ ((2DD'I_2 + D^2 I_2 + DC_1 s(V_{C2} + R_1 I_2) + I_2(D'^2 + D'C_1 R_1 s + C_1 s^2 L_1))(D'(R_2 + R_{pv}) + D(R_2 + R_{pv}) + sL_2)) \end{bmatrix}$$

$$\overline{(D'^4 + D^4 + D^3(C_2(R_2 + R_{pv}) + C_1(R_1 + R_2 + R_{pv}))s + D'^3(4D + C_1 R_1 s + C_2(R_2 + R_{pv})s) + C_1 C_2 s^4 L_1 L_2 + DC_1 C_2 s^3(R_2 L_1 + R_{pv}L_1 + R_1 L_2)}$$
$$+ D^2 s^2(C_2 L_2 + C_1(C_2 R_1(R_2 + R_{pv}) + L_1 + L_2)) + D'^2(6D^2 + 3D(C_1 R_1 + C_2(R_2 + R_{pv}))s + s^2(C_1(C_2 R_1(R_2 + R_{pv}) + L_1) + C_2 L_2)) +$$
$$D'(4D^3 + D^2(3C_2(R_2 + R_{pv}) + C_1(3R_1 + R_2 + R_{pv}))s + 2Ds^2(C_1(C_2 R_1(R_2 + R_{pv}) + L_1) + C_2 L_2) + C_1 C_2 s^3(R_2 L_1 + R_{pv}L_1 + R_1 L_2)))$$

The transfer function of $P(s) = \frac{\Delta I_{em}}{\Delta d}$ from the PVCCS circuit can be obtained by selecting

the second term from $(s - \mathbb{A}(D))^{-1}\mathbb{B}$ as follows.

$$\frac{(D' + D)(2D'DI_2 + D^2 I_2 + DC_1 s(V_{c2} + R_1 I_2) + I_2(D'^2 + D'C_1 R_1 s + C_1 s^2 L_1))}{\begin{array}{c}(D'^4 + D^4 + D^3(C_2(R_2 + R_{pv}) + C_1(R_1 + R_2 + R_{pv}))s + D'^3(4D + C_1 R_1 s + C_2(R_2 + R_{pv})s) + C_1 C_2 s^4 L_1 L_2 + DC_1 C_2 s^3(R_2 L_1 + R_{pv}L_1 + R_1 L_2) + \\ D^2 s^2(C_2 L_2 + C_1(C_2 R_1(R_2 + R_{pv}) + L_1 + L_2)) + D'^2(6D^2 + 3D(C_1 R_1 + C_2(R_2 + R_{pv}))s + s^2(C_1(C_2 R_1(R_2 + R_{pv}) + L_1) + C_2 L_2)) + \\ D'(4D^3 + D^2(3C_2(R_2 + R_{pv}) + C_1(3R_1 + R_2 + R_{pv}))s + 2Ds^2(C_1(C_2 R_1(R_2 + R_{pv}) + L_1) + C_2 L_2) + C_1 C_2 s^3(R_2 L_1 + R_{pv}L_1 + R_1 L_2)))\end{array}}$$

From Control Block Diagram
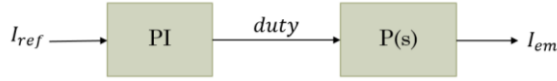
The transfer function of $\frac{\Delta I_{em}}{\Delta I_{ref}}$ is

$$\frac{k(1 + sT)}{sT} \times$$

$$\frac{(D' + D)(2D'DI_2 + D^2 I_2 + DC_1 s(V_{c2} + R_1 I_2) + I_2(D'^2 + D'C_1 R_1 s + C_1 s^2 L_1))}{\begin{array}{c}(D'^4 + D^4 + D^3(C_2(R_2 + R_{pv}) + C_1(R_1 + R_2 + R_{pv}))s + D'^3(4D + C_1 R_1 s + C_2(R_2 + R_{pv})s) + C_1 C_2 s^4 L_1 L_2 + DC_1 C_2 s^3(R_2 L_1 + R_{pv}L_1 + R_1 L_2) + \\ D^2 s^2(C_2 L_2 + C_1(C_2 R_1(R_2 + R_{pv}) + L_1 + L_2)) + D'^2(6D^2 + 3D(C_1 R_1 + C_2(R_2 + R_{pv}))s + s^2(C_1(C_2 R_1(R_2 + R_{pv}) + L_1) + C_2 L_2)) + \\ D'(4D^3 + D^2(3C_2(R_2 + R_{pv}) + C_1(3R_1 + R_2 + R_{pv}))s + 2Ds^2(C_1(C_2 R_1(R_2 + R_{pv}) + L_1) + C_2 L_2) + C_1 C_2 s^3(R_2 L_1 + R_{pv}L_1 + R_1 L_2)))\end{array}}$$

The gain term $\dfrac{k(1+sT)}{sT}$ is in the form according to the gain of the PI Controller in PSIM.

Where k is the gain and T is the time constant.

4.2.2. Parameters

The value of fixed parameters of the PV cell cooperating system are presented in the table below.

Table 4.1 Parameters of the PV cell cooperating system

Parameters	Values
C_1	$6\ F$
C_2	$13.2\ \mu F$
L_1	$10\ mH$
L_2	$7.68\ mH$
R_1	$1\ \Omega$
R_2	$1\ \Omega$
R_{pv}	$5.5486\ \Omega$

The other parameters such as D, V_{c2} or I_2 depend on each operating condition.

4.2.3. Validating the Accuracy of The Transfer Function

The derived transfer function is verified by inputting a signal of the sine wave as a perturbation into the simulating circuit in PSIM to check whether the output is as shown in the Bode diagram of the derived transfer function.

• Bode Magnitude Plot from Transfer Function
• Bode Magnitide Plot from testing FFT of simulation circuit in PSIM
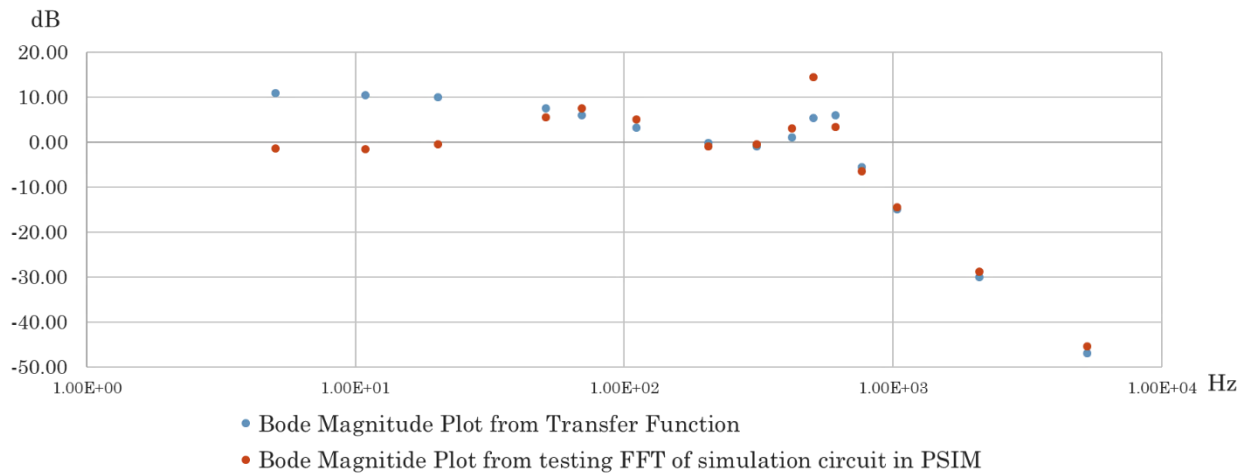
Figure 4.5 Validating result of the derived transfer function

The trend of the Bode plot of both the verifier and the derived transfer function is considered the same in the high-frequency region (>50 Hz). Although, there is an offset error shown from the validation in the low-frequency range (<50 Hz).

The reason for the error might have occurred from the DC terms of the averaged state equations that its value is not zero as same as theoretically. The transfer function is focused on only the first-order AC term and neglected the DC terms and the second-order AC terms. If the value of the DC terms is not zero, then there should be some error caused by this issue.

Another reason might be because of the fluctuation of the operating point in the simulating circuit. Due to the derived transfer function is linearized, therefore there is no influence of the amplitude shown in its plot.

Besides, the derived transfer function might not be correct as the state vector should be defined another way as two separate state vectors because, during the first and second intervals, the circuit is separated apart that the current should not be combined during the averaging method. Another issue, in the derived transfer function, there is an integral term that can cause a very large magnitude in the low-frequency region. The accuracy of the derivation must be considered as well.

4.2.4. Judging System Stability

In order to determine PI controller parameters to improve the stability of the PVCCS, the Bode and Nyquist stability criterion are used to evaluate the system performance by MATLAB. The trial and error method is used to select the PI gains and time constants. The results will be shown in the next part.

4.3. Simulation results

4.3.1. Stability Analysis Results

The test for the proper PI gain (k) and time constant (T) is conducted. The value of k is set to 0.03, 0.06, 0.15 and 0.3; and T is set to 0.001, 0.002, 0.005 and 0.01 respectively. Therefore, there are total 16 cases as follows.

GN1:	GN5:	GN9:	GN13:
T = 0.005 k = 0.03	T = 0.001 k = 0.03	T = 0.002 k = 0.03	T = 0.01 k = 0.03
GN2:	GN6:	GN10:	GN14:
T = 0.005 k = 0.06	T = 0.001 k = 0.06	T = 0.002 k = 0.06	T = 0.01 k = 0.06
GN3:	GN7:	GN11:	GN15:
T = 0.005 k = 0.15	T = 0.001 k = 0.15	T = 0.002 k = 0.15	T = 0.01 k = 0.15
GN4:	GN8:	GN12:	GN16:
T = 0.005 k = 0.3	T = 0.001 k = 0.3	T = 0.002 k = 0.3	T = 0.01 k = 0.3

Bode and Nyquist stability criterions are used to judge the stability. Step response provides information related to the time response of the systems with different gains and time constants.

Among them, there are 8 stable cases, which are GN1, GN2, GN4, GN5, GN9, GN10, GN13 and GN14.

The order of the biggest to the smallest gain margin is GN4, GN5, GN13, GN1, GN9, GN10, GN14 and GN2.

The order of the largest to the tiniest phase margin is GN13, GN1, GN9, GN5, GN14, GN2, GN10 and GN4.

The order of the fastest settling time is GN9, GN5, GN10, GN2, GN1, GN14, GN13 and GN4.

The order of the fastest rise time is GN4, GN10, GN5, GN2, GN9, GN14, GN1, and GN13.

The order of the fastest cases which become steady state is GN5, GN9, GN10, GN2, GN1, GN14, GN13 and GN4.

There are 3 cases with 0% overshoot which are GN1, GN13 and GN14. GN4 produces the largest overshoot with 63.9%. While GN2, GN5, GN9 and GN10 create 0.29%, 9.13%, 2.95% and 10.6% overshoot respectively.

In my opinion, the most proper case is GN5 because it becomes steady state the fastest which is the quality of high responsive. There is 9.13 % overshoot but it is acceptable. It improves 32.2 dB gain margin and 86.7 degrees of phase margin from the plant without PI controller.

The second proper case is GN9 which is very much similar to the GN5 but the time constant is doubled. It comes the second in the fastest steady state time but its settling time is the fastest. It produces lower overshoot with only 2.95%. It improves 27.81 dB gain margin and 93.9 degrees of phase margin from the plant without PI controller.
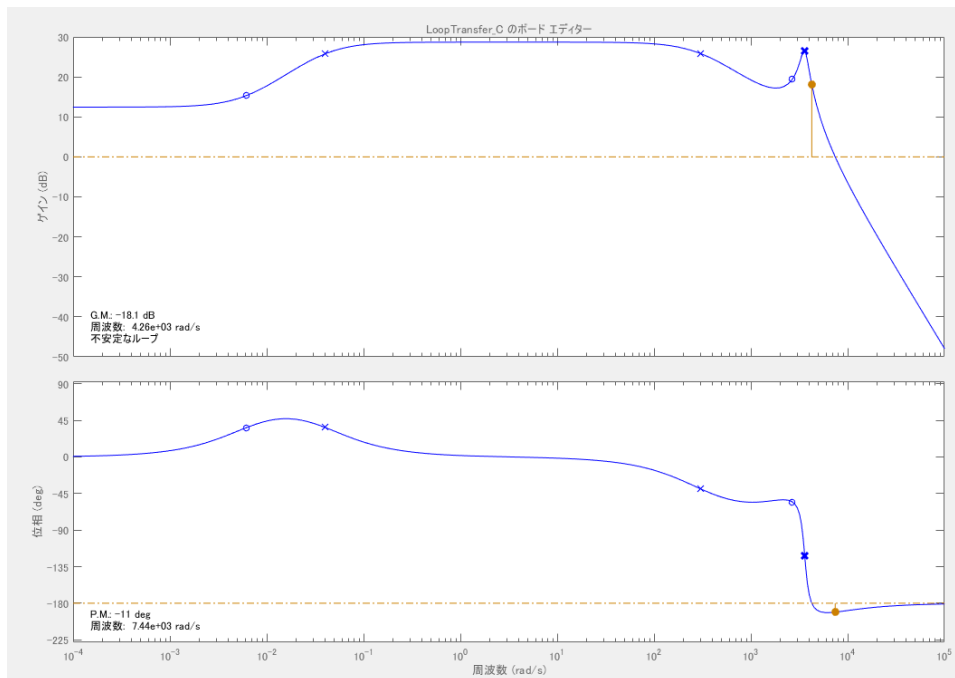
Figure 4.6 Bode Diagram of the plant without PI controller
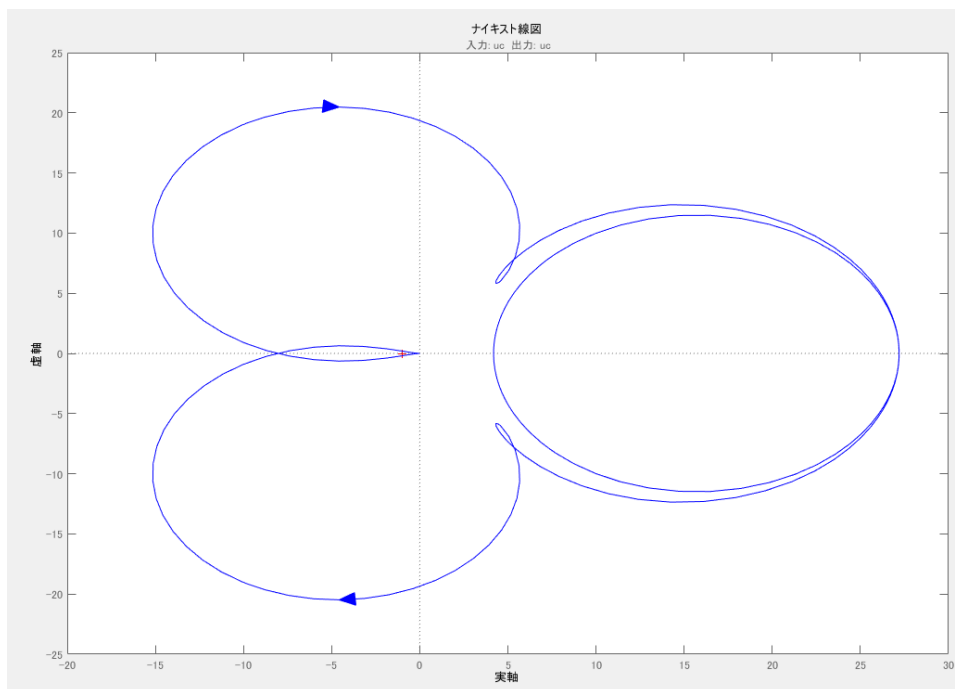
Figure 4.7 Nyquist Diagram of the plant without PI controller

43
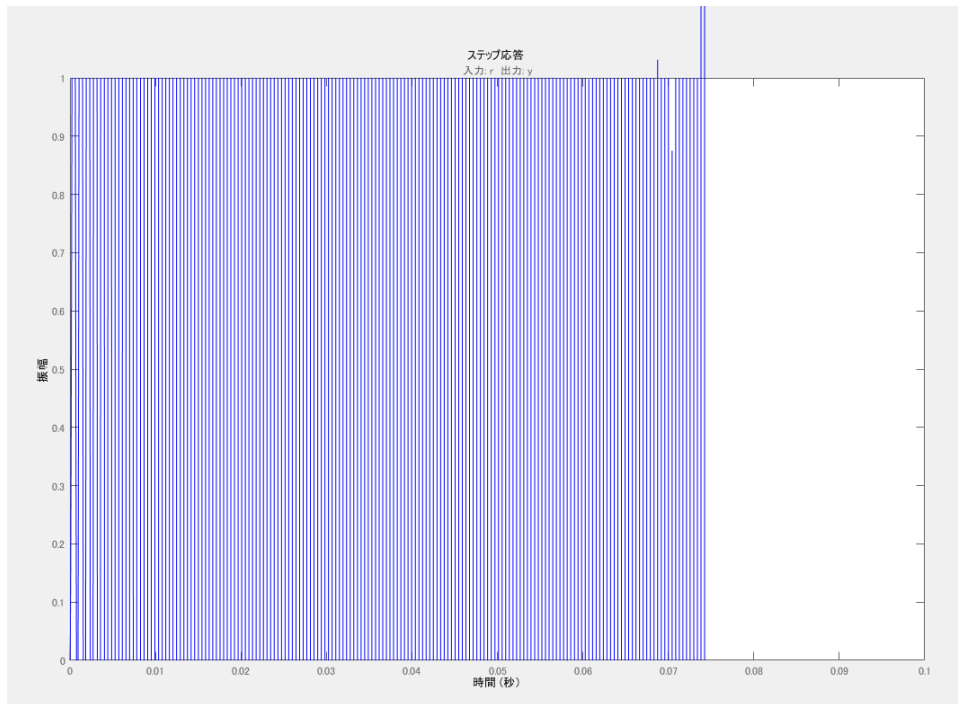
Figure 4.8 Step Response of the plant without PI controller

Stability Analysis Result: Case 1

GN1: T = 0.005 k = 0.03

D = 0.69208456

$I_2 = 4.19\,A$

$V_{C2} = 156.5\,V$

G.M. = 11.2 dB at 4.17e+03 rad/s or 663.676 Hz

P.M. = 105 deg at 193 rad/s or 30.717 Hz

Stable

Peak Response = 1

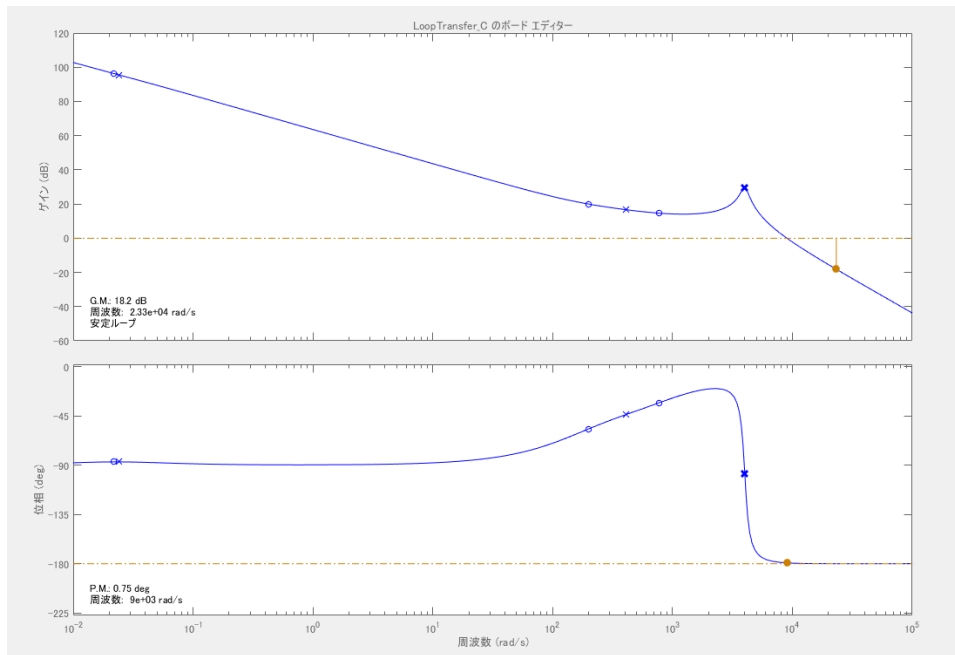Settling Time = 0.0307 s

Rise Time = 0.0155 s

Steady State = 0.06 s
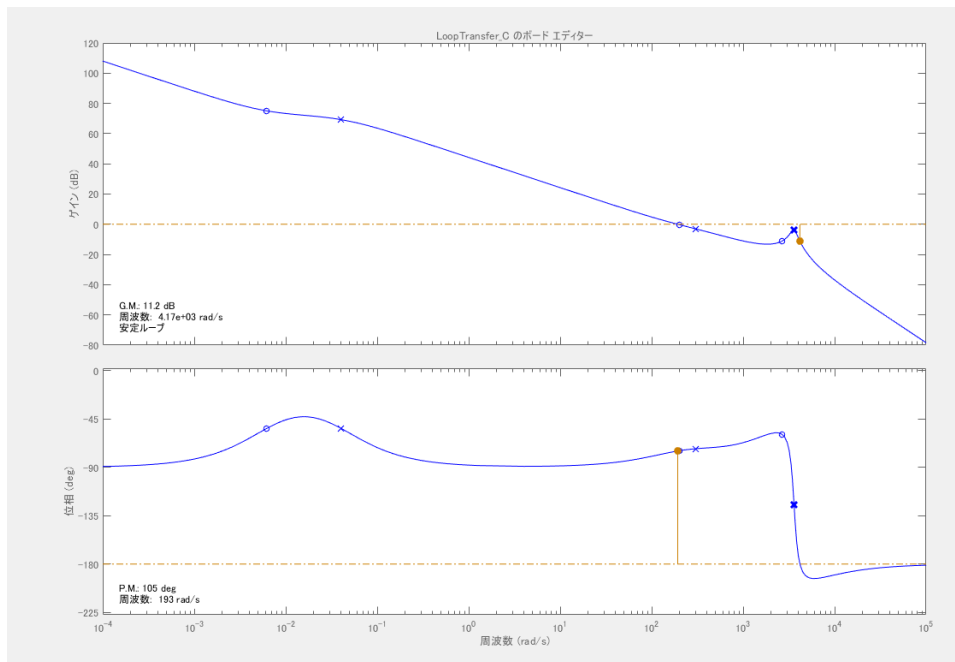
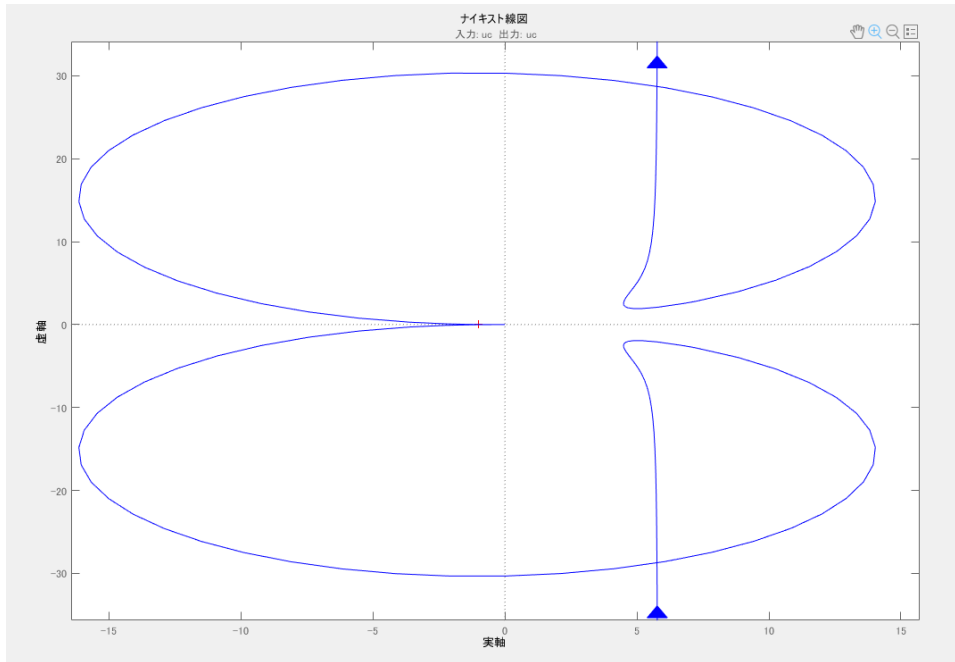Figure 4.9 Bode Diagram of the plant with PI controller parameter T = 0.005 k = 0.03
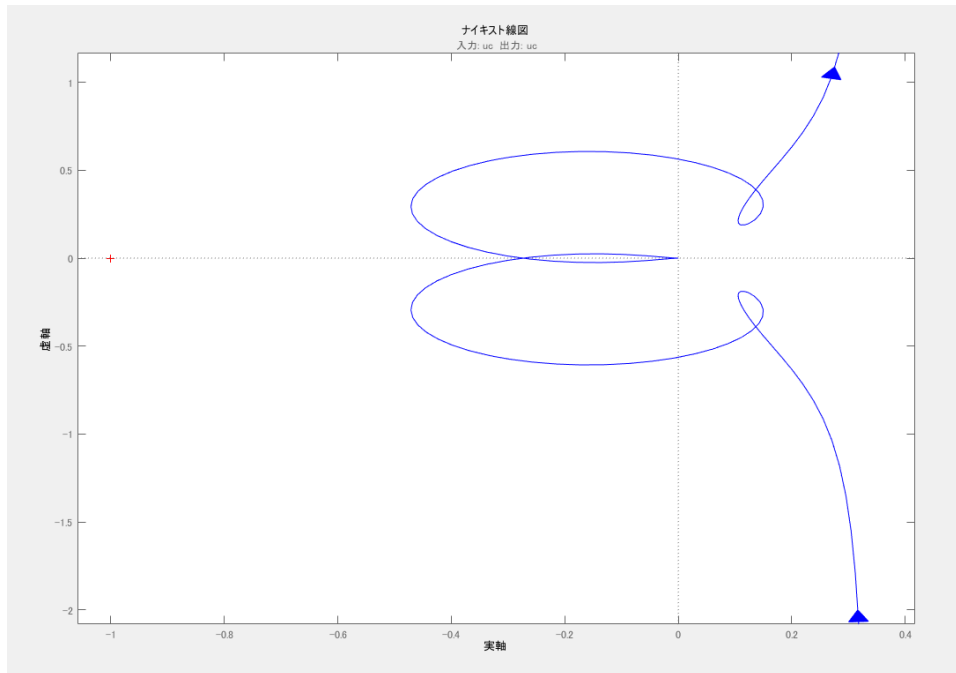
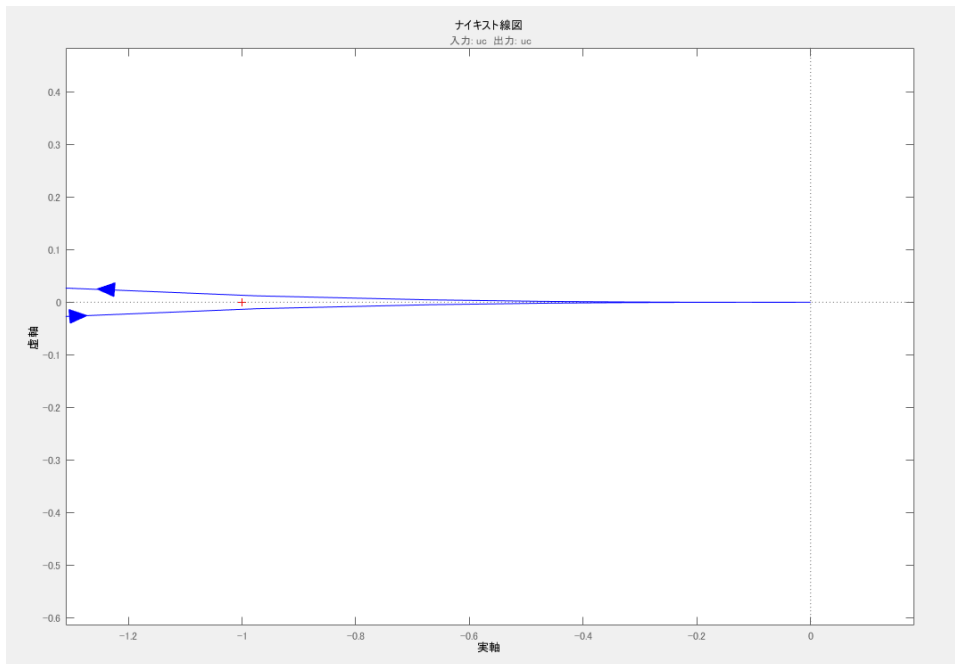Figure 4.10 Nyquist Diagram of the plant with PI controller parameter
T = 0.005 k = 0.03
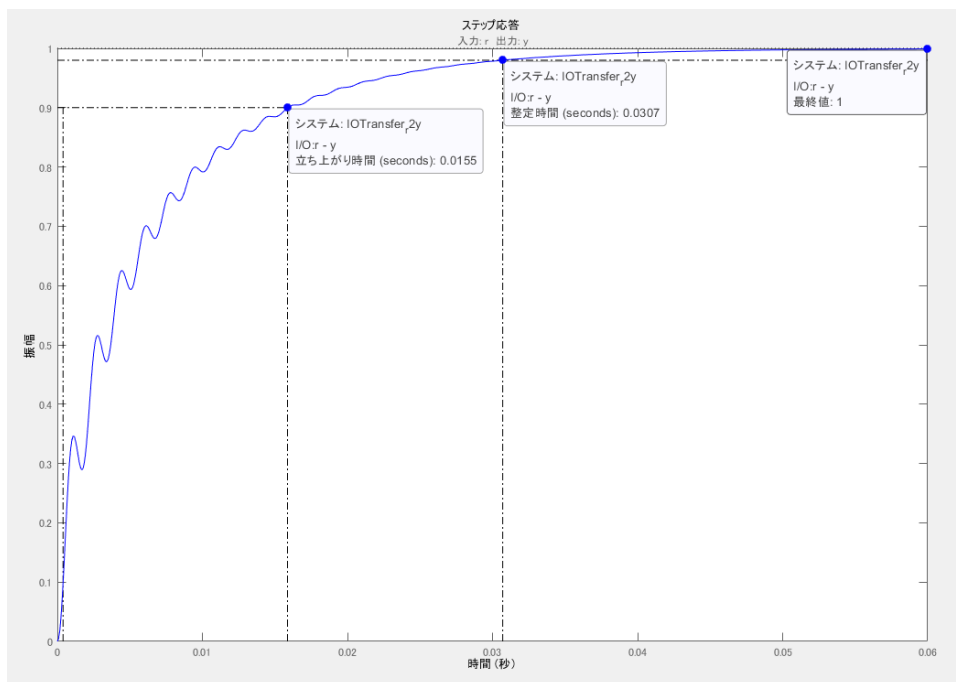
Figure 4.11 Step response of the plant with PI controller parameter T = 0.005 k = 0.03

Stability Analysis Result: Case 2

GN2: T = 0.005 k = 0.06

D = 0.70044457

$I_2 = 4.319118\ A$

$V_{C2} = 158.7667\ V$

G.M. = 5 dB at 4.19e+03 rad/s or 666.8592 Hz

P.M. = 22 deg at 3.85e+03 rad/s or 612.7465 Hz

Stable

Peak Response = 1 at 0.0233 s with 0.29 % overshoot

Settling Time = 0.0227 s

Rise Time = 0.00522 s

Steady State = 0.04 s
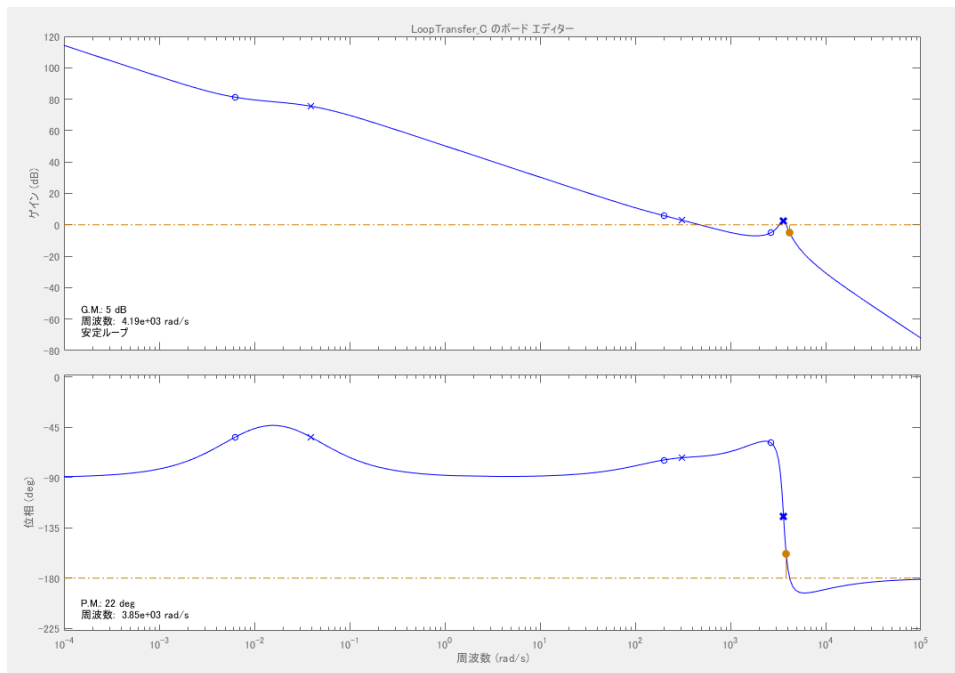
Figure 4.12 Bode Diagram of the plant with PI controller parameter T = 0.005 k = 0.06
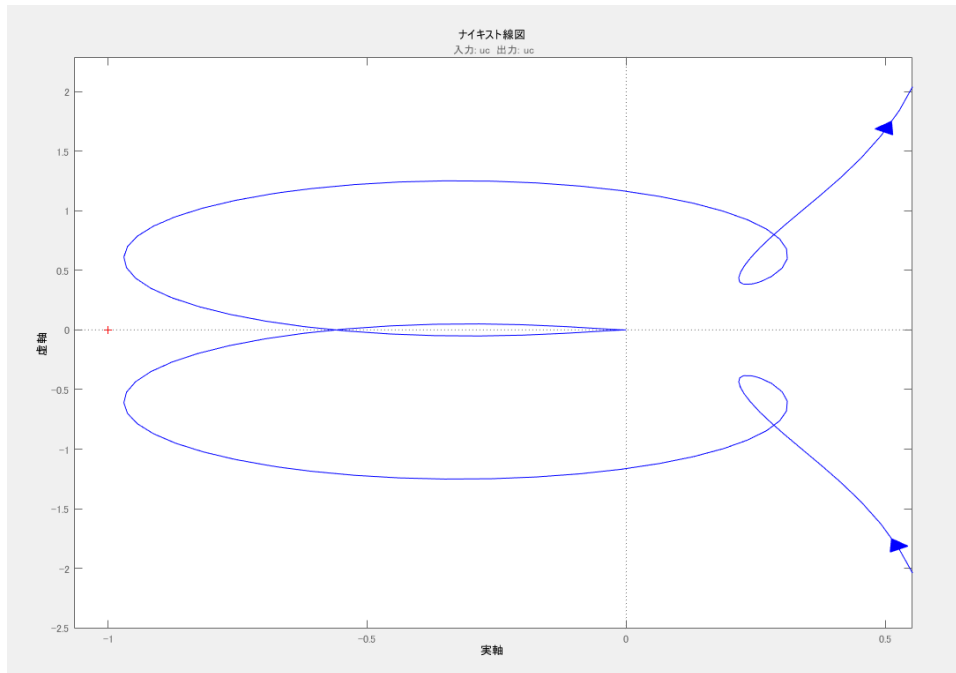
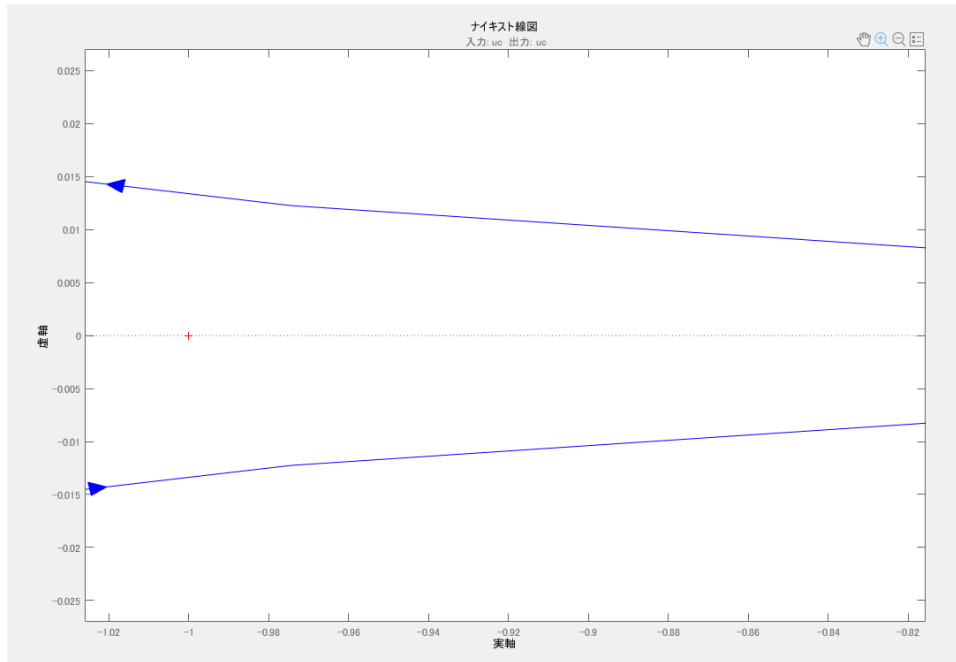Figure 4.13 Nyquist Diagram of the plant with PI controller parameter
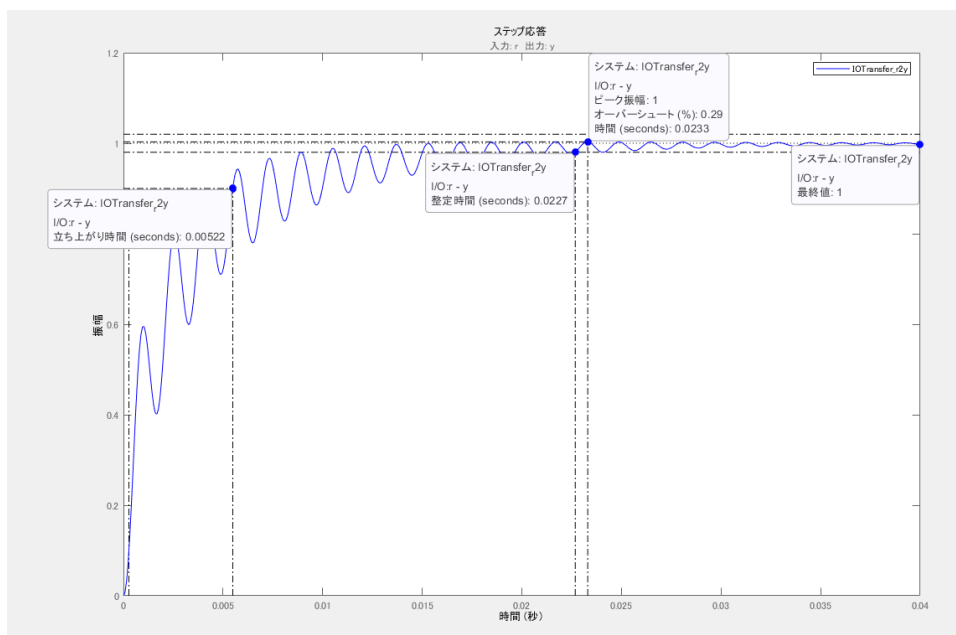
T = 0.005 k = 0.06

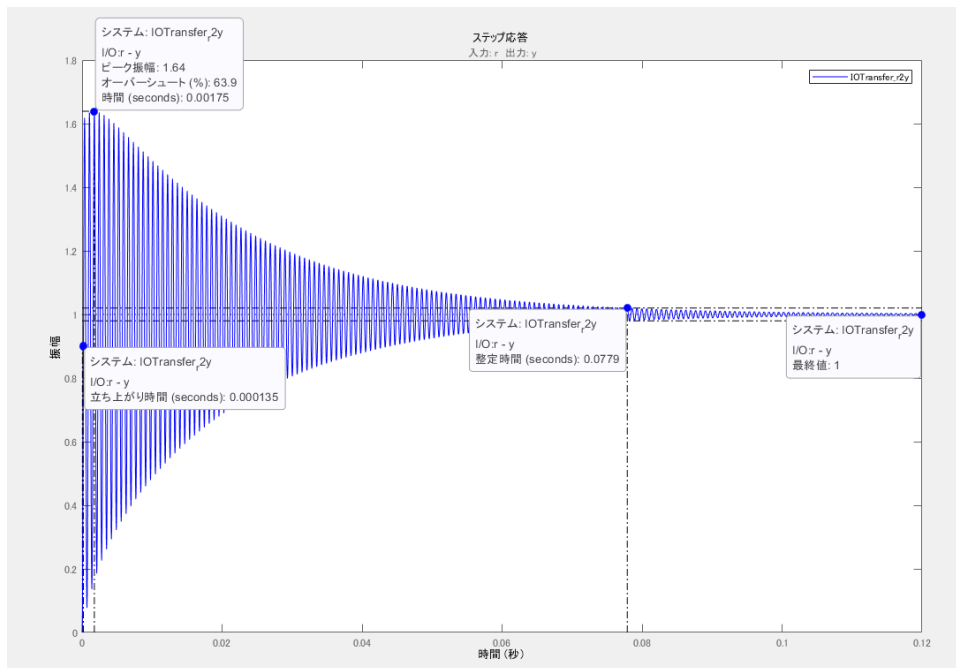

Figure 4.14 Step response of the plant with PI controller parameter T = 0.005 k = 0.06

Stability Analysis Result: Case 3

GN3: T = 0.005 k = 0.15

D = 0.70708403

$I_2 = 4.375\ A$

$V_{C2} = 158.81864\ V$

G.M. = -3.03 dB at 4.2e+03 rad/s or 668.4508 Hz

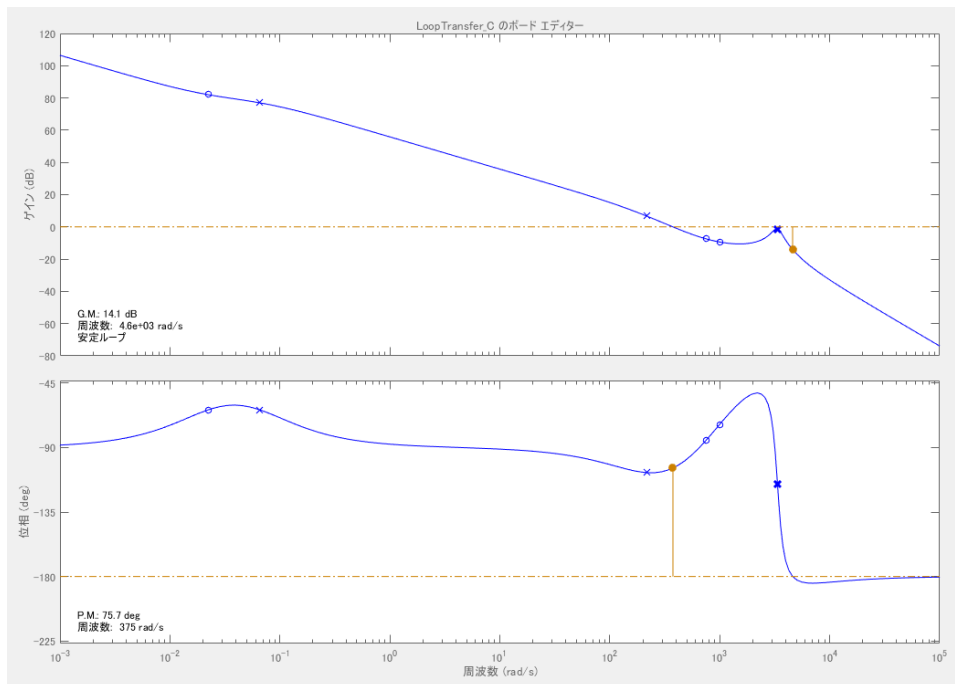P.M. = -6.46 deg at 4.46e+03 rad/s or 709.8310 Hz

Unstable
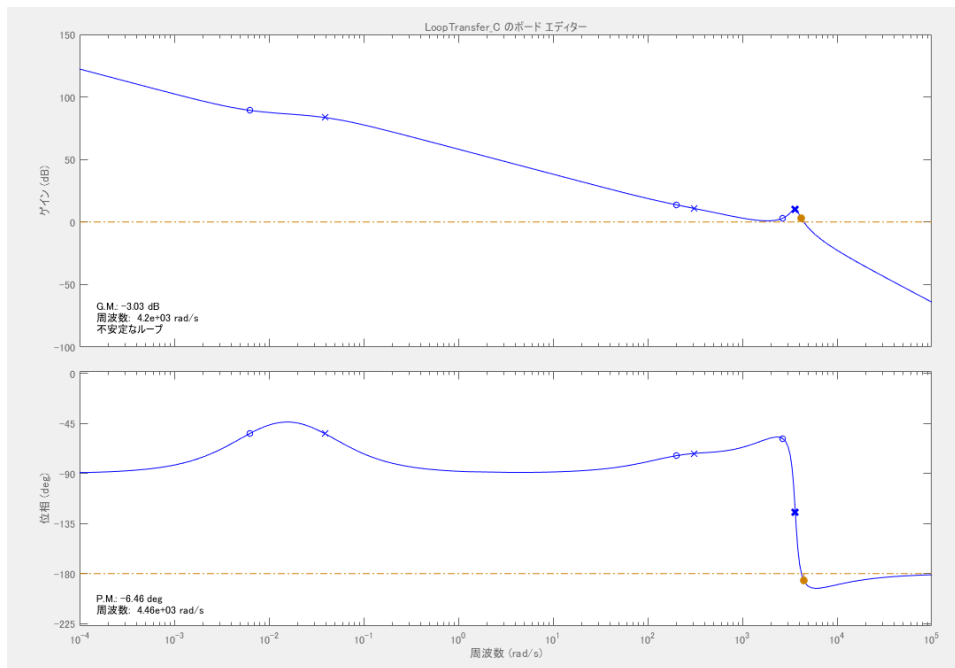
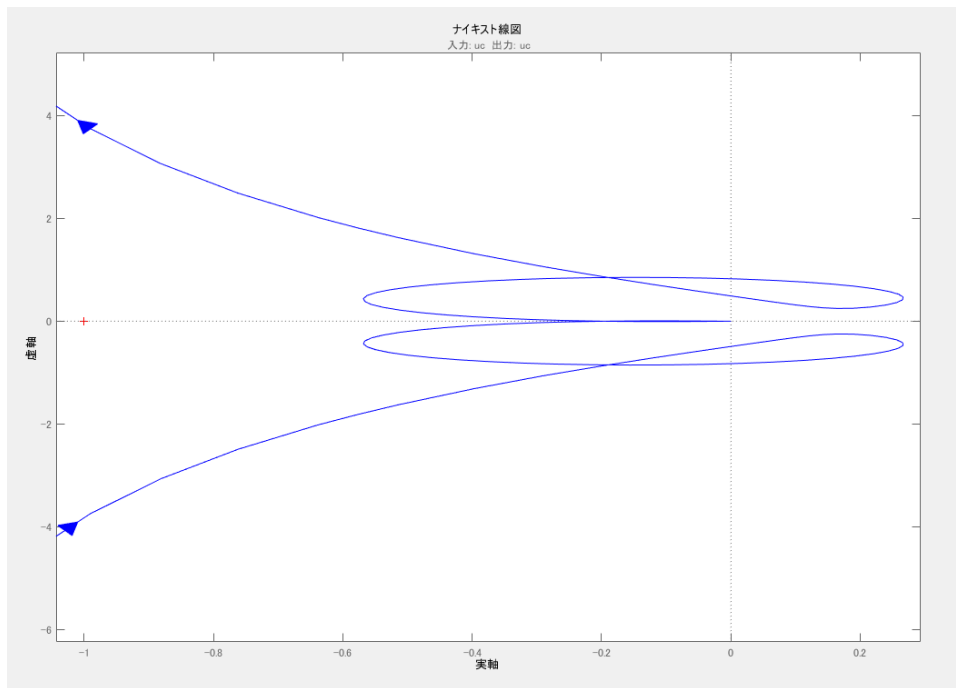Figure 4.15 Bode Diagram of the plant with PI controller parameter T = 0.005 k = 0.15
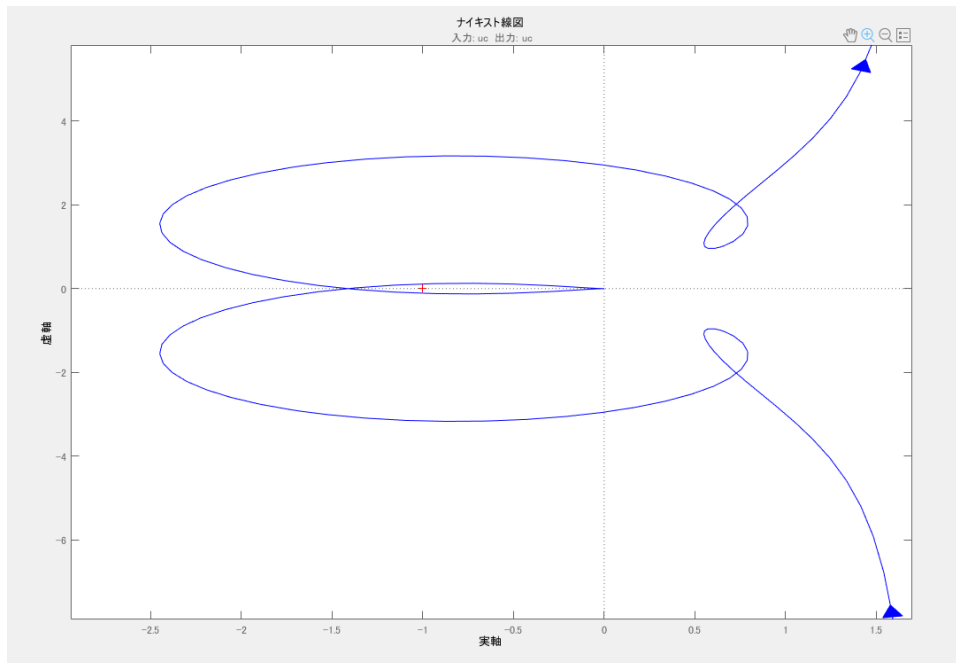
Figure 4.16 Nyquist Diagram of the plant with PI controller parameter
T = 0.005 k = 0.15
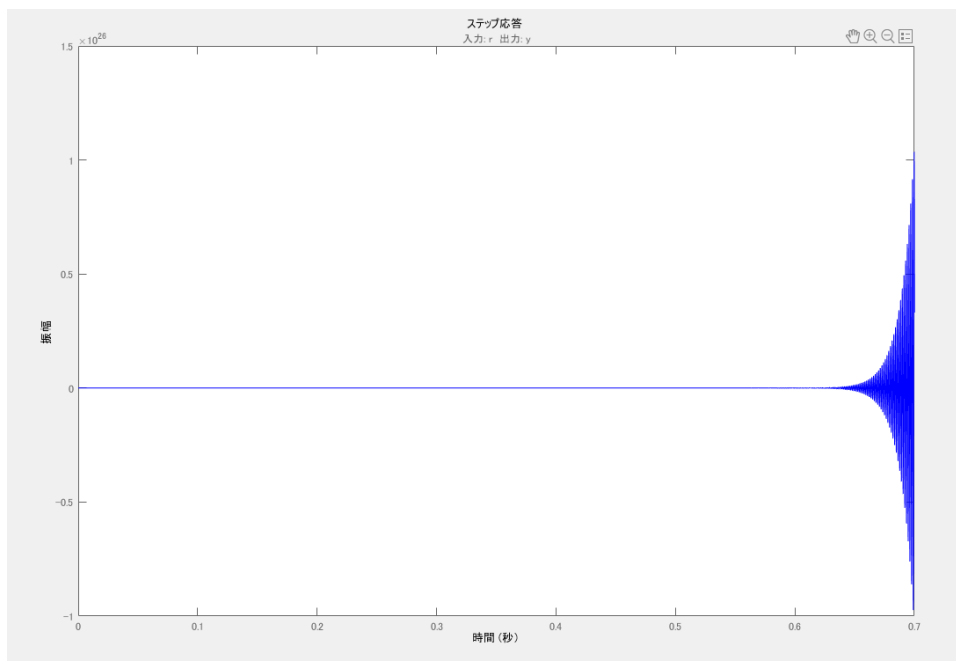
Figure 4.17 Step response of the plant with PI controller parameter T = 0.005 k = 0.15

Stability Analysis Result: Case 4

GN4: T = 0.005 k = 0.3

D = 0.95

$I_2 = 22.577093\,A$

$V_{C2} = 159.08088\,V$

G.M. = 18.2 dB at 2.33e+04 rad/s or 3,708.3102 Hz

P.M. = 0.75 deg at 9e+03 rad/s or 1,432.3945 Hz

Stable

Peak Response = 1.64 at 0.00175 s with 63.9 % overshoot

Settling Time = 0.0779 s

Rise Time = 0.000135 s

Steady State = 0.12 s

Figure 4.18 Bode Diagram of the plant with PI controller parameter T = 0.005 k = 0.3

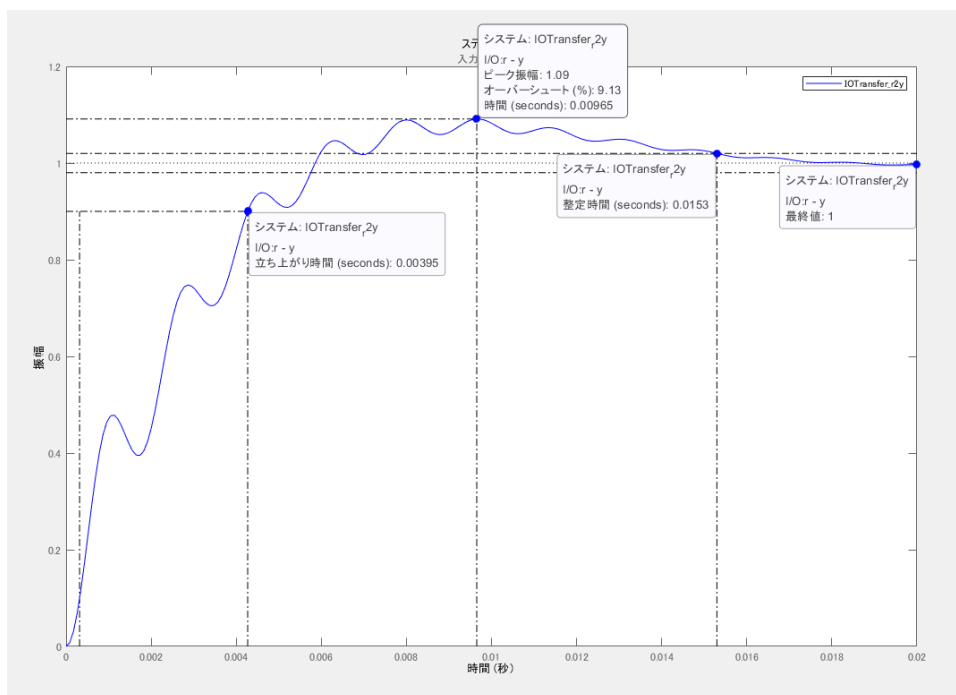Figure 4.19 Nyquist Diagram of the plant with PI controller parameter
T = 0.005 k = 0.3 (1)
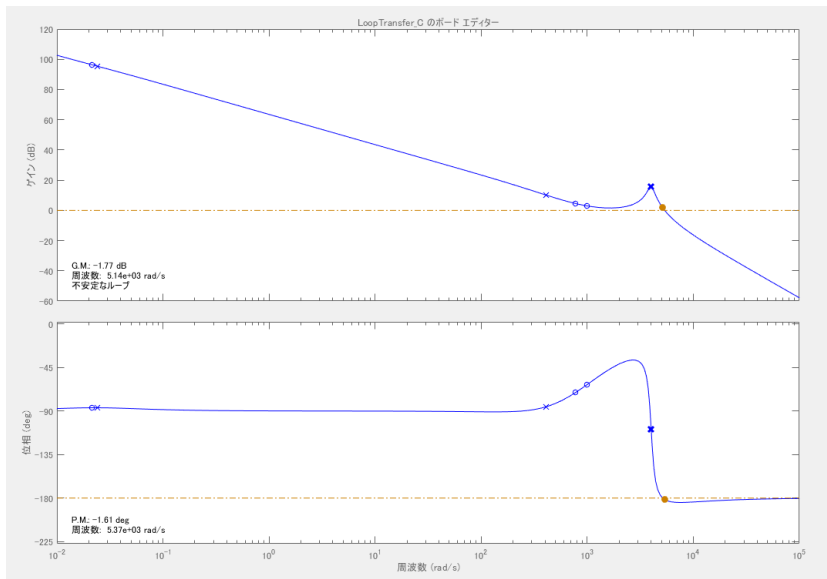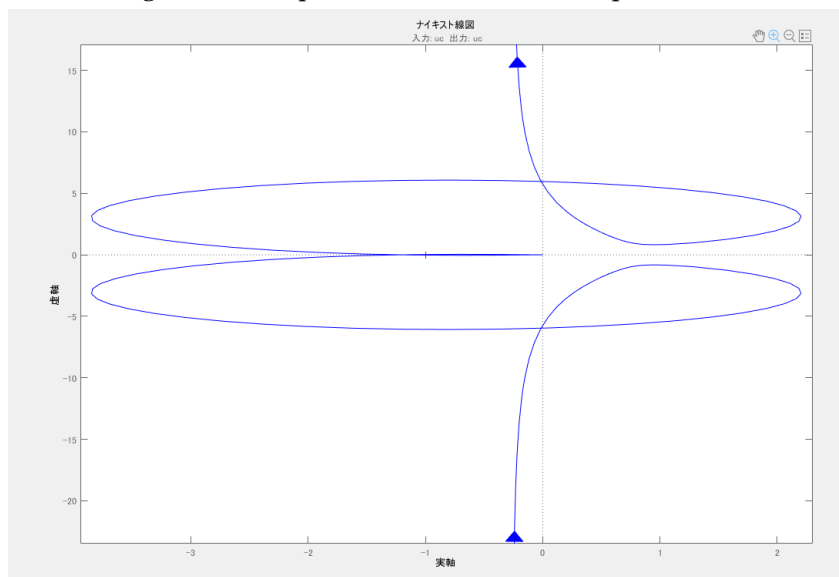

Figure 4.20 Nyquist Diagram of the plant with PI controller parameter
T = 0.005 k = 0.3 (2)

Figure 4.21 Nyquist Diagram of the plant with PI controller parameter

T = 0.005 k = 0.3 (3)

Figure 4.22 Step response of the plant with PI controller parameter T = 0.005 k = 0.3

Stability Analysis Result: Case 5

GN5: T = 0.001 k = 0.03

D = 0.48399361

$I_2 = 7.0024154\ A$

$V_{C2} = 93.896211\ V$

G.M. = 14.1 dB at 4.6e+03 rad/s or 732.1127 Hz

P.M. = 75.7 deg at 375 rad/s or 59.6831 Hz

Stable

Peak Response = 1.09 at 0.00965 s with 9.13 % overshoot

Settling Time = 0.0153 s

Rise Time = 0.00395 s

Steady State = 0.02 s

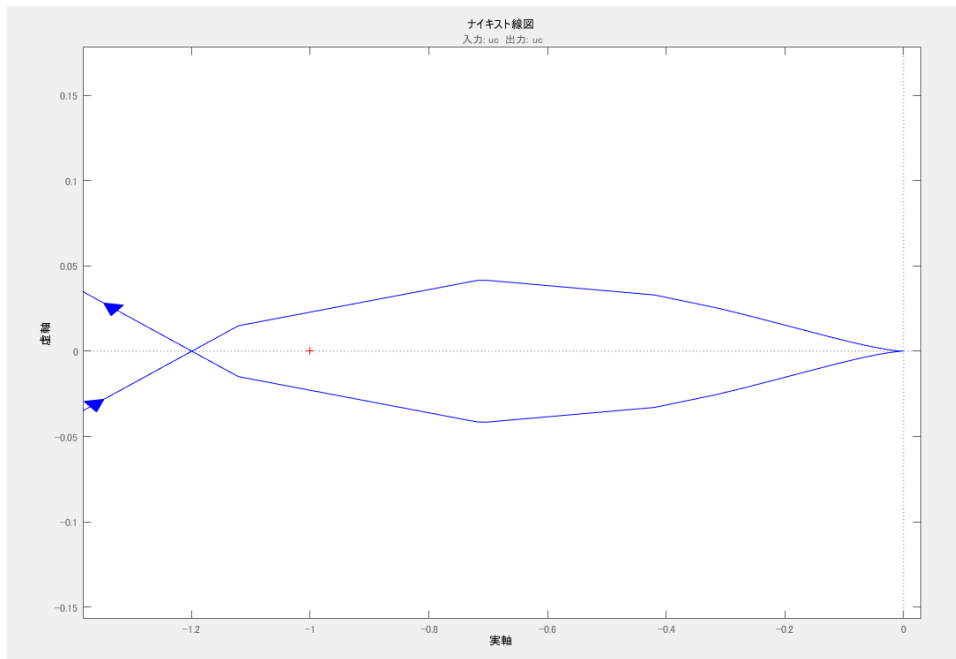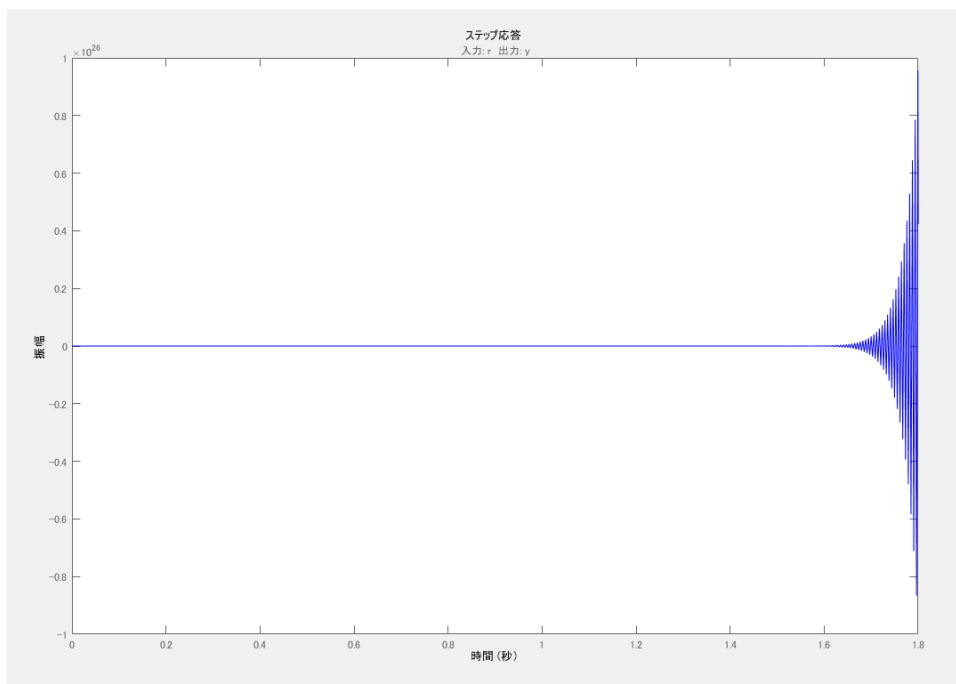Figure 4.23 Bode Diagram of the plant with PI controller parameter T = 0.001 k = 0.03

Figure 4.24 Nyquist Diagram of the plant with PI controller parameter
T = 0.001 k = 0.03

Figure 4.25 Step response of the plant with PI controller parameter T = 0.001 k = 0.03

GN6: T = 0.001 k = 0.06

D = 0.95

$I_2 = 22.286907\ A$

$V_{C2} = 159.03269\ V$

G.M. = -1.77 dB at 5.14e+03 rad/s or 818.0564 Hz

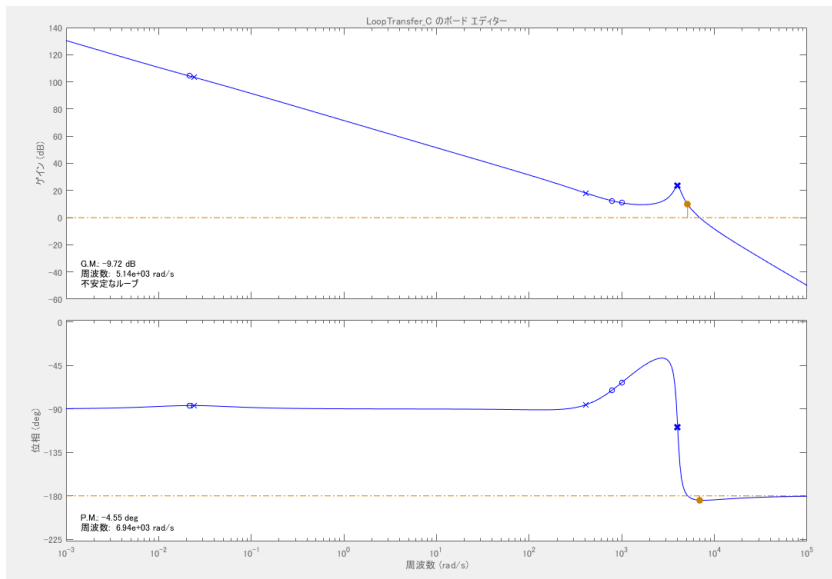P.M. = -1.61 deg at 5.37e+03 rad/s or 854.6620 Hz

Unstable

Figure 4.26 Bode diagram of the plant with PI controller parameter T = 0.001 k = 0.06
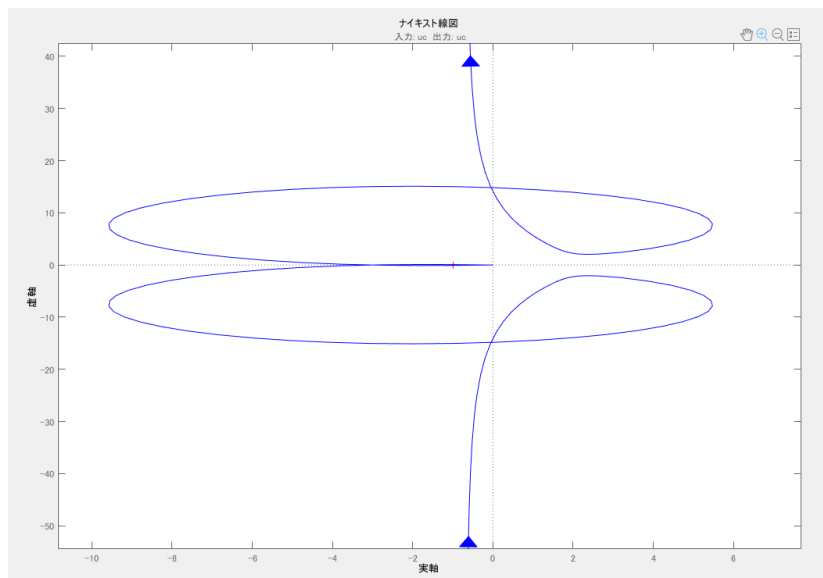

Figure 4.27 Nyquist diagram of the plant with PI controller parameter
T = 0.001 k = 0.06 (1)

Figure 4.28 Nyquist diagram of the plant with PI controller parameter
T = 0.001 k = 0.06 (2)

Figure 4.29 Step response of the plant with PI controller parameter T = 0.001 k = 0.06

Stability Analysis Result: Case 7

GN7: T = 0.001 k = 0.15

D = 0.95

$I_2 = 22.181625\ A$

$V_{C2} = 159.00977\ V$

G.M. = -9.72 dB at 5.14e+03 rad/s or 818.0564 Hz

P.M. = -4.55 deg at 6.94e+03 rad/s or 1,104.5353 Hz

Unstable

Figure 4.30 Bode diagram of the plant with PI controller parameter T = 0.001 k = 0.15

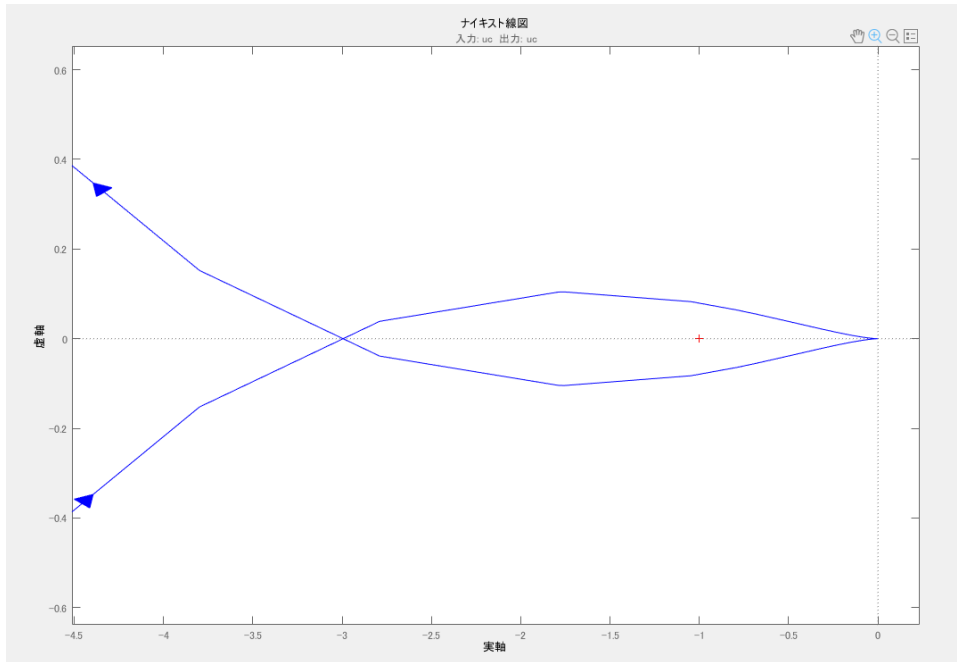Figure 4.31 Nyquist diagram of the plant with PI controller parameter

T = 0.001 k = 0.15 (1)

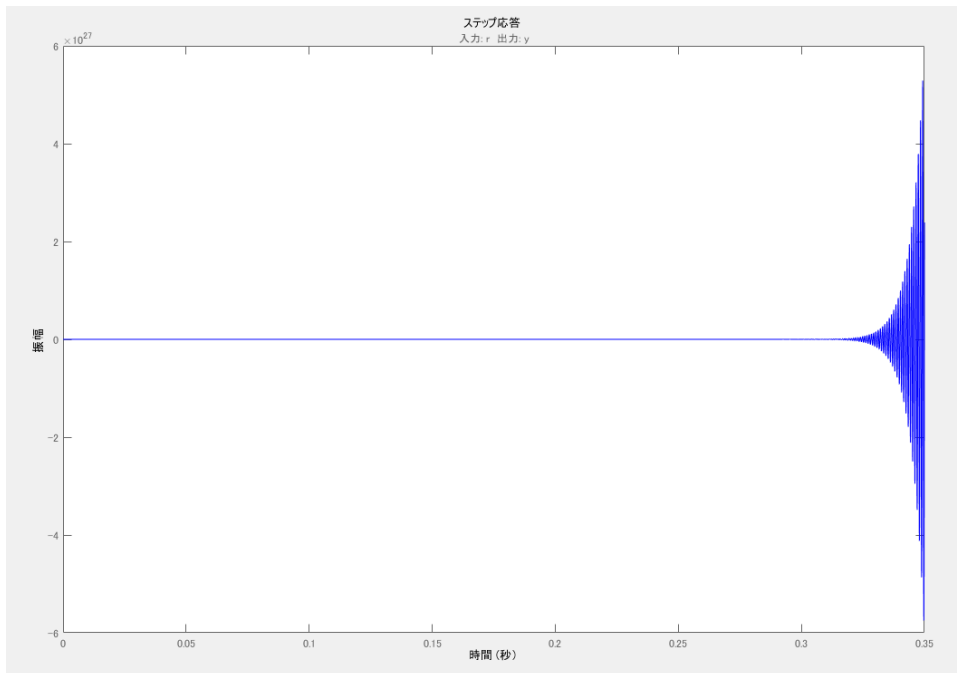Figure 4.32 Nyquist diagram of the plant with PI controller parameter
T = 0.001 k = 0.15 (2)

Figure 4.33 Step response of the plant with PI controller parameter T = 0.001 k = 0.15

Stability Analysis Result: Case 8

GN8: T = 0.001 k = 0.3

D = 0.95

$I_2 = 22.147104\ A$

$V_{C2} = 159.00897\ V$

G.M. = -15.7 dB at 5.14e+03 rad/s or 818.0564 Hz

P.M. = -4.41 deg at 8.95e+03 rad/s or 1,424.4367 Hz

Unstable
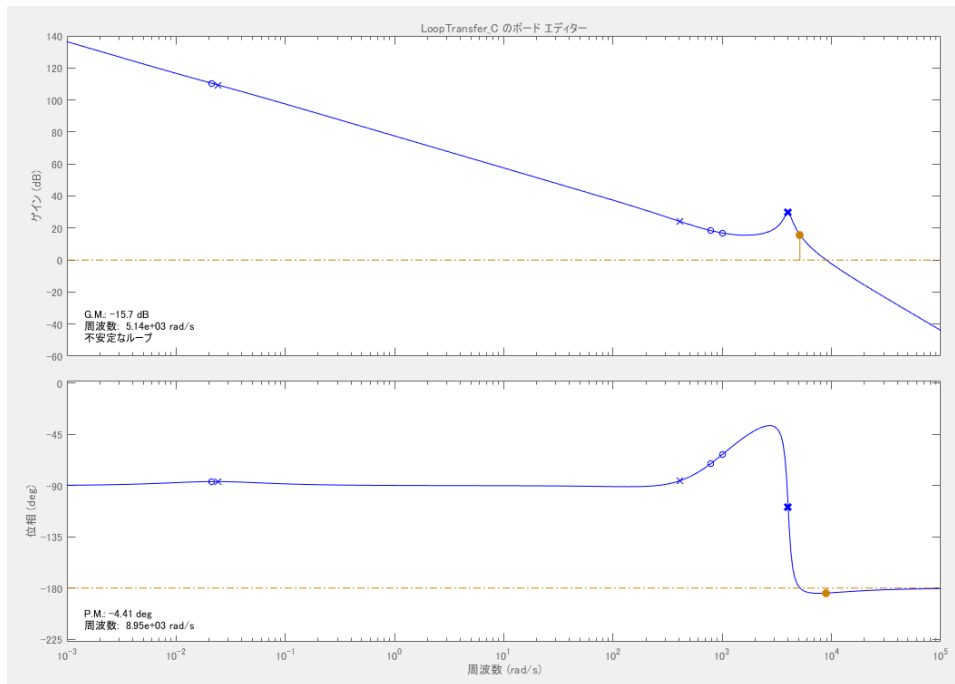

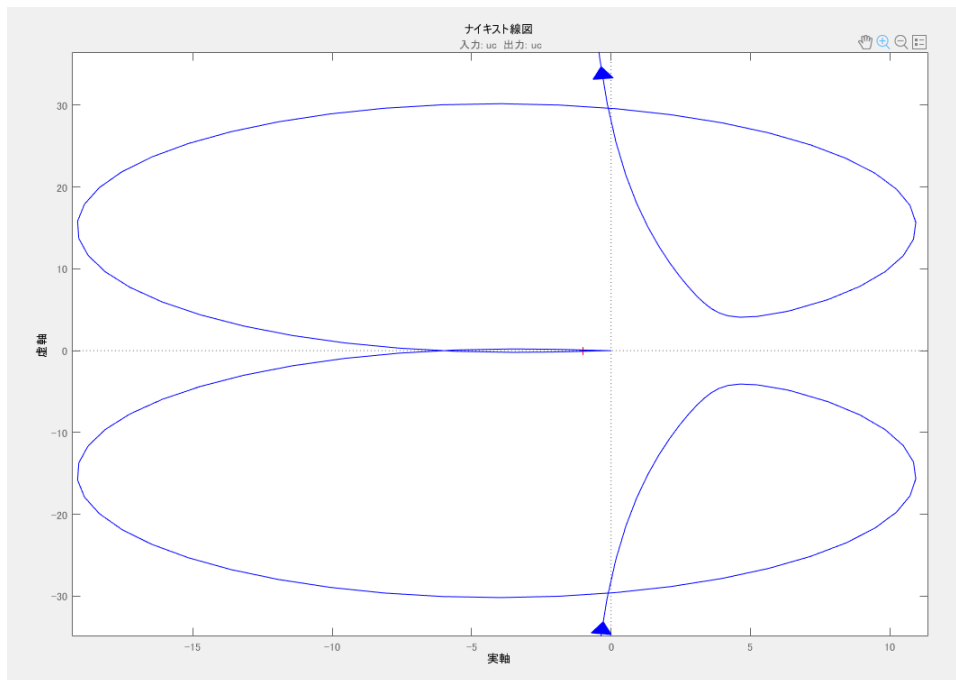Figure 4.34 Bode diagram of the plant with PI controller parameter T = 0.001 k = 0.3

Figure 4.35 Nyquist diagram of the plant with PI controller parameter
T = 0.001 k = 0.3 (1)

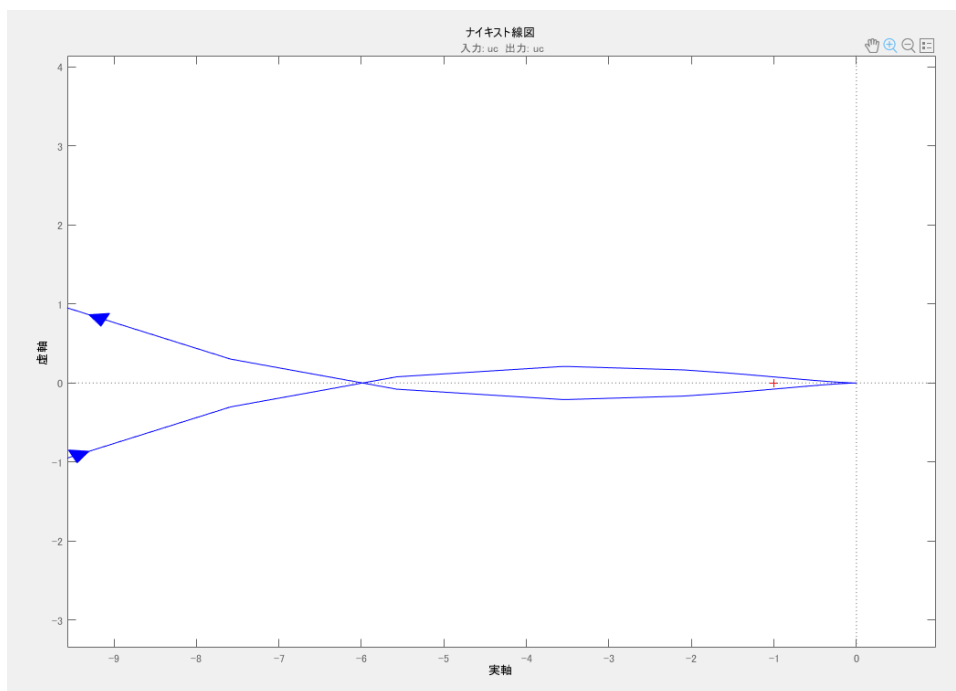

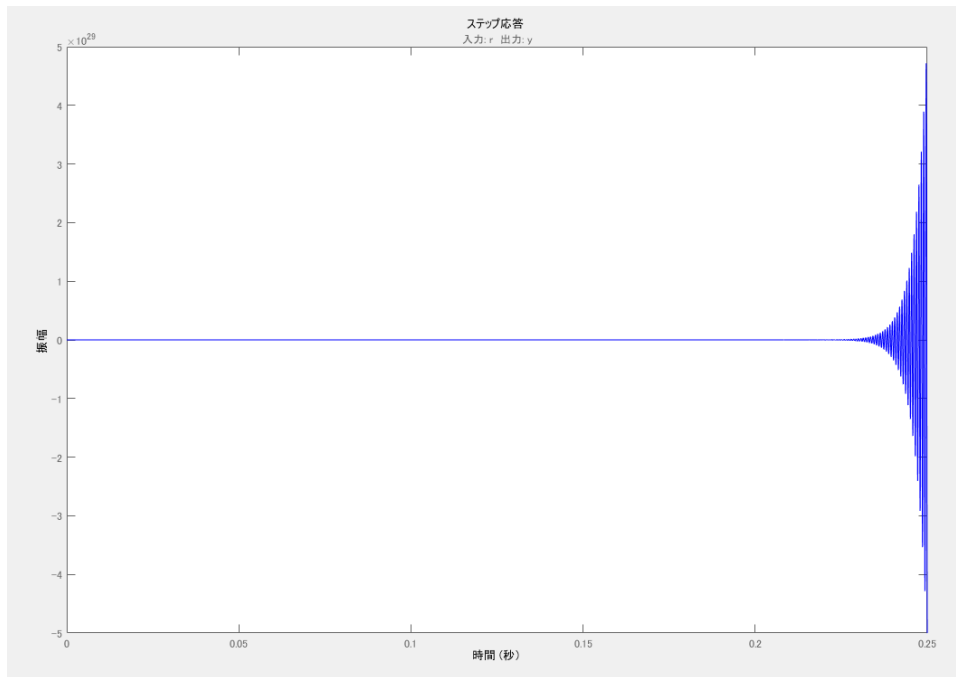Figure 4.36 Nyquist diagram of the plant with PI controller parameter
T = 0.001 k = 0.3 (2)

61

Figure 4.37 Step response of the plant with PI controller parameter T = 0.001 k = 0.3

Stability Analysis Result: Case 9

GN9: T = 0.002 k = 0.03

D = 0.70267176

$I_2 = 4.3262431\ A$

$V_{C2} = 156.52491\ V$

G.M. = 9.71 dB at 4.1e+03 rad/s or 652.5353 Hz

P.M. = 82.9 deg at 336 rad/s or 53.4761 Hz

Stable

Peak Response = 1.03 at 0.011 s with 2.95 % overshoot

Settling Time = 0.0145 s

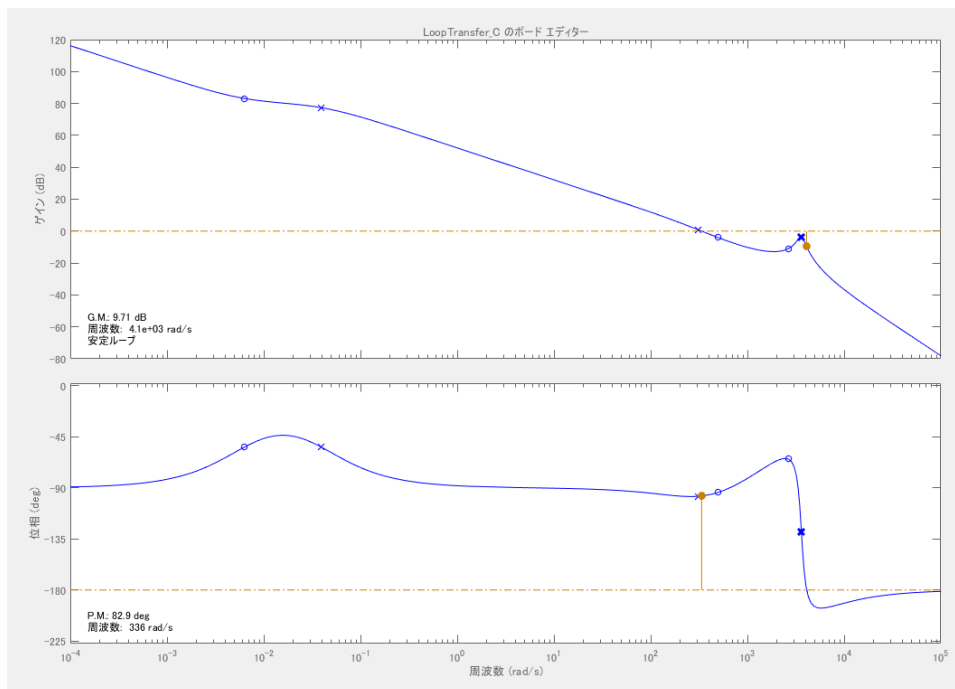Rise Time = 0.0053 s

Steady State = 0.025 s

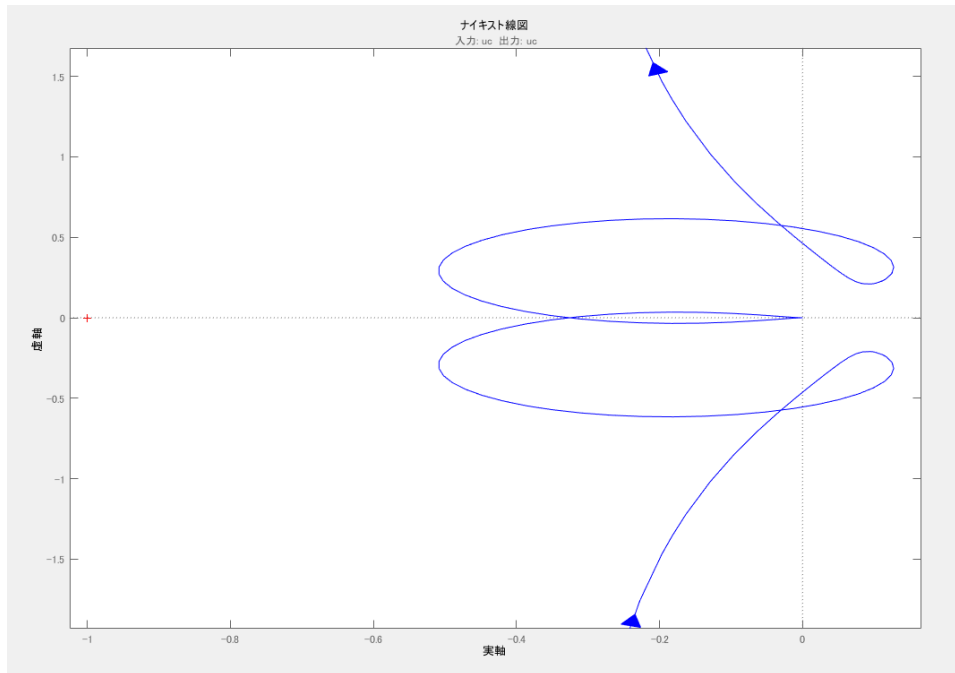Figure 4.38 Bode diagram of the plant with PI controller parameter T = 0.002 k = 0.03

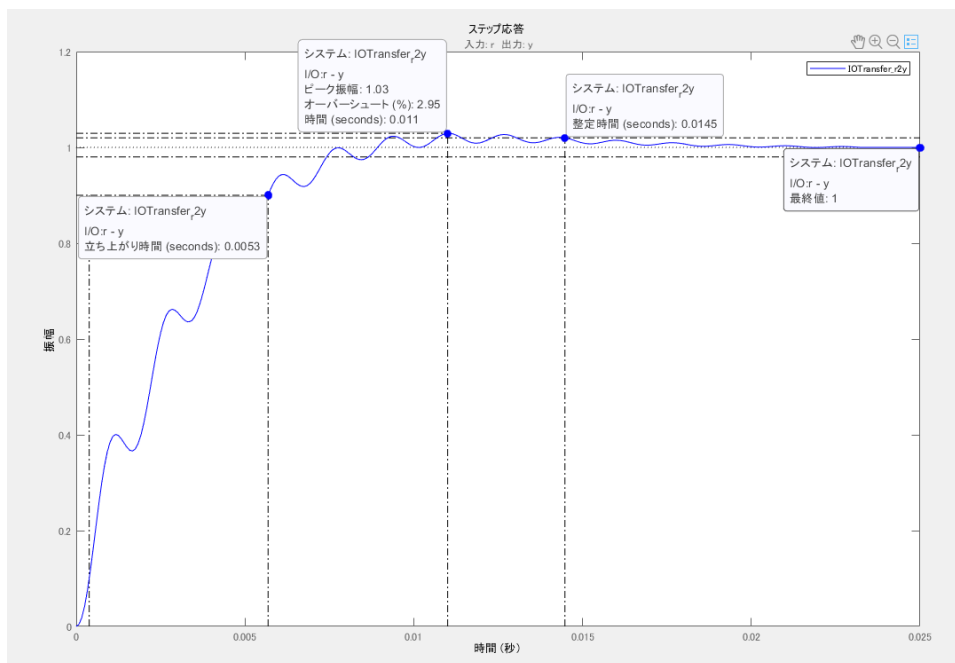Figure 4.39 Nyquist diagram of the plant with PI controller parameter T = 0.002 k = 0.03

Figure 4.40 Step response of the plant with PI controller parameter T = 0.002 k = 0.03

Stability Analysis Result: Case 10

GN10: T = 0.002 k = 0.06

D = 0.66267026

$I_2 = 5.1814049\ A$

$V_{C2} = 136.32745\ V$

G.M. = 6.03 dB at 4.31e+03 rad/s or 685.9578 Hz

P.M. = 21.4 deg at 3.85e+03 rad/s or 612.7465 Hz

Stable

Peak Response = 1.11 at 0.00726 s with 10.6 % overshoot

Settling Time = 0.017 s

Rise Time = 0.00219 s

Steady State = 0.035 s

Figure 4.41 Bode diagram of the plant with PI controller parameter T = 0.002 k = 0.06

Figure 4.42 Nyquist diagram of the plant with PI controller parameter T = 0.002 k = 0.06

Figure 4.43 Step response of the plant with PI controller parameter T = 0.002 k = 0.06

66

GN11: T = 0.002 k = 0.15

D = 0.95

$I_2 = 22.262077\,A$

$V_{C2} = 159.02849\,V$

G.M. = -1.55 dB at 6.54e+03 rad/s or 1,040.8733 Hz

P.M. = -0.447 deg at 6.93e+03 rad/s or 1,102.9438 Hz

Unstable

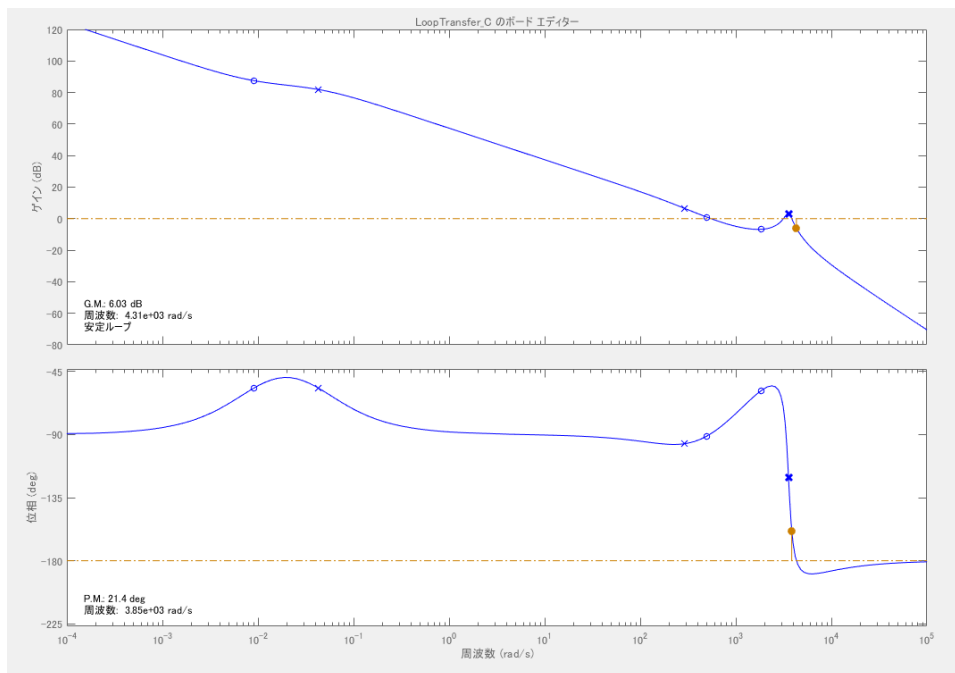Figure 4.44 Bode diagram of the plant with PI controller parameter T = 0.002 k = 0.15

Figure 4.45 Nyquist diagram of the plant with PI controller parameter
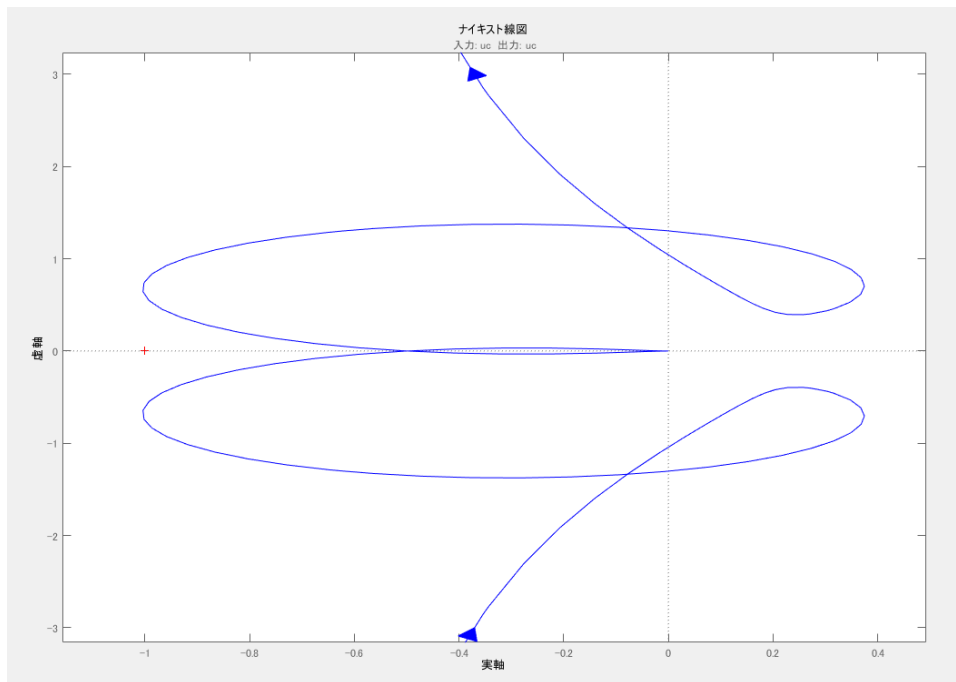T = 0.002 k = 0.15 (1)

Figure 4.46 Nyquist diagram of the plant with PI controller parameter
T = 0.002 k = 0.15 (2)

68

Figure 4.47 Step response of the plant with PI controller parameter T = 0.002 k = 0.15

GN12: T = 0.002 k = 0.3

D = 0.95

$I_2 = 22.245713\ A$

$V_{C2} = 159.02571\ V$

G.M. = -7.58 dB at 6.54e+03 rad/s or 1,040.8733 Hz

P.M. = -1.21 deg at 8.95e+03 rad/s or 1,424.4367 Hz

Unstable

Figure 4.48 Bode diagram of the plant with PI controller parameter T = 0.002 k = 0.3

Figure 4.49 Nyquist diagram of the plant with PI controller parameter
T = 0.002 k = 0.3 (1)

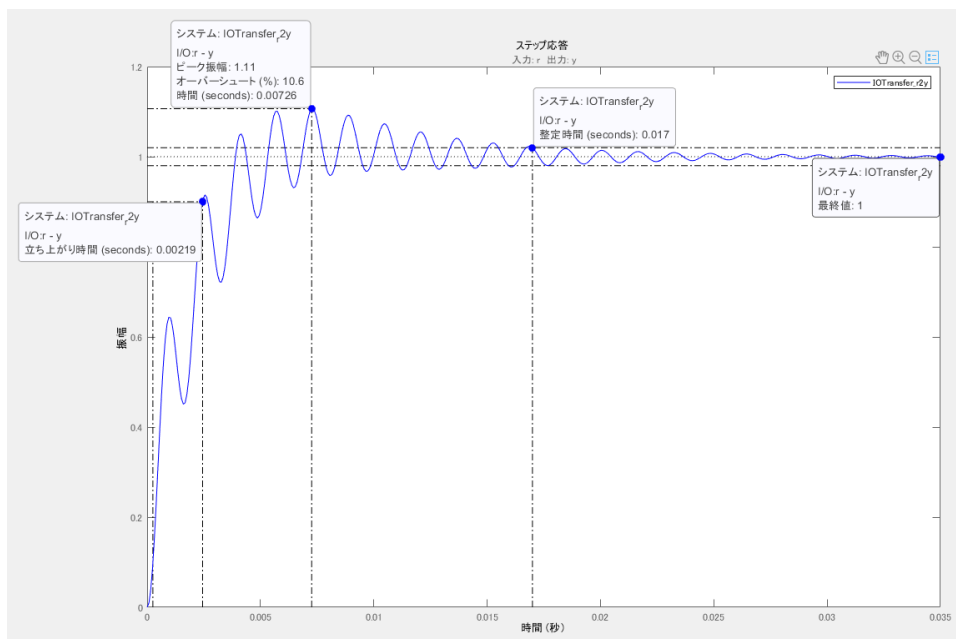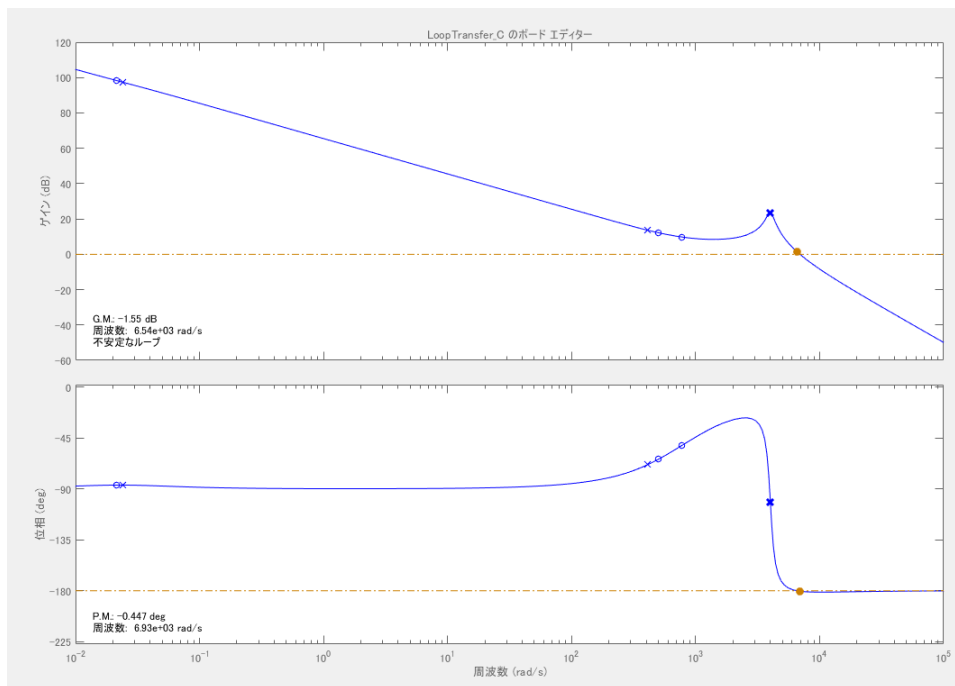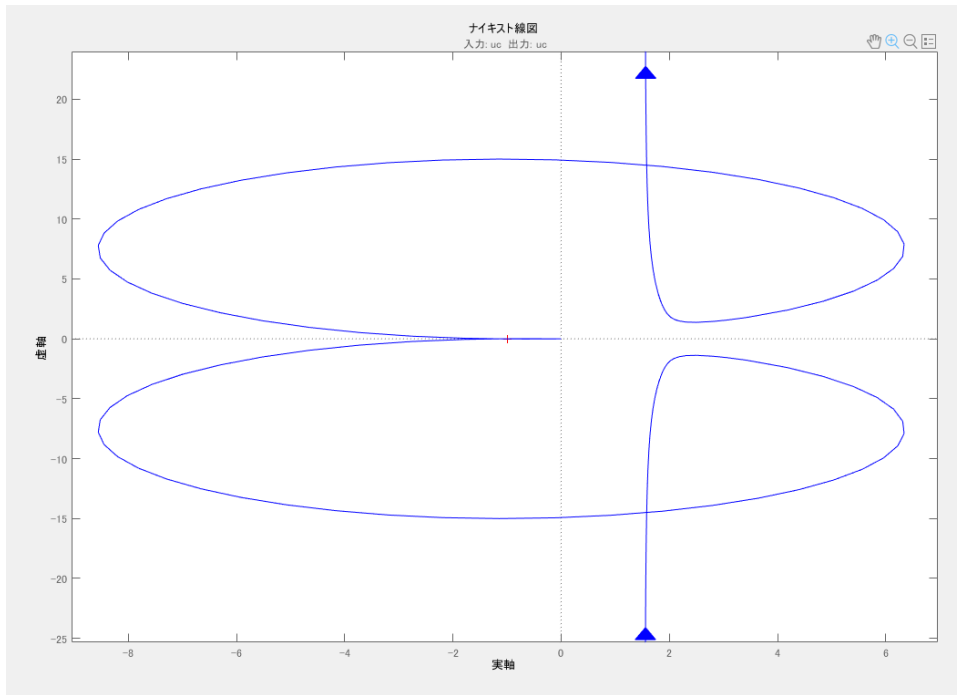Figure 4.50 Nyquist diagram of the plant with PI controller parameter
T = 0.002 k = 0.3 (2)

71

Figure 4.51 Step response of the plant with PI controller parameter T = 0.002 k = 0.3

Stability Analysis Result: Case 13

GN13: T = 0.01 k = 0.03

D = 0.69187785

$I_2 = 4.15\,A$

$V_{C2} = 156.22893\,V$

G.M. = 11.7 dB at 4.21e+03 rad/s or 670.0423 Hz

P.M. = 121 deg at 118 rad/s or 18.7803 Hz

Stable

Peak Response = 0.995 at 0.1 s with 0% overshoot

Settling Time = 0.0687 s

Rise Time = 0.035 s

Steady State = 0.1 s

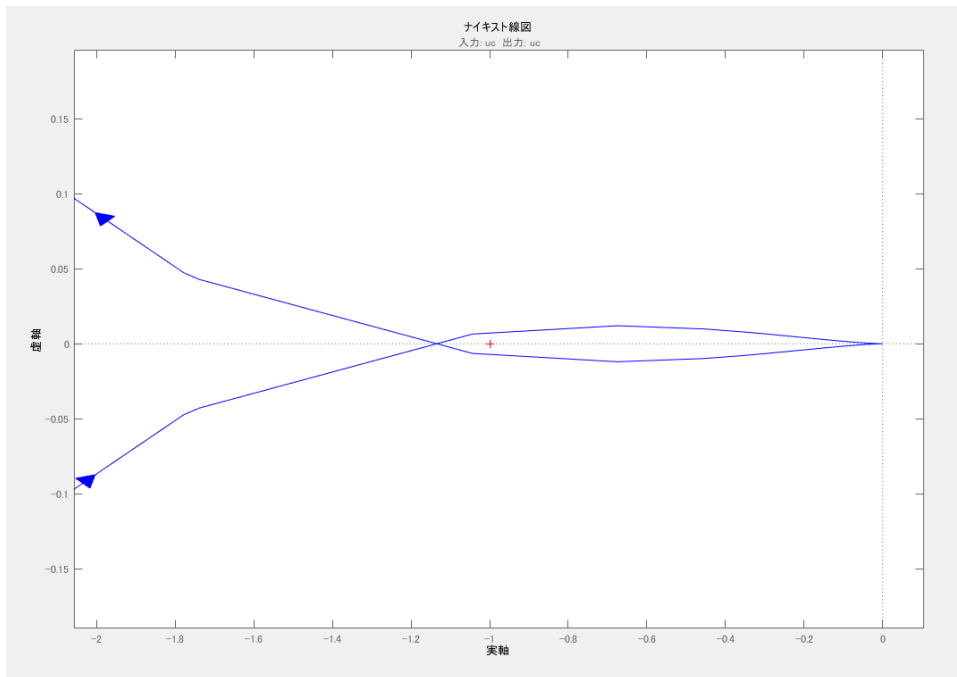Figure 4.52 Bode diagram of the plant with PI controller parameter T = 0.01 k = 0.03

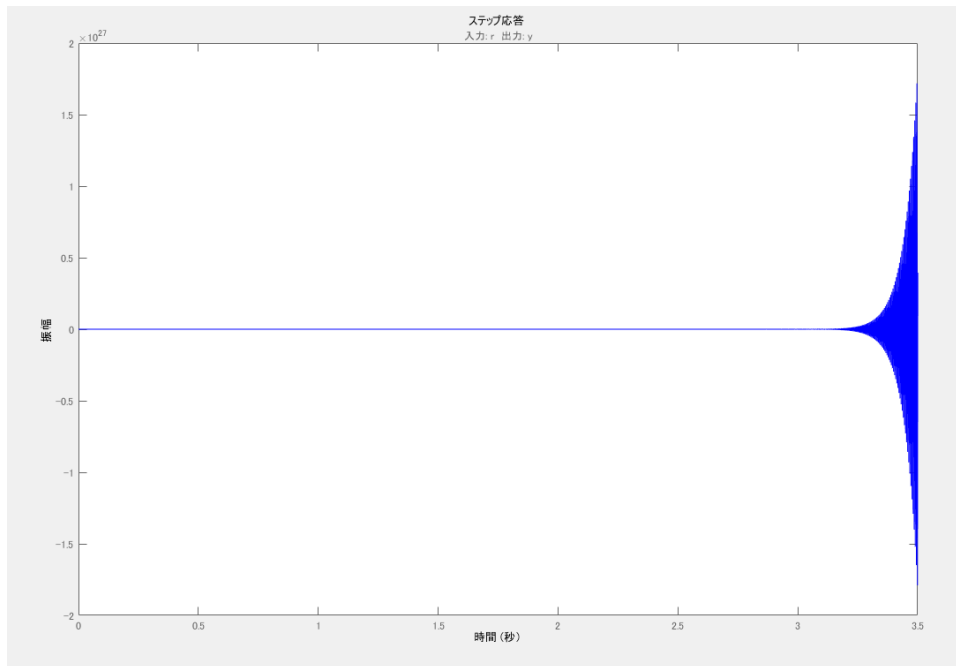Figure 4.53 Nyquist diagram of the plant with PI controller parameter T = 0.01 k = 0.03

Figure 4.54 Step response of the plant with PI controller parameter T = 0.01 k = 0.03

Stability Analysis Result: Case 14

GN14: T = 0.01 k = 0.06

D = 0.69208405

$I_2 = 4.186\ A$

$V_{C2} = 158.75741\ V$

G.M. = 5.55 dB at 4.2e+03 rad/s or 668.4508 Hz

P.M. = 24.7 deg at 3.82e+03 rad/s or 607.9719 Hz

Stable

Peak Response = 0.998 at 0.08 s with 0% overshoot

Settling Time = 0.0424 s

Rise Time = 0.0151 s

Steady State = 0.08 s
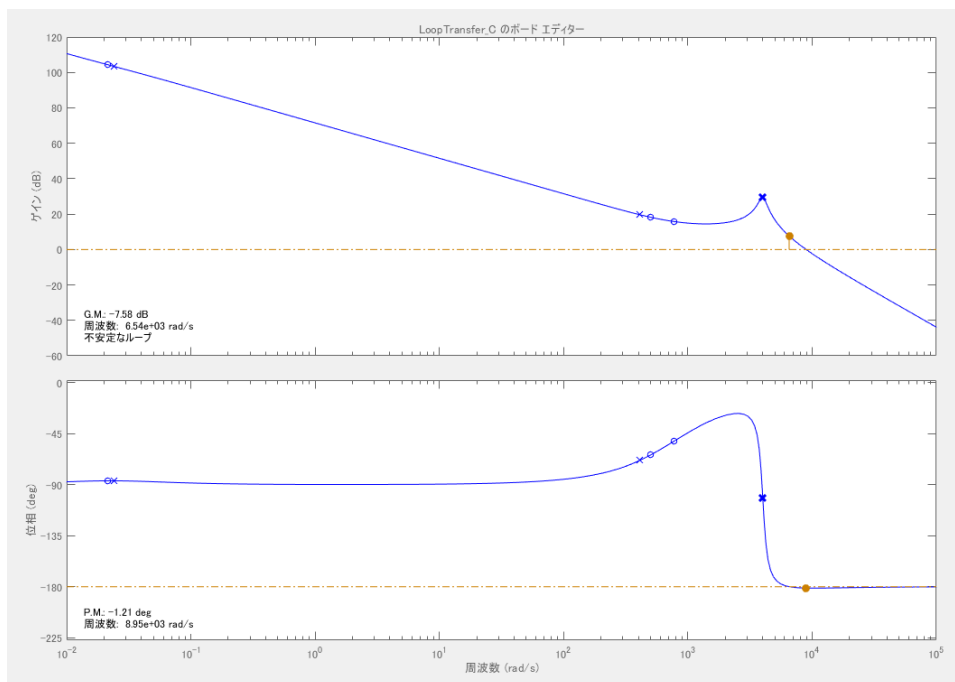

Figure 4.55 Bode diagram of the plant with PI controller parameter T = 0.01 k = 0.06

Figure 4.56 Nyquist diagram of the plant with PI controller parameter T = 0.01 k = 0.06

Figure 4.57 Step response of the plant with PI controller parameter T = 0.01 k = 0.06

Stability Analysis Result: Case 15

GN15: T = 0.01 k = 0.15

D = 0.70232878

$I_2 = 4.21238\ A$

$V_{C2} = 158.79971\ V$

G.M. = -2.56 dB at 4.21e+03 rad/s or 670.0423 Hz

P.M. = -5.5 deg at 4.43e+03 rad/s or 705.0564 Hz

Unstable
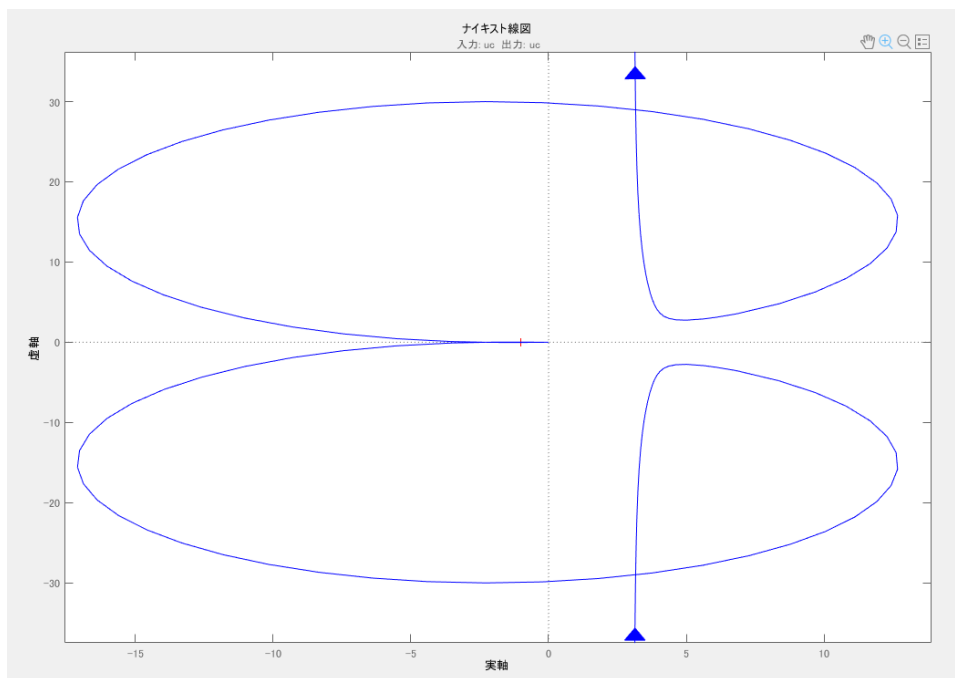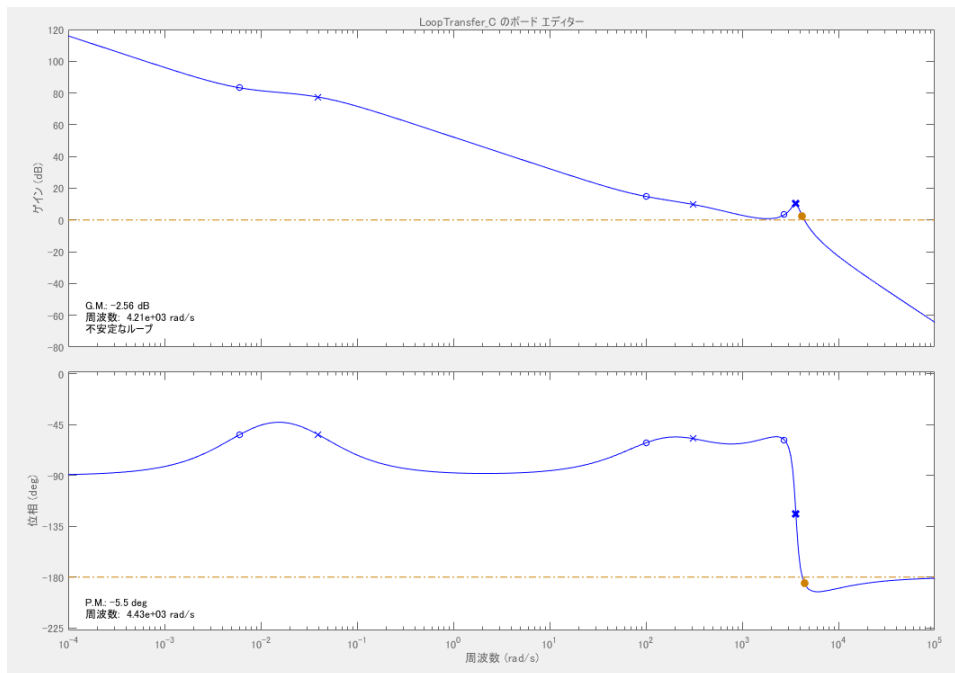

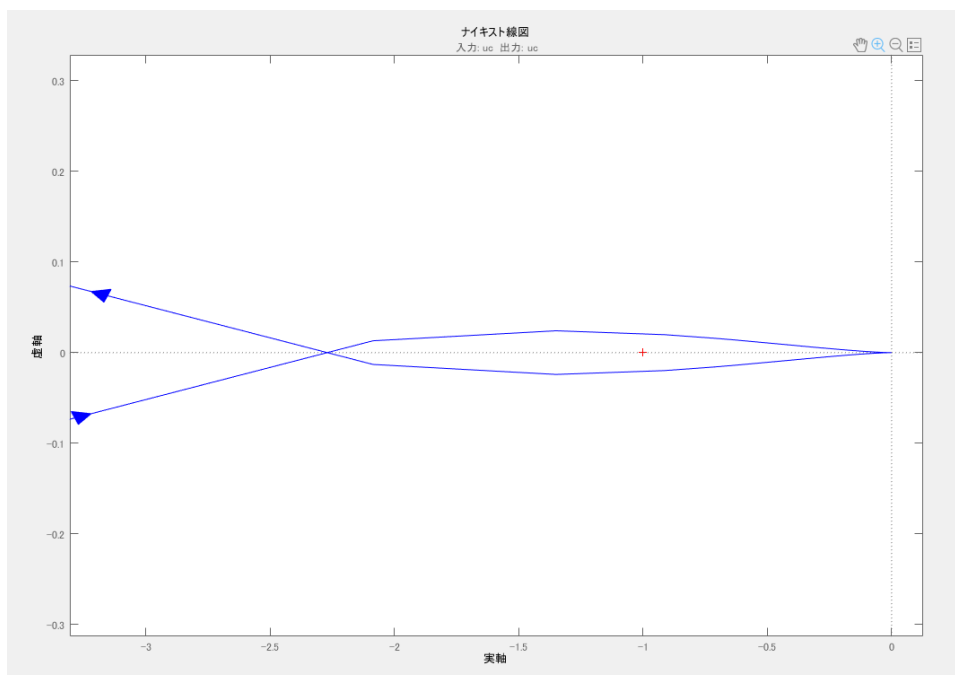Figure 4.58 Bode diagram of the plant with PI controller parameter T = 0.01 k = 0.15
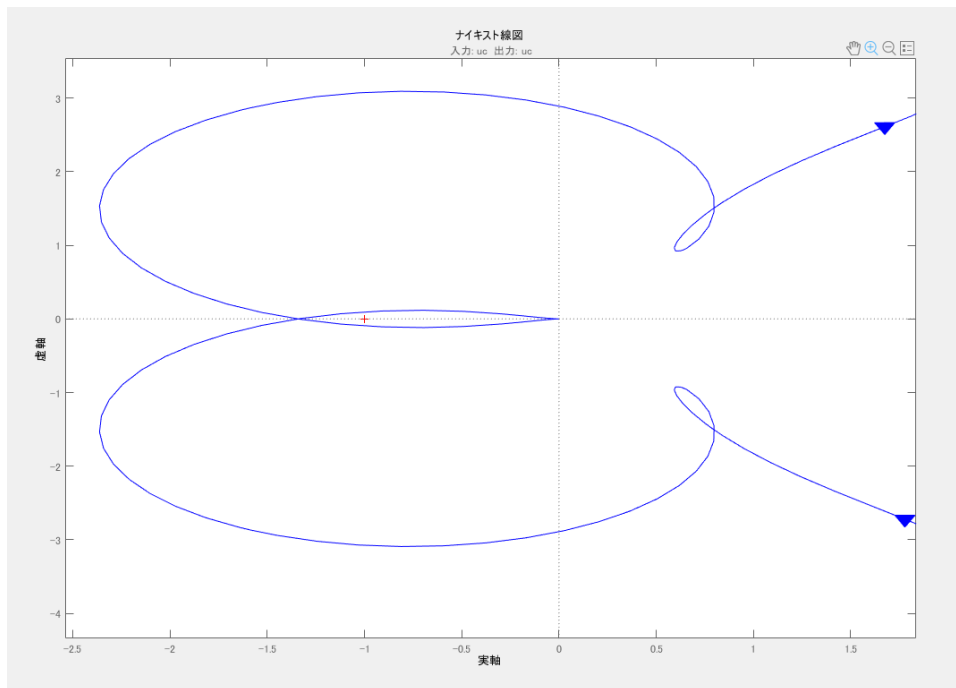
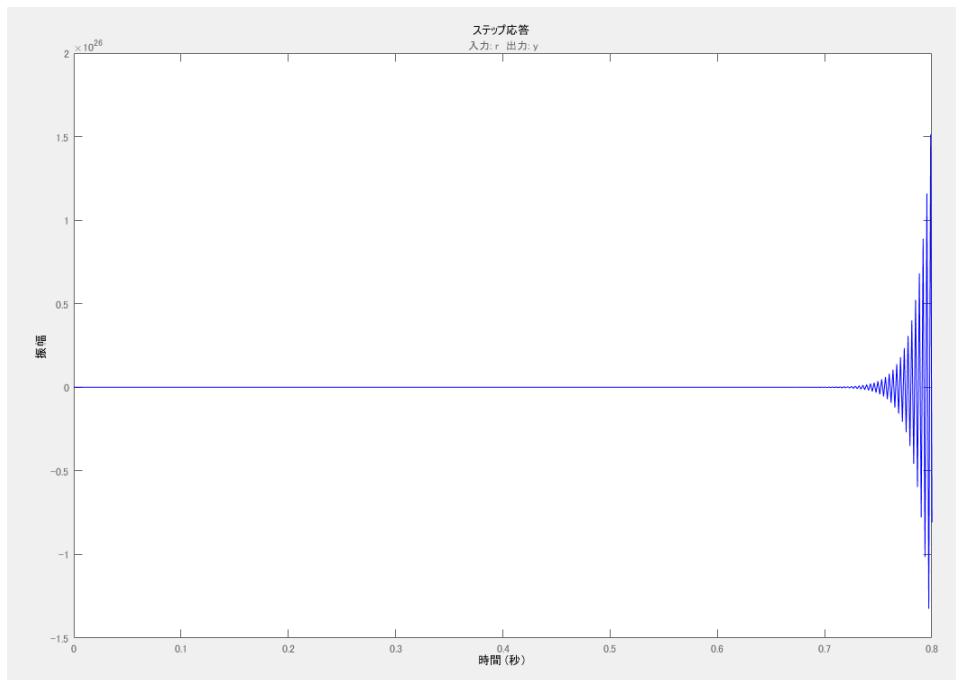Figure 4.59 Nyquist diagram of the plant with PI controller parameter T = 0.01 k = 0.15
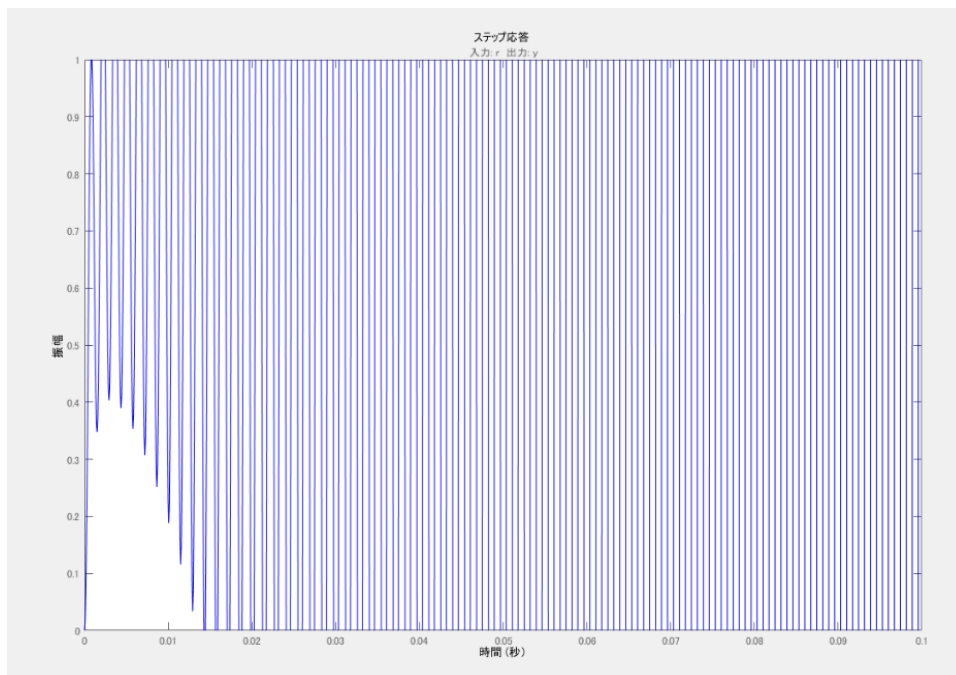
Figure 4.60 Step response of the plant with PI controller parameter T = 0.01 k = 0.15

78

Stability Analysis Result: Case 16

GN16: T = 0.01 k = 0.3

D = 0.95

$I_2 = 2.4170322\ A$

$V_{C2} = 142.09063\ V$

G.M. = -11.6 dB at 4.25e+03 rad/s or 676.4085 Hz
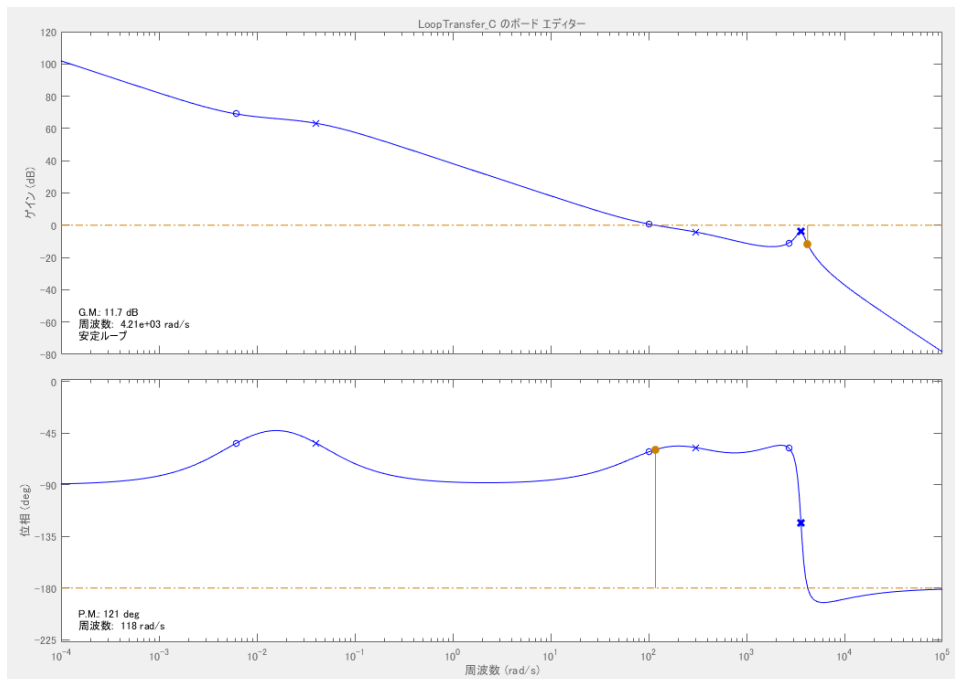
P.M. = -29.1 deg at 5.1e+03 rad/s or 811.6902 Hz

Unstable
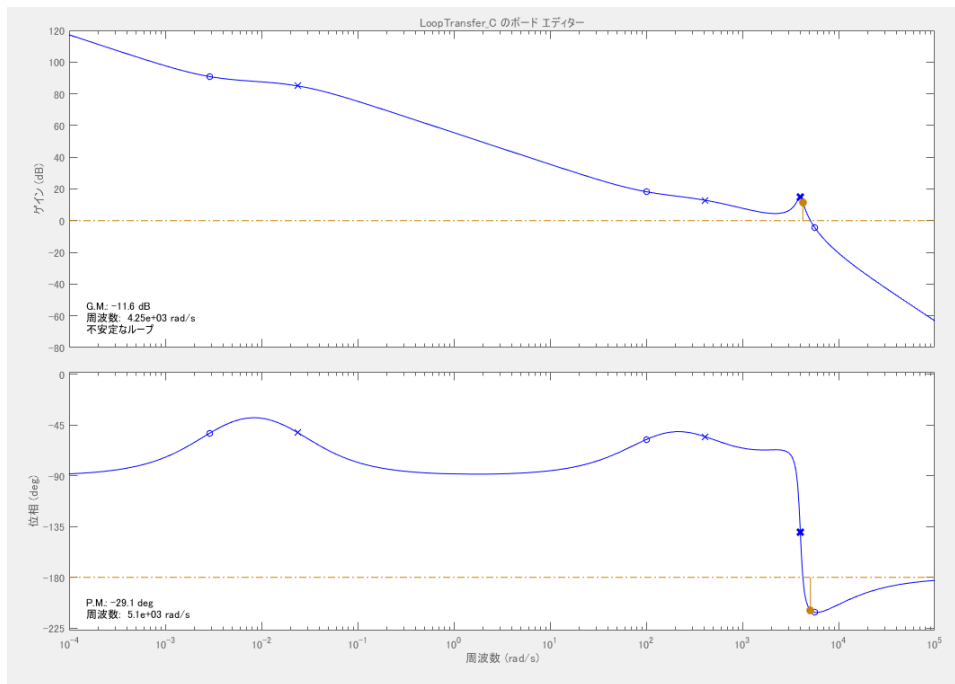
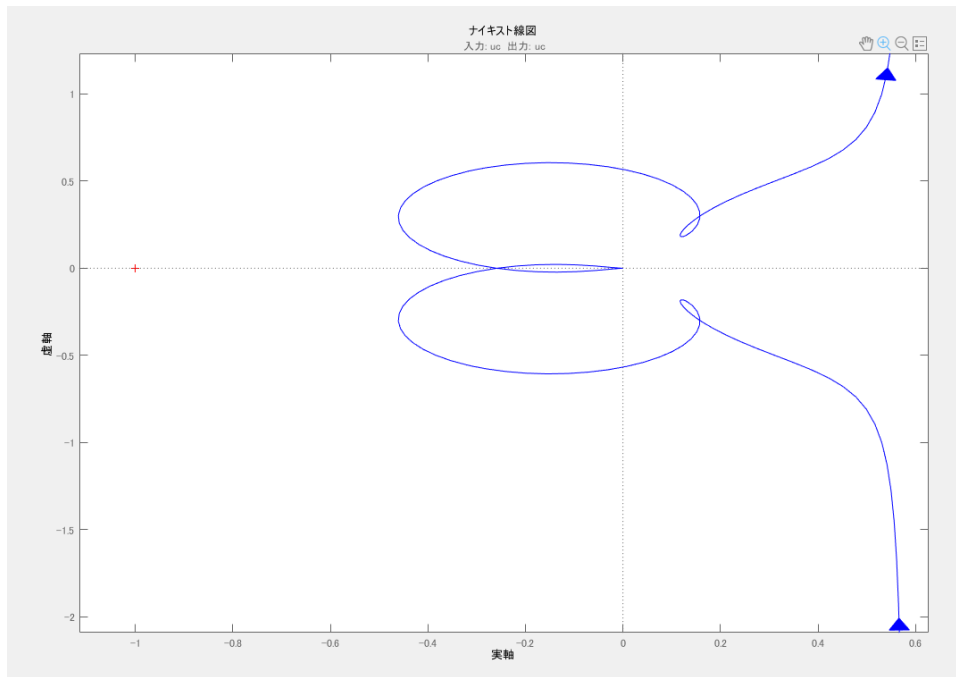Figure 4.61 Bode diagram of the plant with PI controller parameter T = 0.01 k = 0.3

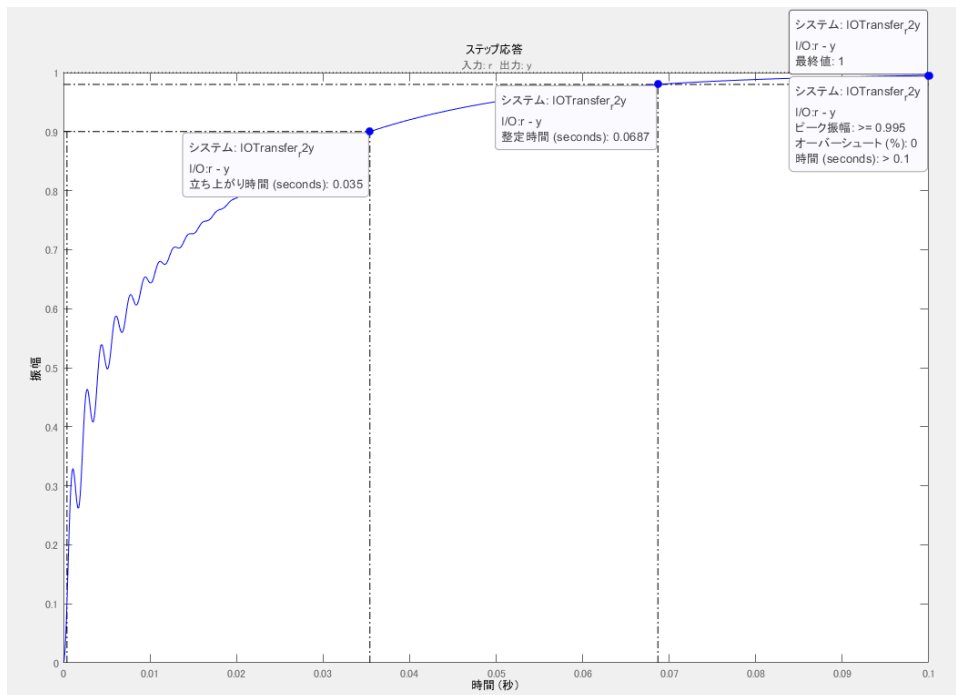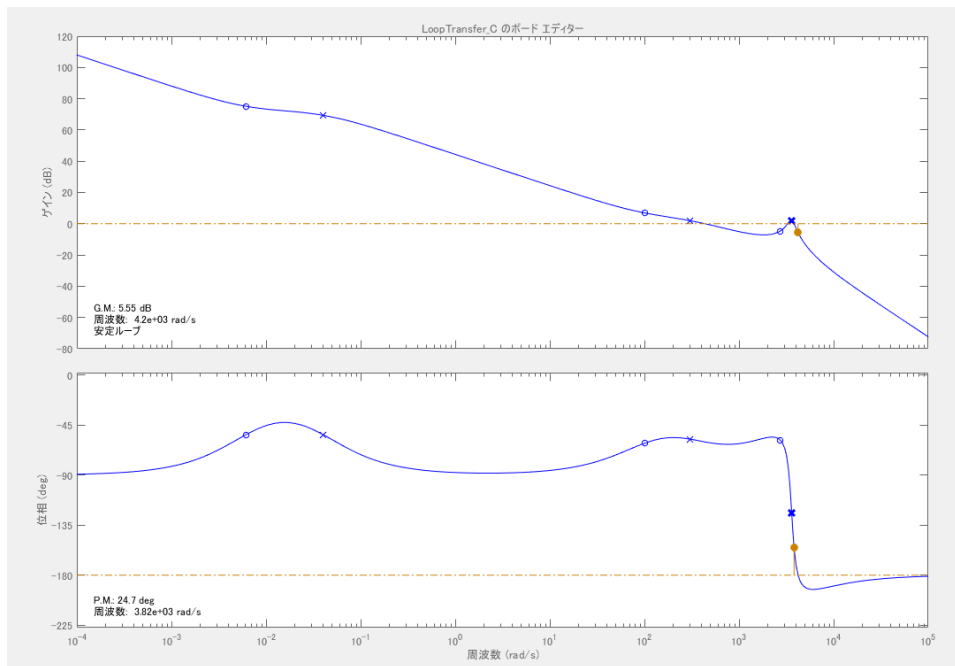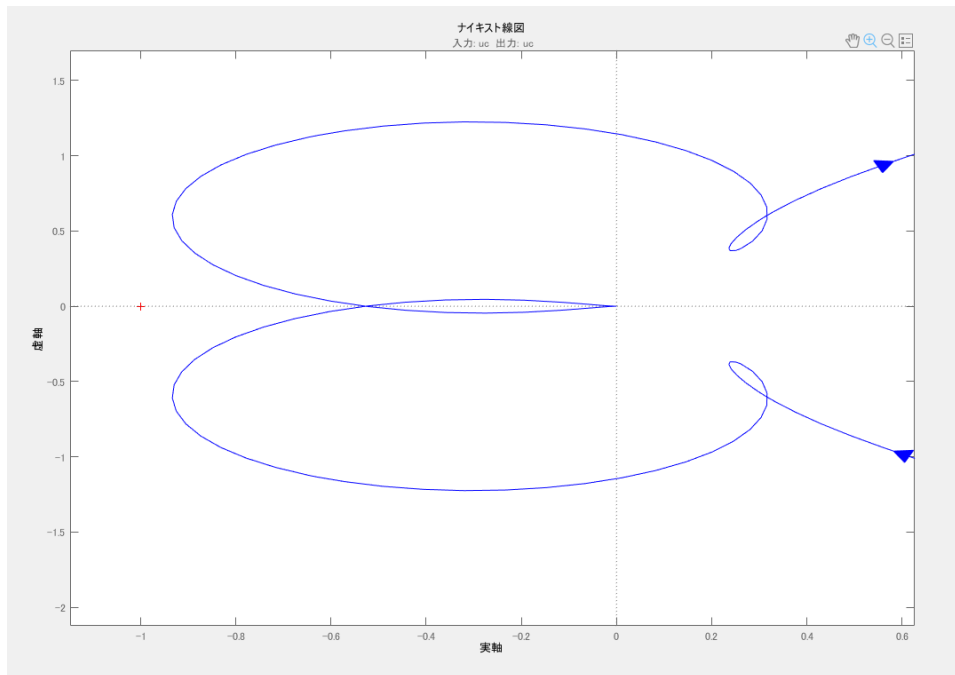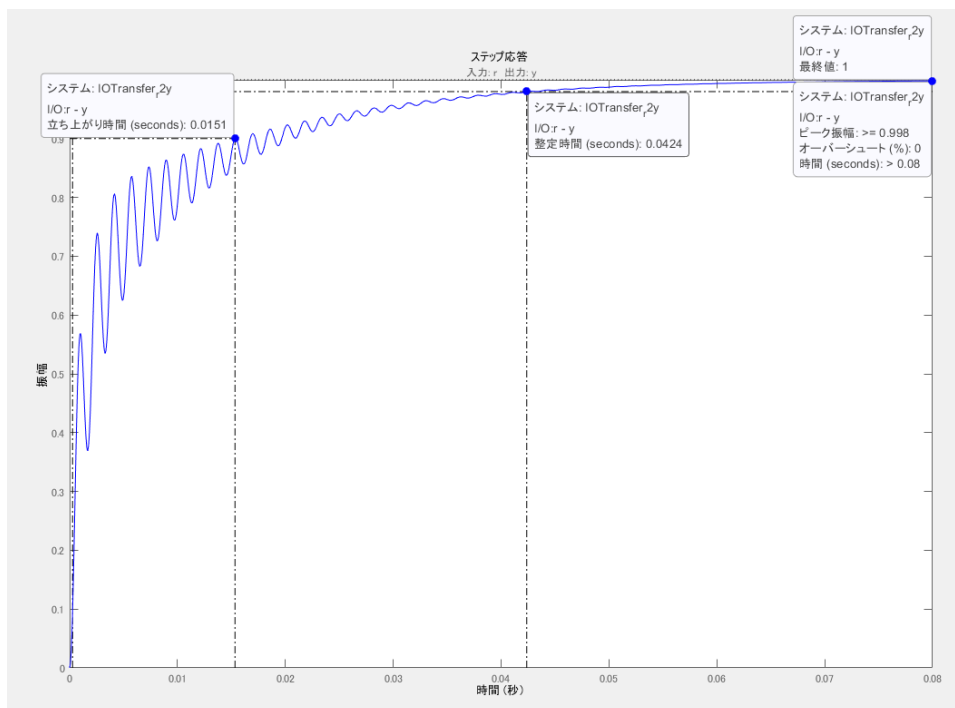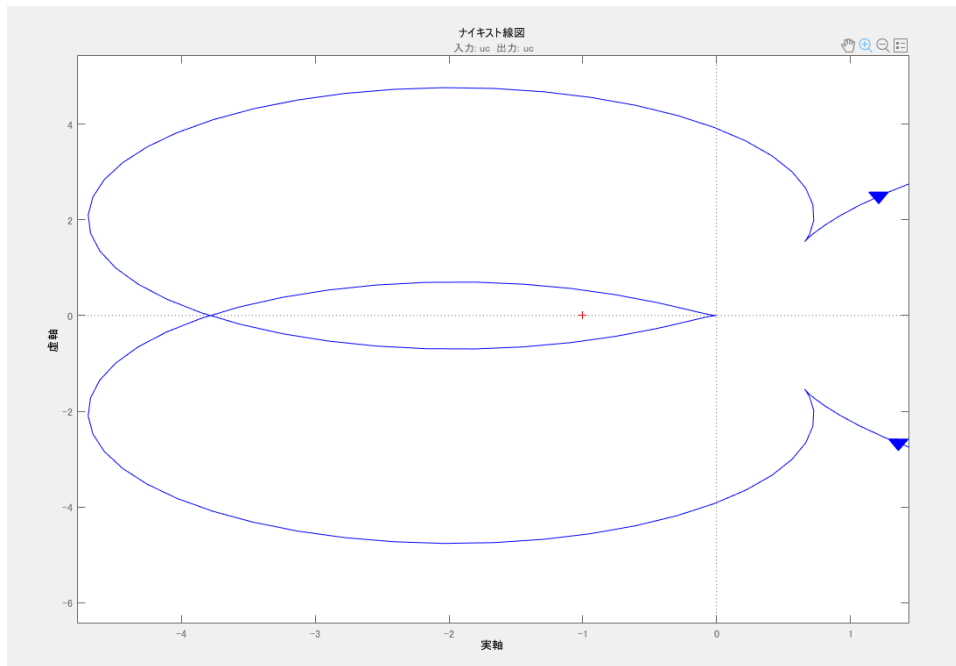Figure 4.62 Nyquist diagram of the plant with PI controller parameter T = 0.01 k = 0.3
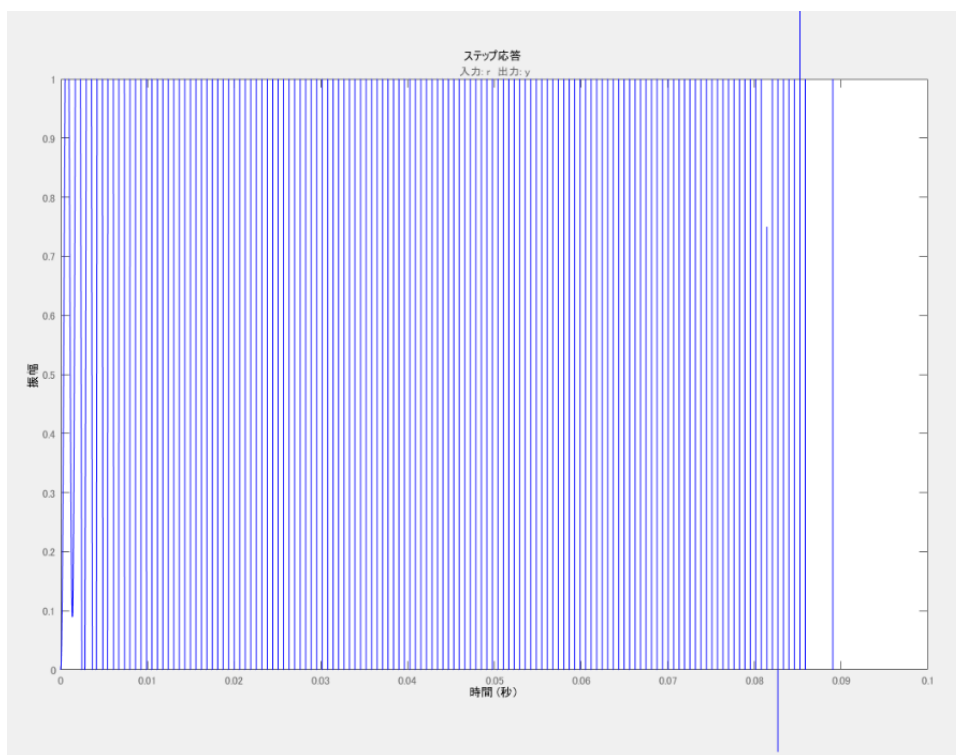
Figure 4.63 Step response of the plant with PI controller parameter T = 0.01 k = 0.3

4.4. Comparing System Performance

Figure 4.64 and 4.65 present a comparison of the system performance between stable and unstable ones. The P_{ref} is changed at the 5th second from 200 W to 100 W.

Figure 4.64 shows a stable system with gain k = 0.1286 and T = 0.1.

Figure 4.65 shows an unstable system with gain k = 0.15 and T = 0.002.

In the stable system, even though the P_{ref} is changed, the system still function properly without any significant fluctuation in any current or voltage signals. On the other hand, in the unstable system, after the change in P_{ref} is changed, there are visible fluctuations shown in every measured signal.

	x1	x2	Δ	平均値
Time	4.00000e+000	6.00000e+000	2.00000e+000	
duty	6.93001e-001	6.73195e-001	-1.98053e-002	6.74301e-001
Iem	1.31509e+000	6.17393e-001	-6.97693e-001	1.00489e+000
Iref	1.28777e+000	6.44358e-001	-6.43411e-001	9.95673e-001
Vedic	5.23483e+001	5.28307e+001	4.82421e-001	5.25823e+001
Vem	1.56558e+002	1.55854e+002	-7.04047e-001	1.51939e+002
IoutEDLC	4.27538e+000	1.86671e+000	-2.38867e+000	3.11675e+000

Figure 4.64 The stable system performance with gain k = 0.1286 and T = 0.1

	x1	x2	Δ	平均値
Time	4.00000e+000	6.00000e+000	2.00000e+000	
duty	9.50000e-001	8.36340e-001	-1.13660e-001	8.24508e-001
Iem	1.38928e+000	2.63846e+000	1.24918e+000	1.01796e+000
Iref	1.44999e+000	6.45063e-001	-8.04931e-001	9.98410e-001
Vedlc	3.46805e+001	3.31695e+001	-1.51099e+000	3.41554e+001
Vem	1.39384e+002	1.68177e+002	2.87930e+001	1.37830e+002
IoutEDLC	2.77452e+001	1.73217e+001	-1.04235e+001	1.71382e+001

Figure 4.65 The unstable system performance with gain k = 0.15 and T = 0.002

4.5. Conclusion

This chapter presents parameters, control, and analysis methods of the PV cell cooperating system. The simulation results are also presented in this chapter along with the stability analysis. There are 8 stable cases from 16 arbitrary chosen cases. From them, 2 new proper gains and time constants values are proposed which are case GN5 (T = 0.001, k = 0.03) and case GN9 (T = 0.002, k = 0.03). Therefore, the stability of the PV cell cooperating system is improved from the normally used value which is the same as case GN1 (T = 0.005, k = 0.03), in comparison with GN5, the gain margin is 2.9 dB increased and the time to reach steady state is reduced from 0.06 s to 0.02 s. Even though GN9 is not improving any gain or phase margin in comparison with GN1 but the steady-state time is also decreased to 0.025 s. This is proof that both new values are highly responsive.

Chapter 5

Conclusions and Future Work

The focus of this thesis is on improving the PV cell cooperating system performance by increasing the stability of the system.

Firstly, the transfer function of the PV cell cooperating system is derived by using the state-space averaging method. Then, the transfer function is verified by inputting a signal of the sine wave to check whether the output is as shown in the Bode diagram of the derived transfer function.

However, even though there is an offset error shown from the validation in the low-frequency range, the stability improving process is conducted by selecting gains and time constants for the PI controller by trial and error method. From that test, after judging the results by the Bode stability criterion, Nyquist stability criterion, and step response, there are 8 stable cases and 2 of them are promising.

The future work in this thesis can be extended according to the proposed ideas as follows:
- Resolve offset error issue by considering DC terms of averaged state equations, Fluctuation of the operating point, and rearrangement of state-space averaged model by redefining state vector I_2 and considering the accuracy of derivation.
- Experiment to confirm the stability improving results

Bibliography

[1] R. ∴. R. NOW, "What are the current trends in renewable energy?," [Online]. Available: https://www.ren21.net/what-are-the-current-trends-in-renewable-energy/. [Accessed 28 6 2020].

[2] "The Cost of Energy, Environmental Impact," The National Academies of SCIENCE, ENGINEERING, MEDICINE, [Online]. Available: http://needtoknow.nas.edu/energy/energy-costs/environmental/. [Accessed 28 6 2020].

[3] "Data and statistics CO2 emissions by energy source, World 1990-2017," International Energy Agency, 23 4 2020. [Online]. Available: https://www.iea.org/data-and-statistics?country=WORLD&fuel=CO2%20emissions&indicator=CO2%20emissions%20by%20energy%20source. [Accessed 28 6 2020].

[4] IRENA, "Global Energy Transformation A Roadmap to 2050," International Renewable Energy Agency, Abu Dhabi, 2018.

[5] G. R. Energy, "What is wind power?," GE, [Online]. Available: https://www.ge.com/renewableenergy/wind-energy/what-is-wind-energy. [Accessed 28 7 2020].

[6] Y. X. a. Z. T. Wenping Cao, Advances in Wind Power, Ontario: IntechOpen, 2012.

[7] W. L. Y. W. J. G. K. P. T. P. Tingzhen Ming, "Chapter 1 - Introduction," in *Solar Chimney Power Plant Generating Technology*, Academic Press, 2016, pp. 1-46.

[8]   A. L. S. Hegedus, Handbook of Photovoltaic Science and Engineering, Second Edition, New Jersey: John Wiley & Sons, Ltd., 2011.

[9]   N. Kishor, M. G. Villalva, S. R. Mohanty and E. Ruppert, "Modeling of PV module with consideration of environmental factors," *2010 IEEE PES Innovative Smart Grid Technologies Conference Europe (ISGT Europe),* pp. 1-5, 2010.

[10] M. M. K. A.-H. Haitham Abu-Rub, Power Electronics for Renewable Energy Systems, Transportation and Industrial Applications, Wiley-IEEE Press, 2014.

[11] M. M. B. Y.S. Mohammed, "Hybrid renewable energy systems for off-grid electric power: Reviewof substantial issues," *Renewable and Sustainable Energy Reviews,* vol. 35, pp. 527-539, 2014.

[12] S. Shiraishi, "Chpater 27 : Electric Double Layer Capacitors," in *Carbon Alloys*, Elsevier Science, 2003, pp. 447-457.

[13] Toshiba, "What is an IGBT?," Toshiba, [Online]. Available: https://toshiba.semicon-storage.com/ap-en/semiconductor/knowledge/faq/mosfet_common/what-is-an-igbt.html. [Accessed 4 August 2020].

[14] T. M. U. W. P. R. Ned Mohan, Power Electronics Converters, Applications, and Design second edition, Canada: John Wiley & Sons, Inc., 1995.

[15] W. W. H. T. D. Y. A Gavrilović, "41 - Reactive Power Plant and FACTS Controllers," in *Electrical Engineer's Reference Book (Sixteenth Edition)*, Newnes, 2003, pp. 41-1-41-40.

[16] C. Study, "Question: 1. Fig. 1 Shows A Single-phase Half-bridge Inverter," Chegg Study, [Online]. Available: https://www.chegg.com/homework-help/questions-and-answers/1-fig-1-shows-single-phase-half-bridge-inverter-fig-2-full-bridge-inverter-determine-equa--q42418725. [Accessed 11 September 2020].

[17] V. M. Phap, "Study on Solar-Wind Hybrid Power System Cooperating with PV Module," Mie University, 2018.

[18] T. M. U. W. P. R. Ned Mohan, Power Electronics: Converters, Applications, and Design, 3rd Edition, John Wiley & Sons, 2002.

[19] N. H. A.W., S. S.F. and M. A. Muin, "Modeling of DC-DC converter for solar energy system applications," *2012 IEEE Symposium on Computers & Informatics (ISCI),* pp. 125-129, 2012.

[20] M. R. G. Y. Z. J. Islam, Power Converters for Medium Voltage Networks, Heidelberg: Springer, 2014.

[21] E. C. M. BSc., "Boost Converters," 18 July 2020. [Online]. Available: https://learnabout-electronics.org/PSU/psu32.php. [Accessed 27 August 2020].

[22] A. Haque, "Maximum Power Point Tracking (MPPT) Scheme for Solar Photovoltaic System," *Energy Technology & Policy,* pp. 115-122, 2014.

[23] M. R. Patel, Wind and Solar Power Systems—Design, Analysis, and Operation, CRC Press, 2006.

[24] E. C. M. BSc., "Buck Converters," 18 July 2020. [Online]. Available: https://learnabout-electronics.org/PSU/psu31.php. [Accessed 27 August 2020].

[25] M.-Y. L. Y.-C. W. a. B.-C. C. Jaw-Kuen Shiau, "Circuit Simulation for Solar Power Maximum Power Point Tracking with Different Buck-Boost Converter Topologies," *Energies,* vol. 7, p. 5027–5046, 2014.

[26] M. J. S. P. M. G. S. S. Sivakumar, "An assessment on performance of DC–DC converters for renewable energy applications," *Renewable and Sustainable Energy Reviews,* vol. 58, p. 1475–1485, 2016.

[27] E. C. M. BSc., "Buck-Boost Converters," 18 July 2020. [Online]. Available: https://learnabout-electronics.org/PSU/psu33.php. [Accessed 28 August 2020].

[28] T. C. S. Jalbrzykowski, "A bidirectional DC-DC converter for renewable energy systems," *Bulletin of the Polish Academy of Sciences Technical Sciences,* vol. 57, no. 4, 2009.

[29] D. S. K. a. N. Hadagali, "Bidirectional DC/DC converter system for solar and fuel cell powered hybrid electric vehicle," *Proc. IEEE International Conference on Emerging Research Areas: Magnetics, Machines and Drives,* pp. 1-6, 2014.

[30] J. T. a. Z. C. Y. Hu, "A bidirectional dc/dc power electronic converter for an energy storage devices in an autonomous power system," *Proc. Power Electron. Motion Conf.,* pp. 171-176, 2004.

[31] H. S. M. B. S. Kolsi, "Amar Design Analysis of DC-DC Converters Connected to a Photovoltaic Generator and Controlled by MPPT for Optimal Energy Transfer throughout a Clear Day," *Journal of Power and Energy Engineering,* vol. 2, pp. 27-34, 2014.

[32] S. M. L. J. Yang H., "The Simulation of the Principle of MPPT Control of PV Systems Based on BOOST Circuit," *Proc. Electrical, Information Engineering and Mechatronics,* p. 2127–2135, 2011.

[33] C. S. Solanki, SOLAR PHOTOVOLTAICS - Fundamentals, Technologies and Applications, PHI Learning Pvt. Ltd, 2015.

[34] S. &. B. N. R. Saravanan, "Maximum power point tracking algorithms for photovoltaic system – A review," *Renewable and Sustainable Energy Reviews,* vol. 57, p. 192–204, 2106.

[35] N. C. Kerim Karabacaka, "Artificial neural networks for controlling wind–PV power systems: A review," *Renewable and Sustainable Energy Reviews,* vol. 29, pp. 804-827, 2014.

[36] N. H. S. A. Z. Yasser E. Abu Eldahab, "Enhancing the maximum power point tracking techniques for photovoltaic systems," *Renewable and Sustainable Energy Reviews,* vol. 40, pp. 505-514, 2014.

[37] D. d. C. P. a. W. J. d. P. Fernando Lessa Tofoli, "Comparative Study of Maximum Power Point Tracking Techniques for Photovoltaic Systems," *International Journal of Photoenergy,* pp. 1-10, 2015.

[38] G. P. G. S. M. V. Nicola Femia, Power Electronics and Control Techniques for Maximum Energy Harvesting in Photovoltaic Systems, CRC Press Taylor & Francis Group, 2013.

[39] K. J. Å. a. R. M. Murray, Feedback Systems: An Introduction for Scientists and Engineers, New Jersey: Princeton University Press, 2020.

[40] A. O. Simon Ang, Power-Switching Converters Second Edition, Florida: CRC Press Taylor & Francis Group, 2005.

[41] gonzo@mit.edu, "Stability Criteria - (Gain Margin and Phase Margin)," MIT, 29 September 2000. [Online]. Available: http://www.mit.edu/afs.new/athena/course/2/2.010/www_f00/psets/hw3_dir/tutor3_dir/tut3_g.html?fbclid=IwAR3x2V7ZORWdgZPBPJ6fyoXE86uI4nSnTztuyogfBey98Nhd0V-F2Ih5aWM. [Accessed 4 August 2020].

[42] Electrical4U, "Bode Plot, Gain Margin and Phase Margin," Electrical4U, 18 May 2020. [Online]. Available: https://www.electrical4u.com/bode-plot-gain-margin-phase-margin/. [Accessed 4 August 2020].

[43] Y. X. a. Z. T. Wenping Cao, "Wind Turbine Generator Technologies," InTechOpen, [Online]. Available: https://www.intechopen.com/books/advances-in-wind-power/wind-turbine-generator-technologies#B7. [Accessed 27 August 2020].

[44] Y. X. a. Z. T. Wenping Cao, "Wind Turbine Generator Technologies," InTechOpen, 2012. [Online]. Available: https://www.intechopen.com/books/advances-in-wind-power/wind-turbine-generator-technologies#B45. [Accessed 27 August 2020].